

UNIVERSITY OF PADOVA

Department of Information Engineering

Ph.D. School in Information Engineering

Information Science and Technology

XXVII Class

Combined Networking and Control Strategies for Smart Micro Grids

Analysis, Co-simulation and Performance Assessment

Ph.D. candidate:

Riccardo BONETTO

Supervisor:

Prof. Michele ROSSI

Course coordinator:

Prof. Carlo FERRARI

Ph.D. School director:

Prof. Matteo BERTOCCO

Academic Year 2014-2015

Abstract

The constantly increasing number of power generation devices based on renewables calls for a transition from the centralized control of electrical distribution grids to a distributed control scenario. In this context, distributed generators are exploited to achieve other objectives beyond supporting loads, such as the minimization of the power losses along the distribution lines, the sustainability of the electrical network when operated in islanded-mode (i.e., when the the energy flow from the main energy supplier is not available) and the power peaks shaving.

In order to fulfill the aforementioned goals, optimized techniques aimed at managing the electrical behavior of the distributed generators (i.e., the amount of active and reactive power injected into the grid by the distributed generators at any given time), are needed. These techniques, in order to dispatch information regarding the actual state of the network agents, rely on smart metering devices (measuring instantaneous electrical quantities as, for example, active and reactive power, loads impedance and loads voltage) and on a communication infrastructure (i.e., Powerline Communication - PLC) interconnecting the smart-grid agents and allowing for the exchange of the measured quantities. Moreover, suitable communication protocols, supporting the transmission channel access and data routing, are needed.

In this doctoral thesis, firstly, a full-fledged system that extends existing state-of-the-art algorithms for the distributed minimization of power losses in smart micro grids is presented. There, practical aspects such as the design of a communication and coordination protocol that is resilient to link failures and manages channel access, message delivery and distributed generator coordination is taken into account. Design rules for the networking strategies that best fit the selected optimization approaches are provided. Finally, in the presence of lossy communication links, the impact of communication and electrical grid features is as-

sessed. Specifically, communication failures, scheduling order for the distributed control, line impedance estimation error, network size and number of distributed generators are considered as major issues.

Next, it will be shown that the convergence rate of the optimization algorithms, implemented in the aforementioned system, can be improved by suitably scheduling the order in which the smart-grid agents are activated. For stability purposes, a token ring approach is often implemented for the control, where at any given time a single node with communication and control capabilities (referred to as *smart node*) has the token and is the only node in charge of implementing the control action entailed by the algorithms (i.e., power injection). It will be shown that the token ring approach does not always ensure the fastest convergence rate. In order to improve the convergence rate of the selected optimization techniques, optimality criteria are defined and a lightweight, distributed and heuristic (suboptimal) scheduling algorithm is designed.

Another important aspect considered in this thesis, is the one concerning the power demand peak shaving. Algorithms that exploit the distributed energy sources and rely on the smart-grid communication infrastructure in order to level out the peaks in the electrical power demand, can greatly reduce the workload of the main energy supplier, thus preventing unexpected hardware failures and blackouts. The importance of leveling out the power demand peaks is even greater when dealing with smart-grids operating in islanded mode, since avoiding power demand peaks can substantially improve the self-sustainability of the electrical grid. To this end, a lightweight and effective approach for the management of prosumer communities through the synergistic control of the power electronic converters acting therein is designed. An islanded operating mode is considered, and the control strategy aims at leveling peaks in the use of energy drained from or injected into the connection point with the main power supplier.

All the aforementioned techniques rely on the use of distributed generators (whose energy comes from renewable sources) to contribute to the overall grid electrical efficiency. In a real-world setting, such control actions will however depend on market models and on the revenue (monetary income) that the final users will accrue through energy trading with other users and with the smart grid operator. For this reason, an optimized market model accounting for electrical efficiency constraints, along with the demand-offer rule, is designed. Novel market

rules designed to provide economical benefits to all the smart grid players (i.e., the users and the grid operator), while also driving the power grid toward a satisfactory solution in terms of electrical performance are designed. To the best of the author's knowledge, a general framework for the study of the interaction between power grid optimization algorithms (electrical performance) and energy pricing and trading strategies (revenue) is not yet available in the related scientific literature.

Sommario

In questi anni, si sta verificando una costante diffusione di dispositivi atti alla produzione di energia elettrica basati su fonti energetiche naturali e rinnovabili. Questo fenomeno, a sua volta, sta portando a una decentralizzazione del controllo delle reti di distribuzione elettrica.

I generatori di energia elettrica basati su fonti rinnovabili, chiamati nel seguito generatori distribuiti, oltre che per l'alimentazione dei carichi elettrici delle sedi in cui sono installati, possono altresì essere utilizzati per numerosi altri scopi, come, ad esempio: la minimizzazione della potenza dissipata lungo le linee di trasmissione elettrica; il mantenimento delle condizioni operative della rete anche qualora il principale fornitore di energia venisse disconnesso e, infine, il livellamento dei picchi di domanda di potenza elettrica.

Al fine di supportare queste funzionalità addizionali, è necessario che vengano implementate politiche efficienti di controllo del comportamento dei generatori distribuiti. Tali politiche dovranno permettere a ciascun generatore distribuito di conoscere, in ogni momento, gli esatti riferimenti di potenza attiva e reattiva che debbono essere iniettati nella rete elettrica. Affinché le suddette tecniche possano essere implementate, è necessaria l'esistenza di un'infrastruttura di comunicazione che permetta agli elementi attivi della rete elettrica di scambiare informazioni.

In questa tesi, verranno considerati aspetti pratici, fondamentali al corretto funzionamento di una rete elettrica intelligente quali, ad esempio la progettazione di protocolli di comunicazione e di controllo robusti rispetto agli errori di comunicazione e in grado di garantire la corretta sincronizzazione dei generatori distribuiti nell'applicazione della politica di controllo selezionata. Verranno inoltre studiate tecniche in grado di incrementare la velocità di convergenza di alcuni algoritmi atti alla minimizzazione della potenza dissipata nella fase di distribuzione. Verrà, a questo proposito, presentato un algoritmo euristico e distribuito

in grado di uncremente la velocità di convergenza delle tecniche selezionate senza, tuttavia, influire in misura degna di nota sul numero di messaggi che è necessario scambiare per la corretta esecuzione delle suddette tecniche.

Un secondo aspetto di considerevole importanza considerato in questa tesi, è il livellamento dei picchi nella potenza totale richiesta dai carichi presenti nella rete. A tal proposito verrà presentato un algoritmo distribuito in grado di livellare con successo i picchi di domanda sia nel caso la rete elettrica sia connessa al fornitore ufficiale di energia sia nel caso contrario.

Infine, basandosi sulla considerazione che, affinché i generatori distribuiti collaborino all'efficienza energetica della rete elettrica, è necessario questi ultimi ottengano un ritorno economico derivante dal loro comportamento virtuoso, verrà definito un nuovo modello di mercato energetico. Tale modello permetterà la compravendita diretta di energia (non ci sarà quindi più bisogno che il fornitore ufficiale agisca da intermediario) e, allo stesso tempo, consentirà ad un'entità regolatrice di indirizzare il mercato verso configurazioni energetiche efficienti.

Contents

Abstract	i
Sommario	v
1 Introduction	1
2 Networking for Power Loss Minimization in Smart Micro Grids: Design Rules and Performance Assessment	5
2.1 Introduction	5
2.2 Background	8
2.2.1 Grid Model	8
2.2.2 Local Control	10
2.2.3 Current Based Surround Control	10
2.2.4 Voltage Based Surround Control	12
2.2.5 Distributed Optimal Reactive Power Flow Control	14
2.3 Clustering	14
2.4 Communication Procedures	17
2.4.1 Communication Infrastructure and Requirements	17
2.4.2 Token Ring Protocol for Tree Networks	19
2.5 Simulation setup	21
2.6 Numerical Results	24
2.6.1 Dissipated Power	24

2.6.2	Convergence Time	25
2.6.3	Resilience to Link Failures	26
2.6.4	PCC Workload	27
2.6.5	Impact of the EC Procedure	29
2.6.6	Performance Assessment with Time Varying PV Generation and Power Demand	30
2.6.7	Lessons Learned	33
2.7	Conclusions	35
3	When Order Matters	39
3.1	Introduction	39
3.2	System Model	41
3.2.1	Grid Model	41
3.2.2	Distributed Optimization Algorithms	42
3.3	Token Ring Control	43
3.4	Electrical Grid Topology Generation	45
3.5	Numerical Results	46
3.6	Conclusions	50
4	Peak Shaving	53
4.1	System Model	55
4.2	Microgrid control strategy	57
4.2.1	Islanded Operation – Active Power	59
4.2.1.1	$P_{Ltot}(\ell + 1) < P_{Gtot}^{\min}(\ell + 1)$	59
4.2.1.2	$P_{Gtot}^{\min}(\ell + 1) \leq P_{Ltot}(\ell + 1) < P_{Gtot}(\ell + 1)$	59
4.2.1.3	$P_{Gtot}(\ell + 1) \leq P_{Ltot}(\ell + 1) \leq P_{Gtot}^{\max}(\ell + 1)$	60
4.2.1.4	$P_{Ltot}(\ell + 1) > P_{Gtot}^{\max}(\ell + 1)$	60
4.2.2	Islanded Operation – Reactive Power	60
4.2.2.1	$Q_{Ltot}(\ell + 1) \leq Q_{Gtot}^{\max}(\ell + 1)$	60
4.2.2.2	$Q_{Ltot}(\ell + 1) > Q_{Gtot}^{\max}(\ell + 1)$	61
4.2.3	Grid connected operation	61
4.2.4	Islanded operation.	63

4.2.4.1	Over-generation ($P_{Gtot} > P_{Ltot}$)	63
4.2.4.2	Under-generation ($P_{Gtot} < P_{Ltot}$)	64
4.3	Results	64
4.4	Conclusions	68
5	Optimized Energy Pricing for Smart Grid Efficiency Enforcement	71
5.1	Introduction	71
5.2	Scenario	74
5.2.1	Electrical Scenario	74
5.2.2	Communication Scenario	75
5.2.3	Market Scenario	75
5.3	Notation	77
5.3.1	Domains	77
5.4	Multi-Objective Optimization Problem	79
5.4.1	Objective Functions	80
5.4.2	Constraints	80
5.4.3	Optimization Problem	82
5.4.4	Geometric Programming Formulation	85
5.4.5	Solution	86
5.5	Simulation Setup	87
5.6	Results	89
5.6.1	Tight Power Offer	90
5.6.2	Unbalanced Tight Power Offer	92
5.6.3	Loose Power Offer	93
5.7	Conclusions	95
6	Conclusions	97
	List of Publications	99
	Bibliography	100

The term Smart Grid refers to the integration of the traditional power distribution network with communication and information technologies and the constantly increasing number of distributed energy production plants based on renewables [1]. The grid resulting from this integration allows for the implementation of autonomous control and actuation systems.

Among the many opportunities offered by the emerging Smart Grids, in this work we focus on three main topics:

- distribution power loss minimization;
- peak shaving;
- new energy market models accounting for the concurrent maximization of the power grid efficiency (e.g., using the techniques of the previous two points).

In particular, the distribution power loss minimization allows the boosting of the grid electrical efficiency. Effective power loss minimization techniques have been proposed in previous work [2–7] and have been shown to effectively reduce the main energy supplier workload, allowing to serve more users with a higher electrical power quality. In this doctoral thesis, we explore the performance of state-of-the-art control schemes for the power loss minimization in residential micro grids [5–7] providing design rules for the networking strategies that best fit the selected optimization approaches. In the presence of lossy communication links the impact of communication and electrical grid features is assessed. Specifically, as major issues we consider communication failures, scheduling order for the distributed control, line impedance estimation error, network size and number of DGs. The performance of control

algorithms is evaluated in terms of power loss reduction, reduction of aggregate power demand, convergence rate, resilience to impairments and injected current from DGs. Once the impact of communication impairments on the selected power loss minimization techniques has been assessed, the effect of the control actions scheduling is taken into account. To this respect, we investigate the impact of the control action scheduling on the convergence rate of selected optimization techniques, defining optimality criteria, devising lightweight suboptimal rules and assessing the performance of the optimal and suboptimal but online techniques. The performance of the selected techniques has been assessed by extensive simulation campaigns using topologies generated through a statistical approach [8] and real-world energy photovoltaic production [9] and power demand profiles.

Peak shaving strategies aim at leveling peaks in the use of the energy drained from or injected into the main power supplier. In this thesis, we investigate and evaluate a lightweight and effective approach for the management of prosumer communities. The management process is made possible by the presence of controllable elements cooperating through a common communication infrastructure. These controllable elements are the utility interface, installed at the point of common coupling with the electrical utility, and the energy gateways, interfacing distributed generation units and energy storage devices with the distribution grid. The user interface acts as the control master for the microgrid, that collects information on generators and loads activity and dispatches a control parameter that regulates both energy storage devices and generators. The proposed control strategy is tested on a residential microgrid model, 100 kVA rated, which has been developed and utilized to analyze selected performance metrics. As for the previous case, real-world energy photovoltaic production and power demand profiles have been used.

Both power loss minimization and peak shaving rely on the collaboration of the distributed energy production plants to drive the power grid toward a stable and electrically efficient operating regime. In real-world scenarios, this collaboration is mainly driven by economical benefits. For this reason, an optimized market model accounting for electrical efficiency constraints, is designed. Novel market rules conceived to provide economical benefits to all the smart grid players (i.e., the end-users and the grid operator), while also driving the power grid toward a satisfactory solution in terms of electrical performance are designed. To the best of our knowledge, a general framework for the study of the interaction between power grid

optimization algorithms (electrical performance) and energy pricing and trading strategies (economical benefit) is not yet available in the related scientific literature. This framework is then validated, accounting for the salient characteristics of power grids, i.e., electrical optimization, communication infrastructure and a dynamic and distributed energy market. The developed market model is finally optimized by means of multi-objective optimization tools that allows to find the set of all the optimal energy trading policies.

The rest of this work is structured as follows.

Chapter 2: In this chapter, the impact of communication impairments on the performance of four selected distributed power loss minimization techniques is assessed.

Chapter 3: In this chapter, the impact of the control action scheduling on two selected power loss minimization techniques is assessed. Moreover, a heuristic scheduling optimization technique is presented and evaluated.

Chapter 4: In this chapter, a new peak shaving procedure leveling peaks in the use of energy drained from or injected into the main power supplier is presented.

Chapter 5: In this chapter, a new energy market model, jointly accounting for distributed power generation and electrical efficiency enforcement is presented. A multi-objective optimization problem yielding the optimal energy trading policies is defined and its solution is discussed.

Chapter 6: In this chapter, we draw our conclusions.

Networking for Power Loss Minimization in Smart Micro Grids: Design Rules and Performance Assessment

2.1 Introduction

The traditional centralized power distribution grid is nowadays facing two important trends: the constantly increasing power demand and the worldwide diffusion of electrical power generation devices based on renewables [1]. While the former calls for radical changes in the way the energy is generated and delivered to the final users, we note that electrical power generation is still mostly based on biofuels, fossil fuels and nuclear plants [10]. Currently, distributed generation devices are used either to sell power to the energy provider or to fulfill the owner's power demand, without interactions with the distribution grid, other users, or the utility provider. However, a more flexible use of the distributed generator (DG) devices is expected both to boost the grid efficiency [11–14] in terms of power distribution, reactive power compensation and frequency stability, and to relieve electricity production plants from some of the power load [15]. This however requires the addition of communication and smart metering capabilities to the power grid. In the last few years, several grid optimization techniques have been proposed [16–18], each exploiting some existing communication infrastructure and relying on online smart metering procedures [19].

In this chapter, we target residential micro grids where some of the end users behave as DGs, due to the exploitation of some form of renewable energy such as solar, wind, biomass, geothermal, etc. Instead of injecting all excess power into the grid, after local load satisfaction, the end users control their energy injection into the electricity grid in order to reduce the distribution power losses and the total power demand to the mains. Our objective is

twofold: a) providing an insight into the *impact of communications* on control strategies, and b) assessing relevant performance metrics of control algorithms over *a set of comprehensive and realistic network topologies*. For the first objective, we focus on the communication infrastructure, devising suitable communication protocols and assessing the impact of routing of control messages and communication failures on the performance of selected algorithms (discussed shortly) for the distributed control of the DGs. As a reasonable starting point for an initial design of distributed control schemes, previous research has taken the communication infrastructure for granted [2], assuming fully connected communication networks and perfect (and real time) estimation of salient grid parameters. However, practical networks are subject to communication link failures, and grid features (e.g., line lengths or network topology) must be estimated through dedicated algorithms that rely on communication protocols. These algorithms are explicitly designed and evaluated in this chapter. For the second objective, we devise an accurate co-simulation (electricity grid, communication and control) framework that allows the assessment of relevant performance metrics in the presence of realistic network topologies and time varying power demand and energy inflow from solar sources. Our models are statistically generated so as to faithfully mimic the characteristics of real-world networks. This allows the evaluation of the performance metrics of interest over a large number of network realizations, as opposed to what is currently done in the Smart Grid literature, where a single network setup is often considered [3]. Our methodology makes it possible to control all network parameters, such as the number of nodes, the communication and electrical topologies, the impedance of network lines, the number of DGs and their renewable energy availability. Thus, we obtain accurate and statistically relevant results, characterizing the selected control algorithms in terms of convergence rate, resilience to communication failures, impact of the number of nodes with DG capabilities and of electrical parameters (such as line impedances).

Control techniques for DGs have been initially studied through centralized approaches [4]. Subsequently, concerns on the required computational power and on the required information about the grid status [20] have led to the study of distributed optimization techniques [5–7]. These distributed approaches still require some network knowledge, e.g., its topology to build clusters of generators and loads (to be used in the distributed control of the DGs), or its line impedances (to estimate power losses). Here, we consider four state-of-the-art distributed

optimization techniques, namely a) local control (LC) [5], b) current based surround control (CBSC) [6], c) voltage based surround control (VBSC) [6], and d) distributed optimal reactive power flow control (DORPF) [7]. For a *powerline communication* (PLC) communication infrastructure [21–23], we focus on its most critical issues for the selected optimization approaches, i.e., the communication requirements for *clustering*, practical communication protocols for the exchange of control signals, and the robustness of the communication and control solutions to link failures.

Hence, we present a thorough comparison of the four selected algorithms in terms of power loss reduction, reduction of the aggregate power demand to the distribution network, convergence rate and resilience to communication link failures. In order to obtain statistically relevant results, we use the smart grid topology generator proposed in [24] (see also [25]), which is based on the *small world* model of [8]. Hence, by spanning a wide range of networks we provide more extensive (and general) results with respect to those in the existing literature, which are obtained for example networks and, in turn, can not be easily extended to more general cases.

To summarize, the main contributions of this chapter are:

- a communication and coordination protocol designed to operate on residential smart grids in the presence of nodes with communication and metering capabilities. This protocol ensures that the channel access is contention free, the shortest path is chosen in multi-hop communication scenarios and only one node performs a control action at any given time;
- a new design of clustering for CBSC [6] able to further reduce the distribution power losses with respect to those obtained by the original protocol;
- a comparative study of the performance, in terms of distribution power loss reduction and convergence rate, of four selected control techniques for micro-grids [5–7], which are recent and promising distributed techniques for power loss minimization;
- a comparative study of the performance, in terms of resilience to link failures, convergence time, and impact of line impedance of the four selected control techniques over a relevant number of network topologies;

- a detailed assessment of the impact of realistic power demand and distributed generation from solar sources.

Our results reveal that the convergence and stability performance of the selected algorithms vary greatly. Typical network configurations provide convergence of the optimization algorithms within five to ten communication steps. When just 30% of the nodes are DGs, the aggregate power demand is roughly halved. Also, some of the considered approaches are quite robust against link failures as they still provide gains with respect to the localized solutions for failure rates as high as 50%.

The rest of this chapter is structured as follows. In Section 2.2 we introduce the electrical grid model (see Section 2.2.1) and we subsequently describe (see Sections 2.2.2, 2.2.5) the four distributed optimization techniques that we analyze in this work.

In Section 2.3 we discuss an original clustering technique to further enhance the performance of the selected schemes. In Section 2.4 we present the communication infrastructure, discussing the communication requirements of the distributed control algorithms and present a novel resilient token ring protocol, specifically designed for tree networks. In Section 2.5 we detail the simulation setup and we also describe the procedure used to generate the test networks for the simulations. In Section 2.6 we present and discuss the numerical results. Finally, in Section 2.7 we draw our final considerations.

2.2 Background

In this section, we specify the electrical model used to characterize the micro grid. In addition, four different distribution losses minimization techniques are reviewed. Note that the complexity of the algorithms is minimal, also considering the fact that they must be operated on rather relaxed time-scales with respect to the typical processing and communication speed provided by state-of-the-art controllers.

2.2.1 Grid Model

TokenRing, SurroundControl, dyngridmap, DORPF, DORPFConvergence

We consider a power micro grid modeled as a directed tree. The root of the tree represents the point of common coupling (PCC) and the other nodes represent loads, distributed

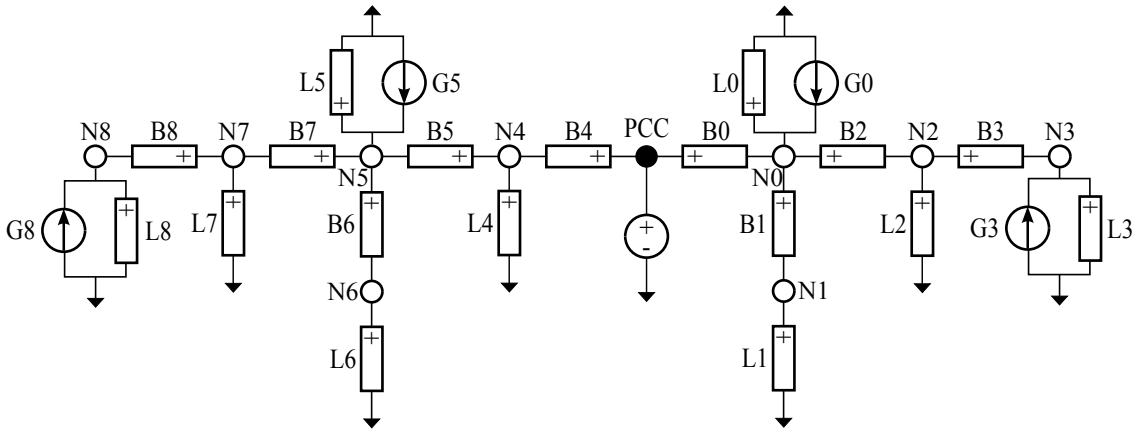


Figure 2.1. Power micro grid example.

Lengths [m]								
B0	B1	B2	B3	B4	B5	B6	B7	B8
100	23	45	26	35	67	32	12	66

Table 2.1. Branch Lengths of Fig. 2.1 in meters

generators (DGs) and connection points. Loads are represented either by constant complex impedances or by constant current sources, the PCC is modeled as a voltage generator setting the voltage reference for the entire grid, while DGs are modeled as current generators. This model has been widely considered in the literature, and in particular for power loss minimization algorithms [6,7,26–28]. Considering both constant-impedance and constant-current loads allows a large flexibility in the model.

Fig. 2.1 shows an example of a power grid. Node i is denoted by label N_i , load z and DG m are denoted respectively by L_z and G_m , and the impedance of branch j is denoted by B_j . Moreover, we assume that all the branches have constant impedance per unit length [6,7]. Note that each DG has an *associated* load. This models, for example, a house (i.e., an aggregated load fed by photovoltaic panels on the rooftop). DGs, besides feeding the respective *associated* loads, are operated in order to reduce the power distribution losses through suitable control algorithms. From Fig. 2.1 we see that two main portions of the grid can be identified: one connecting nodes PCC, N_0, \dots, N_3 (see right hand side of Fig. 2.1) and the other one connecting nodes N_4, \dots, N_8 (left hand side). These two portions are electrically independent and hence the DGs can be controlled separately. Generalizing this concept, if a power grid has $n \in \mathbb{N}$ branches exiting from the PCC node, then the corresponding n

sub-grids can be controlled in parallel. Note that Fig. 2.1 is only an example network, while the results presented in this chapter are obtained for a broad range of randomly generated networks according to suitable statistics, as described in Section 2.5.

The control algorithms considered in this chapter require a communication network among the controlled nodes, which is here assumed to be a powerline communication (PLC) infrastructure [23]. Nodes equipped with PLC transceivers are referred to as smart nodes (SNs) and suitable communication protocols are assumed to allow the communication between any pair of SNs, possibly by appropriate routing of messages through intermediate SNs, as we detail shortly. We assume that SNs are also capable of measuring instantaneous electrical quantities (i.e., voltage, current and power) absorbed (by the loads) or injected (by DGs).

2.2.2 Local Control

With the local control (LC) technique [5, 29], each DG provides the reactive power absorbed by its *associated* load. Assuming that only the reactive component injected by the inverter is controllable by the optimization process [5, 29], LC only uses local information available at the inverter, namely the active and reactive powers absorbed by the load connected to the same node. As an extension of LC, we consider the case where both the active and the reactive power generated by the DG are the powers absorbed by its *associated* load and we denote this control technique as extended LC (ELC).

2.2.3 Current Based Surround Control

According to the current based surround control (CBSC) [6], the grid is divided into clusters. Each cluster is composed of a pair of DGs (G_A and G_B) such that the path connecting the DGs only contains loads. Considering a single cluster, let $I_{G_A G_B}$ be the current injected by node G_A towards G_B and, conversely, refer to $I_{G_B G_A}$ as the current from G_B to G_A . The aim of CBSC is to find, for each cluster, the optimal currents $I_{G_A G_B}$ and $I_{G_B G_A}$, as we describe next. According to [6], fixing the initial DG, termed G_A , we find all the possible generators, termed G_h , that form a cluster with it, i.e., the portion of network between G_A and G_h only contains loads. $\mathcal{N}(G_A)$ is the set of indices of all generators G_h (including the PCC) found through this procedure. Hence, the optimal current injected by G_A that minimizes the

distribution losses is found as:

$$I_{G_A}^{\text{CBSC}} = \sum_{h \in \mathcal{N}(G_A)} I_{G_A G_h}^{\text{opt}}, \quad (2.1)$$

where:

$$I_{G_A G_h}^{\text{opt}} = \frac{1}{R_{G_A, G_h}} \sum_{i \in \mathcal{L}(G_A, G_h)} I_i R_{G_h, L_i} \quad (2.2)$$

and:

- R_{G_A, G_h} is the real part of the impedance Z_{G_A, G_h} of the lines connecting DGs G_A and G_h ;
- R_{G_h, L_i} is the real part of the (total) impedance Z_{G_h, L_i} of the lines connecting DG G_h and load L_i ;
- $\mathcal{L}(G_A, G_h)$ is the set of indices of the loads in cluster (G_A, G_h) ;
- I_i , $i \in \mathcal{L}(G_A, G_h)$ is the current absorbed by load L_i .

A variant of CBSC provides that only the reactive current injected by the DGs is controlled in order to reduce distribution losses, while the active current is regulated by other mechanisms, e.g., business contracts, or fully injected into the grid. In this case, the current injected by DG G_A is $0 + j\Im(I_{G_A}^{\text{CBSC}})$.

In order to operate CBSC, G_A first builds a list of the clusters it belongs to. This list contains the set $\mathcal{N}(G_A)$ and, $\forall h \in \mathcal{N}(G_A)$, the set $\mathcal{L}(G_A, G_h)$. Moreover, $\forall h \in \mathcal{N}(G_A)$ and $\forall i \in \mathcal{L}(G_A, G_h)$, G_A estimates the resistances R_{G_h, L_i} and R_{G_A, G_h} . Once the list of clusters has been set up, Algorithm 1 shows the actions taken by G_A in order to estimate and inject $I_{G_A}^{\text{CBSC}}$. Firstly G_A creates and sends to G_h a special packet denoted as DataGatheringPacket (see line 2). This packet is routed to its destination by the loads whose indices are in $\mathcal{L}(G_A, G_h)$. Once G_h receives the DataGatheringPacket, it sends back an acknowledgment which, according to line 3, is stored in the Ack variable. Each load involved in the routing process adds to the acknowledgment its own index and actual current demand. Function UpdateCluster(Ack) called in line 4 builds the vector CurrentDemand containing the current demands stored in the Ack variable. The elements of CurrentDemand are indexed using the indices of $\mathcal{L}(G_A, G_h)$, as shown in line 7. Once the optimum current has been computed, G_A injects I^{CBSC} as dictated by the function InjectCurrent in line 12.

Algorithm 1 CBSC Pseudocode**Require:** List of clusters

```

1: for all  $h \in \mathcal{N}(G_A)$  do
2:   SendDataGatheringPacket( $h$ )
3:   Ack  $\leftarrow$  WaitForGatheringAck()
4:   CurrentDemand  $\leftarrow$  UpdateCluster(Ack)
5:    $I \leftarrow 0$ 
6:   for all  $i \in \mathcal{L}(G_A, G_h)$  do
7:      $I_i \leftarrow$  CurrentDemand[ $i$ ]
8:      $I \leftarrow I + \frac{1}{R_{G_A, G_h}} I_i R_{G_h, L_i}$ 
9:   end for
10:   $I^{\text{CBSC}} \leftarrow I^{\text{CBSC}} + I$ 
11: end for
12: InjectCurrent( $I^{\text{CBSC}}$ )

```

Since the voltage reference imposed by the PCC stabilizes the grid, the current injected by the DGs does not influence the loads' total current demand. Hence CBSC requires that each DG runs Algorithm 1 only once in order to drive the grid's state towards the minimum distribution loss.

2.2.4 Voltage Based Surround Control

The voltage based surround control (VBSC) algorithm [6] aims at reducing the communication requirements with respect to CBSC. VBSC is based on the observation that losses are minimized when all DG voltages are as close as possible to the PCC voltage. Let U_{G_i} be the voltage of DG G_i and let G_A be the generator performing the control action, then the voltage that G_A should reach is:

$$U_{G_A}^{\text{opt}} = \frac{\sum_{h \in \mathcal{N}(G_A)} \frac{R_{G_A, G_h}}{|Z_{G_A, G_h}|^2} U_{G_h}}{\sum_{h \in \mathcal{N}(G_A)} \frac{R_{G_A, G_h}}{|Z_{G_A, G_h}|^2}}. \quad (2.3)$$

Given (2.3), the variation of the current injected by G_A is:

$$\Delta I_{G_A} = \frac{U_{G_A}^{\text{opt}} - U_{G_A}^0}{Z_{G_A}^{\text{eq}}}, \quad (2.4)$$

Algorithm 2 VBSC Pseudocode**Require:** List of neighbors $\mathcal{N}(G_A)$ **Require:** Impedance $Z_{G_A, G_h} \forall h \in \mathcal{N}(G_A)$

- 1: $I^{\text{VBSC}} \leftarrow$ current required by G_A 's load
- 2: $U_{G_A}^0 \leftarrow \text{GetMyVoltage}()$
- 3: $U_{num} \leftarrow 0$
- 4: $U_{den} \leftarrow 0$
- 5: **for all** $h \in \mathcal{N}(G_A)$ **do**
- 6: $\text{SendVoltageGatheringPacket}(h)$
- 7: $\text{Ack} \leftarrow \text{WaitForGatheringAck}()$
- 8: $U_{G_h} \leftarrow \text{UpdateNeighborVoltage}(\text{Ack})$
- 9: $U_{num} \leftarrow U_{num} + \frac{\text{real}(Z_{G_A, G_h})}{\text{abs}(Z_{G_A, G_h})^2} U_{G_h}$
- 10: $U_{den} \leftarrow U_{den} + \frac{\text{real}(Z_{G_A, G_h})}{\text{abs}(Z_{G_A, G_h})^2}$
- 11: **end for**
- 12: $Z_{G_A}^{eq} \leftarrow \text{MeasureEquivalentImpedance}()$
- 13: $U_{G_A}^{opt} \leftarrow \frac{U_{num}}{U_{den}}$
- 14: $I^{\text{VBSC}} \leftarrow I^{\text{VBSC}} + \frac{U_{G_A}^{opt} - U_{G_A}^0}{Z_{G_A}^{eq}}$
- 15: $\text{InjectCurrent}(I^{\text{VBSC}})$

where $U_{G_A}^0$ is the actual voltage of G_A and $Z_{G_A}^{eq}$ is the Thevenin impedance of the whole grid as seen by G_A . As for CBSC, if the active power is regulated by mechanisms other than power loss minimization, only the reactive current can be injected (see [6]). In this case, the variation of the current injected by G_A will be $0 + j\Im(\Delta I_{G_A})$.

Note that the update of the current according to (Eq. 2.4) changes the voltages of all the other nodes, including the value of U_{G_h} , $\forall h \in \mathcal{N}(G_A)$. Therefore, the optimum voltage is obtained through multiple control actions that gradually drive towards zero the absolute voltage difference between the DGs and the PCC. In order to operate VBSC, G_A must know the indices of the neighboring DGs ($\mathcal{N}(G_A)$) and the impedance of the path connecting G_A and G_h , $\forall h \in \mathcal{N}(G_A)$. Algorithm 2 shows the procedure that G_A executes every time it performs the control action. According to line 2, G_A firstly stores its voltage, then for each DG whose index is in $\mathcal{N}(G_A)$ it sends a `VoltageGatheringPacket` (see line 6). Once

G_h receives the VoltageGatheringPacket, it measures its instantaneous voltage and sends it back to G_A as an acknowledgment. Once the acknowledgment is received and the neighbor's voltage has been updated (see lines 7 and 8), G_A computes the numerator and denominator of (Eq. 2.3) corresponding to neighbor G_h . Once this operation has been performed for all neighboring DGs, the equivalent Thevenin impedance seen by G_A (see line 12) is measured and the current step is computed (see lines 13 and 14).

2.2.5 Distributed Optimal Reactive Power Flow Control

The distributed optimal reactive power flow control (DORPF) algorithm, proposed in [7], assumes that only the reactive power is controlled for distributed loss minimization. DORPF groups the DGs into (possibly overlapping) clusters and, for each cluster, a portion of the full optimization problem is solved using an approximate representation of the grid. DORPF is based on a distributed linearization of the optimal reactive power flow problem which is not reported here for the sake of conciseness (see [7]). The most effective clustering strategy appears to be that of [6], used also for CBSC.

2.3 Clustering

As discussed in the previous sections, the ability to build clusters of DGs is an essential feature of all the considered distributed algorithms. In this section we describe an online procedure to build clusters in a distributed fashion, by also describing a novel approach that extends the work of [6], and makes the optimization more robust to certain topologies. Here we do not build the neighbors table for each DG, but we rather assume that a neighbors table exists, which is a reasonable assumption due to the static nature of electrical grid topologies.

In [6] and [7] pairs of generators (including the PCC) such that the path connecting them only includes loads (and no generators) are defined as clusters. According to this definition, considering Fig. 2.1, four clusters can be identified: C1 with the PCC and G0; C2 with G0 and G3; C3 with the PCC and G5; C4 with G5 and G8.

For VBSC and DORPF only distributed generators are required to have metering and communication capabilities (in the following, nodes with these features will be referred to as smart nodes, SNs), hence the clustering process is reduced to a neighbor discovery process. The CBSC algorithm, on the contrary, requires detailed information about the loads (which

are SNs too) along each cluster's path. Let G_A be the DG performing the clustering procedure shown in Algorithm 3, then to obtain this information, once $\mathcal{N}(G_A)$ has been set up, G_A sends a special information gathering packet (called `BuildClusterPacket`, see line 2) to all DGs $G_h : h \in \mathcal{N}(G_A)$. Each load $L_k : k \in \mathcal{L}(G_A, G_h)$ appends to this packet its current demand, the impedance of the lines connecting it to G_A and its identifier k , and forwards it to the next node in the path between G_A and G_h . This procedure is repeated for all nodes in the path, until the `BuildClusterPacket` reaches the destination, as shown in Algorithm 4 (see lines 2, 3 and 4). G_h stores the received load current demands and impedances from G_A in the clusters table in the position corresponding to the sender's identifier and then sends back an acknowledgment which piggybacks the loads' current demands and line impedances. Once the clusters table has been set up, changes in loads current demands can be dynamically updated by the loads.

Since CBSC requires that all the nodes are SNs, the optimization process can be improved. The clustering obtained through Algorithms 3 and 4 considers only couples of neighboring DGs, thus leaving out of the optimization process portions of the network ending with a leaf node with a single connected load. In Fig. 2.1 two portions of the network are isolated: one made by edge B1 and node N1 and the other made by edge B6 and node N6. Since the leaf nodes have just one neighbor, they are able to determine their position in the network and hence to communicate to the nearest DG the presence of a portion of the network that would not be optimized using the standard clustering approach. Once a DG learns of such a portion of the network, which can be achieved through a simple probing procedure, it considers it as a special cluster and fully feeds such portion of the grid. This clustering procedure (called enhanced clustering, EC) enhances the performance of CBSC, with respect to the standard clustering scheme, when an appropriate number of DGs is accounted for. As an example, Fig. 2.2 shows the performance in terms of dissipated power when EC is used. For this plot, CBSC has been executed on the topology of Fig. 2.1 using the parameters reported in the same figure and a specific line impedance of $(0.8 + j0.8)10^{-6} \Omega/\text{m}$. In Section 2.6.5, EC is further investigated for a higher number of topologies and system parameters.

Algorithm 3 Basic Clustering Pseudocode, Generator side

Require: Nodes are synchronized to central clock

Require: List of neighboring generators N

```
1: for all Neighbor  $n$  in  $N$  do
2:   SendBuildClusterPacket(CurrentTime);
3:   WaitForAck();
4:   if ReceivedAck() then
5:      $D \leftarrow$  SetImpVector(Ack.Impedances);
6:      $PW \leftarrow$  Ack.CurrentDemand;
7:     UpdateClusterTable( $n$ ,  $D$ ,  $Pw$ );
8:   end if
9: end for
```

Algorithm 4 Basic Clustering Pseudocode, Load side

Require: Nodes are synchronized to central clock

```
1: if BuildClusterPacketRx() then
2:    $d \leftarrow$  EstimateImpFromSource();
3:   UpdatePacket(GetCurrentDemand(),  $d$ );
4:   SendPacket(Packet);
5: end if
```

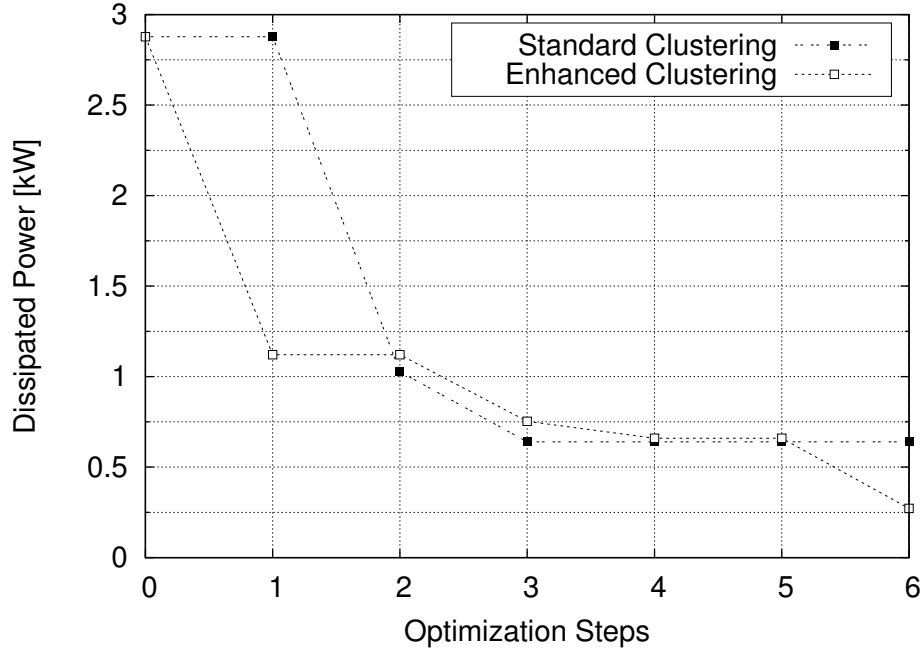


Figure 2.2. Dissipated power vs optimization steps for CBSC for standard clustering and the enhanced clustering technique. Active and reactive current injection.

2.4 Communication Procedures

In this Section we first analyze the communication requirements of LC, CBSC, VBSC and DOPRF and then we propose a token ring protocol tailored for the distributed solution and for tree networks.

2.4.1 Communication Infrastructure and Requirements

The control algorithms considered in this chapter require a communication network among the controlled nodes, which is here assumed to be a powerline communication (PLC) infrastructure. SNs are equipped with PLC transceivers and suitable communication protocols are assumed to enable the communication between any pair of SNs, possibly by appropriate routing of messages through intermediate SNs, as we detail shortly. We assume that SNs are also capable of measuring instantaneous electrical quantities (i.e., voltage, current and power) absorbed (by the loads) or injected (by DGs).

The communication requirements for the distributed control algorithms of Section 2.2 are:

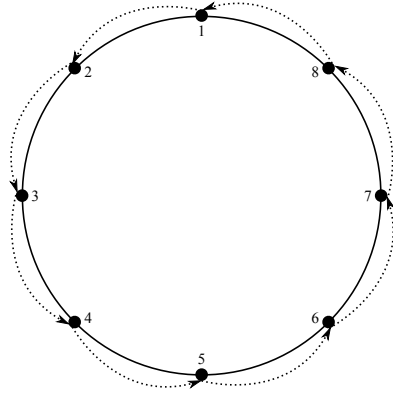


Figure 2.3. *Token ring network example. The arrows indicate the token's path.*

2.4.1.0.1 LC and ELC these schemes only use local information and, in turn, do not require any communication among SNs.

2.4.1.0.2 CBSC for this algorithm, very fast convergence rates are obtained at the cost of requiring that each node is a SN, which means that each node must have communication and metering capabilities (to measure or estimate the quantities required by the scheme). This may be difficult to achieve in practice, especially when retrofitting existing grids that use old equipment.

2.4.1.0.3 VBSC this scheme does not collect any information about the loads and requires that only the DGs are SNs. This considerably reduces the communication requirements of VBSC with respect to CBSC. The reduced amount of information needed to perform the optimization makes the implementation of this technique easier, while yielding a slower convergence rate.

2.4.1.0.4 DORPF for this algorithm, the DGs in a cluster are required to estimate the PCC's voltage, the line impedance, and the neighbor's voltage. In order to acquire this information, only DGs need to be SNs and, thus, the communication requirements of DORPF are similar to those of VBSC.

An update in the current injected by the DGs alters the operating points of all other grid nodes. To ensure convergence, an iterative approach to update the injected currents has been proposed in [26], which uses a round robin scheme whereby *token-passing* is utilized to arbitrate control among the nodes.

To make sure that, at any one time, the token is owned by a single node (which performs the control actions as dictated by the selected algorithm), a token ring communication protocol is exploited. The token ring protocol (known as IEEE 802.5) has originally been developed for networks whose nodes are connected in a ring fashion. Hence, a special packet called *token* is circulated in the network and node n receiving the token has the right to transmit packets while all the other nodes remain silent, unless they receive a specific request from node n . Once the token's owner has completed its operations, it sends the token to the next neighbor, selected according to a certain schedule. Fig. 2.3 shows an example of a token ring network. Solid lines connecting the nodes numbered from 1 to 8 represent the actual communication links between them, while the counterclockwise pointed lines represent the token's path in the network.

2.4.2 Token Ring Protocol for Tree Networks

In this section, we propose a failure resilient token ring protocol for tree networks. This protocol is then used in conjunction with the clustering algorithm of Section 2.3, obtaining the final distributed algorithms that will be evaluated in Section 2.6.

To adapt the standard token ring protocol to the tree topology treated in this work, a new token's owner selection procedure is devised. Let $N > 1$ be the number of SNs. Let the SNs be identified by the unique identifiers $0, \dots, N - 1$ and let the current token's owner identifier be $i \in \mathbb{N}$ with $i < N$, then the next token's owner is obtained as $j = (i + 1) \bmod N$. This owner selection rule ensures that when SN i releases the token, all the other SNs will receive it before i owns it again, thus promoting fairness in the communication process.

Fig. 2.4 shows an example of the token path on the power grid of Fig. 2.1 assuming that all nodes are SNs (i.e., $N = 9$). Nodes receive the token on the basis of their identifiers (on the contrary, in regular token ring networks the token exchange is based on the actual physical position of the nodes). It is also worth noting that, by correctly setting the nodes' identifiers, the token's path can be forced into a depth first path search on the tree, as illustrated in Fig. 2.4. Note that this minimizes the number of jumps of the token between non-adjacent nodes.

Lost Token Recovery The circulating token can be lost for various reasons such as, for example, external electromagnetic interference, communication link and device failures on the

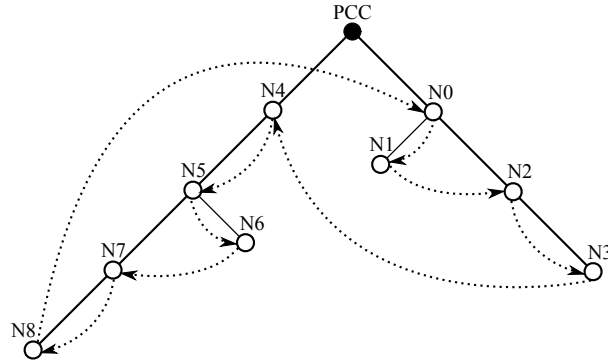


Figure 2.4. Example of the token's path in the communication network associated to the power grid of Fig. 2.1.

token's path. In order to recover from these events, the token reception must be acknowledged to the sender. Node i releasing the token remains the owner until it successfully receives the acknowledgment sent by node j . If after a timeout time T (also dependent on the network size and on the transmission rate) no acknowledgment is received, then the token exchange procedure is repeated until either the token reception is acknowledged or the maximum number of transmission attempts is exceeded. In the latter case, we skip the next node in the path and start a new exchange procedure with the following node $j' = (j + 1) \bmod N$. If the token is correctly received by node j , but the acknowledgment is lost, the aforementioned procedure is performed as for the lost token case. After the reception of the new token, node j will send back an acknowledgment and discard the newly received token.

Handling Disconnected Portions of the Network When a portion of the network gets disconnected from a communication perspective, the nodes therein first have to discover that such an event has occurred. To this end, each SN utilizes the following approach. A timeout timer is reset at every node, every time the token is received (the timeout period must be the same for all the SNs and must be dispatched by a coordinator). If the timeout timer of a given SN counts down to zero, then the SN promotes itself as the new coordinator for the disconnected portion of the network and from a communication standpoint starts acting as the coordinator. It performs a new neighbor discovery, and each node involved in such process updates its routing tables according to the new information it receives. Once this process is completed, the obtained subtree will be optimized independently, using as a reference voltage the PCC's voltage estimated (or measured) by the new coordinator before the failure.

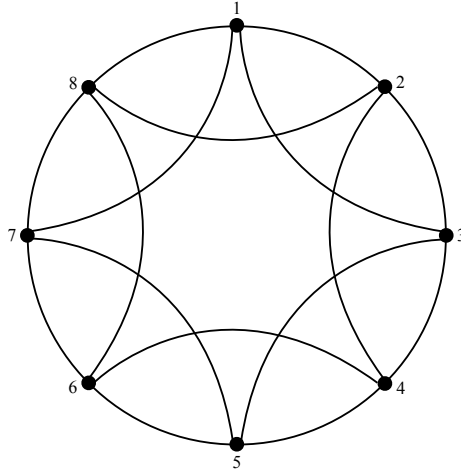


Figure 2.5. *Regular ring lattice with eight nodes.*

2.5 Simulation setup

Numerical results (obtained through the use of our simulation framework, implemented in Matlab) comparing the performance of the considered algorithms have been obtained over a large set of randomly generated grids. Instead of relying on standard test feeders as proposed in [30] or on a single case study as in [3], we have adopted the approach of [25]. Using the generator from [24], we generated more than a thousand power distribution grids and averaged the numerical results obtained by testing the optimization techniques on every single grid. The impact of communication and clustering protocols has also been assessed.

After assessing the performance of the selected algorithms in the ideal case (i.e., in the case in which all the DGs are able to inject the optimal power), we assessed the performance of the selected algorithms (in terms of power loss reduction) in the case in which the available power is limited to a 28 Ah battery installed at each DG and charged by photovoltaic panels, and the power demand from the loads is based on a statistical model derived from real world data.

Random Grid Generation For a meaningful performance evaluation, we have considered a large number of networks, which have been obtained using a network generator that accounts for the theoretical and experimental results of [8] and has been adopted for topology design [24] and performance assessment of smart grids [25]. According to this approach, power micro grids are modeled as directed graphs (with the orientation of the edges determined by the direction of the active current). These graphs are included in the class of small-world

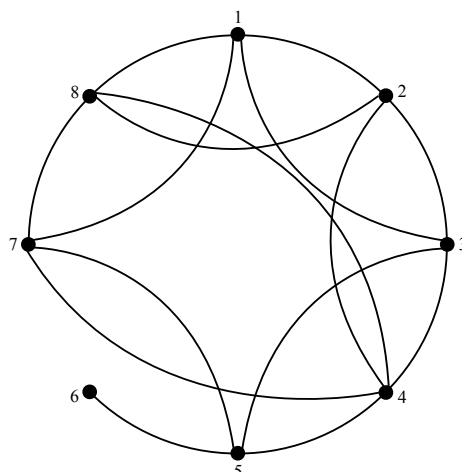


Figure 2.6. *Small world graph obtained from Fig. 2.5.*

networks which are connected graphs characterized by a large number of vertices with sparse connections and fill the gap between completely random graphs and regular graphs. With this approach, we can generate numerous synthetic networks by fixing their relevant parameters such as the number of nodes, the number of generators, the depth of the tree, etc., by making sure that the generated networks have statistical properties resembling those of real power grids. In order to build a small-world network we start from a ring lattice. Then for each edge e a so called rewiring procedure is performed: one of its endpoints is replaced with probability p (called rewiring probability) by another node, chosen uniformly at random among all other nodes.

Tree networks with n nodes and $n - 1$ branches and shaped according to a given rewiring probability are generated. Branch lengths are then generated according to an exponential distribution with tunable mean. The number of nodes, the rewiring probability and the mean of the exponential distribution generating the branch lengths are user defined parameters. The rewiring probability determines the shape of the generated tree: when this probability is zero, the generated tree has exactly 1 leaf, when this probability is one, the generated tree has exactly $n - 1$ leaves. Fig. 2.5 shows an example of regular ring lattice with 8 nodes. Instead, Fig. 2.6 shows a small-world graph generated from the regular lattice of Fig. 2.5 when edges e_a and e_b connecting nodes (6, 7) and (4, 6) are rewired to links (4, 7) and (4, 8), respectively.

Electrical Parameters Setup We assume that the generated grids operate in steady state and that they are single phased electrical networks whose distribution lines have a constant

specific impedance of $(0.08 + j0.08)10^{-6} \Omega/\text{m}$. The phase voltage at the PCC is set at 230 V and the voltage drops along the distribution lines are neglected in determining the loads' instantaneous power demand, as assumed in [6]. DGs with associated loads automatically feed them with the required current. Moreover, we do not assume any limitations on the maximum current that can be injected by the DGs.

Communication Assumptions From a communication standpoint, a first assumption is that a routing protocol connecting each pair of SNs in the grid exists. A second assumption is that no packet is lost or corrupted along a communication path unless at least one of the links in the path is broken (which is accounted for using an independent and identically distributed process with a certain probability). In order to obtain statistically relevant results, the optimization methods treated in Section 2.2 and the communication procedures treated in Section 2.3 and Section 2.4 have been tested over a large number of grids and the corresponding communication network conditions. In particular, we have considered networks with 30 nodes, a specific line impedance of $(0.08 + j0.08)10^{-6} \Omega/\text{m}$, average line length of 30 m, and a rewiring probability of 0.5.

Renewable source model energy traces for photovoltaic (PV) sources have been obtained using the SolartStat tool [9]. In detail, energy generation statistics (cumulative distribution functions, cdf) have been generated for each month of the year and for each hour of the day for the city of Los Angeles. For the solar modules, we have considered the Panasonic N235B solar panel technology, accounting for a surface of about 10 m^2 (delivering a nominal power of about 4 kW), which represents a reasonable size for residential users. The solar modules have a tilt angle of 45° and an azimuthal displacement, with respect to the real South, of 30° . The statistics generated for this setup have been utilized to generate the current harvested from each solar module with a time granularity (time slot) of 1 minute.

Modeling power demand an accurate statistical model has been derived from the household electric power consumption data set of [31]. This database contains fine-grained (one per minute) measurements of active and reactive power demands from residential structures, collected between December 2006 and November 2010. Following the approach of [9], we have obtained power demand statistics for each month of the year, day of the week and hour of the

day. A power demand process is then updated for each end-user every minute according to these statistics. Note that although the same cdf is considered for different end-users within the same time slot, their demands are independently drawn from this cdf.

2.6 Numerical Results

In this section, we show the numerical results obtained considering the simulation setup described in Section 2.5.

2.6.1 Dissipated Power

Figs. 2.7 and 2.8 show the average dissipated power over one hundred random network realizations where both active and reactive current injection is allowed and where only reactive current injection is allowed, respectively. For each network, 30% of the nodes are DGs. For all algorithms, the starting point of the iterative optimization procedure provides that the DGs do not inject any current.

When both active and reactive current is injected, only ELC, CBSC and VBSC are considered. A first important result is that CBSC and VBSC achieve a considerably lower power distribution loss than ELC, due to their exploitation of communication capabilities. With reference to Fig. 2.7, while ELC reduces the power loss by more than 4 kW with respect to the starting point, CBSC further reduces losses by over 2 kW in less than ten iterations. VBSC exhibits a much slower convergence rate while reducing power loss by nearly 1 kW with respect to ELC (at convergence, not shown in the plot, see also Fig. 2.9 for the convergence rate of VBSC).

When only reactive current is controlled (Fig. 2.8), LC reduces the power losses by nearly 1.75 kW with respect to the starting point. It is worth noting that all the distributed algorithms exploiting communication capabilities still allow the reduction of the power loss by (up to) 0.5 kW with respect to ELC. Overall, CBSC outperforms all other approaches, relying on a complete knowledge of the clusters, since each DG has a complete knowledge of the branches connecting it to other neighboring DGs, and hence can compute the exact amount of power that is needed in each branch to minimize the loss.

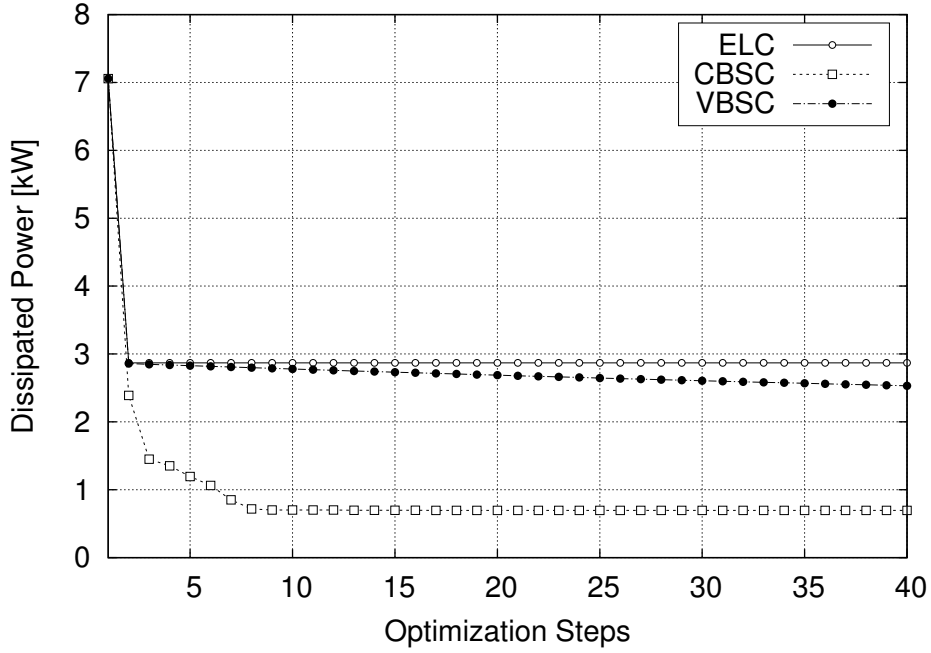


Figure 2.7. Average dissipated power vs optimization steps for ELC, CBSC and VBSC. 30% of nodes are DGs. Active and reactive current injections.

2.6.2 Convergence Time

As shown in Figs. 2.7 and 2.8, all algorithms converge to a minimum dissipated power after a certain number of iterations. In Fig. 2.9, we show the average number of control steps (over the network realizations) that are required, for each algorithm, so that its performance falls within 5% of the associated minimum power loss. This number of steps is plotted against the dissipated power by varying, as a free parameter, the percentage of DGs from 10% to 95% of the nodes.

A first important result is that CBSC, VBSC and DORPF guarantee that the dissipated power is comparable to that of LC even when only 10% of the nodes are DGs. Moreover, the aforementioned algorithms achieve a power loss very close to zero when the DGs are about 70% of the nodes (or more). CBSC, once again, exhibits the fastest convergence rate and the lowest power loss at each point. It is remarkable that this algorithm always converges within a few (at most twenty for the considered networks) iterations and that this number weakly depends on the percentage of DGs.

When only the DGs are SNs, only DORPF and VBSC can be applied, as explained in Section 2.4.1. In this case, we note that DORPF ensures the best convergence time for the

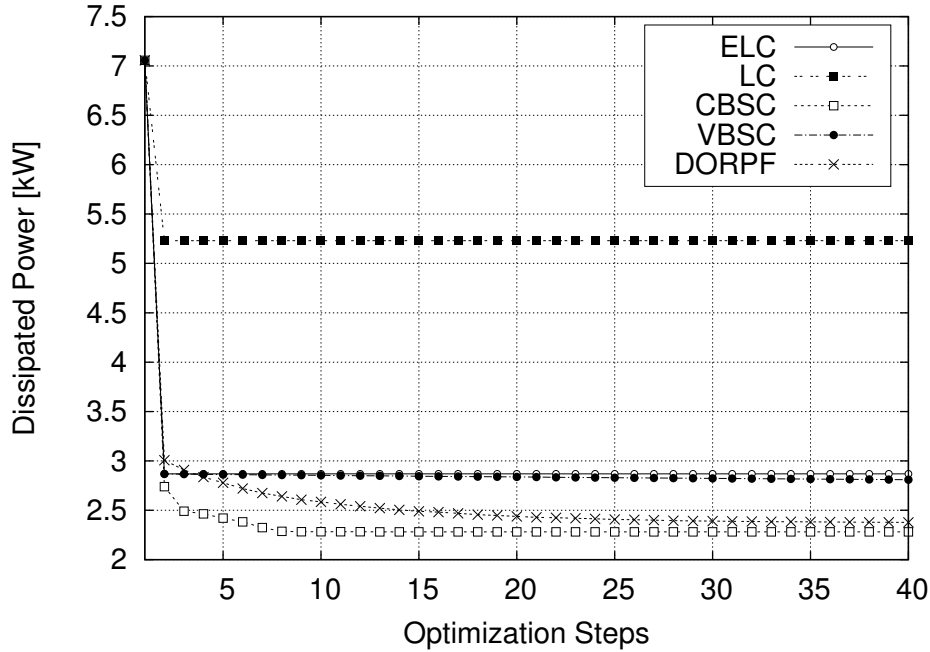


Figure 2.8. Average dissipated power vs optimization steps for LC, ELC, CBSC, VBSC and DORPF. 30% of nodes are DGs. Reactive current injection.

same dissipated power performance. Nevertheless, from Fig. 2.10, we note that when the specific line impedance grows, the performance gap between DORPF and VBSC increases, leading to a higher dissipated power, up to 25%, for DORPF with respect to VBSC for a specific line impedance of $(0.08 + j0.08)10^{-3} \Omega/\text{m}$. Thus, DORPF appears to be less robust for increasing line impedance, and this fact should be carefully evaluated in practical implementations of this algorithm. In particular, when the specific line impedance is well known and ensures that the voltage drops along the power lines are less than 3% of the PCC's voltage, DORPF can be successfully used (see [28]). On the contrary, when the specific line impedance is not known in advance or the voltage drops are not within the 3% range (as it may occur in rural or isolated areas), optimization should be performed through VBSC since this technique exhibits a higher robustness with respect to the grid parameters.

2.6.3 Resilience to Link Failures

In the two previous sections we assumed a communication network with error free links. In this section, instead, the algorithms' resilience to link failures is considered. In the following

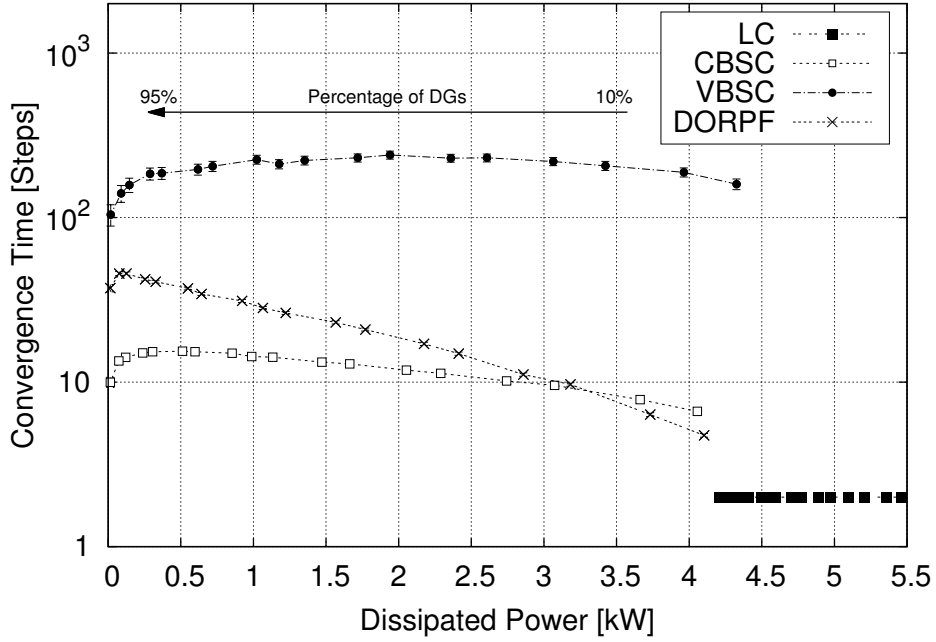


Figure 2.9. Average convergence time vs dissipated power for ELC, CBSC, VBSC and DORPF. DGs are from 10% to 95% of nodes. Reactive current injection.

results, broken links are chosen uniformly at random among all links according to a given percentage.

Fig. 2.11 shows the average dissipated power as a function of the percentage of broken links; we note that despite high percentages of broken links, CBSC and VBSC achieve a lower dissipated power than ELC. On the contrary, when the percentage of broken links exceeds 25%, DORPF performs worse than ELC. We recall that, when only DGs are SNs only VBSC and DORPF can be used. VBSC exhibits a considerably higher degree of resilience to link failures with respect to DORPF. The higher resilience to link failures, together with the independence from the specific line impedance discussed in the previous section, make VBSC the best algorithm when scarce information is available about the grid or when link failures are frequent.

2.6.4 PCC Workload

Fig. 2.12 shows the average PCC's workload as a function of the percentage of DGs in the grid. A first noticeable result is that, for at least 10% of DGs, at least 40 kW are saved when using LC. When ELC is used, at least 60 kW can be saved. Distributed optimization

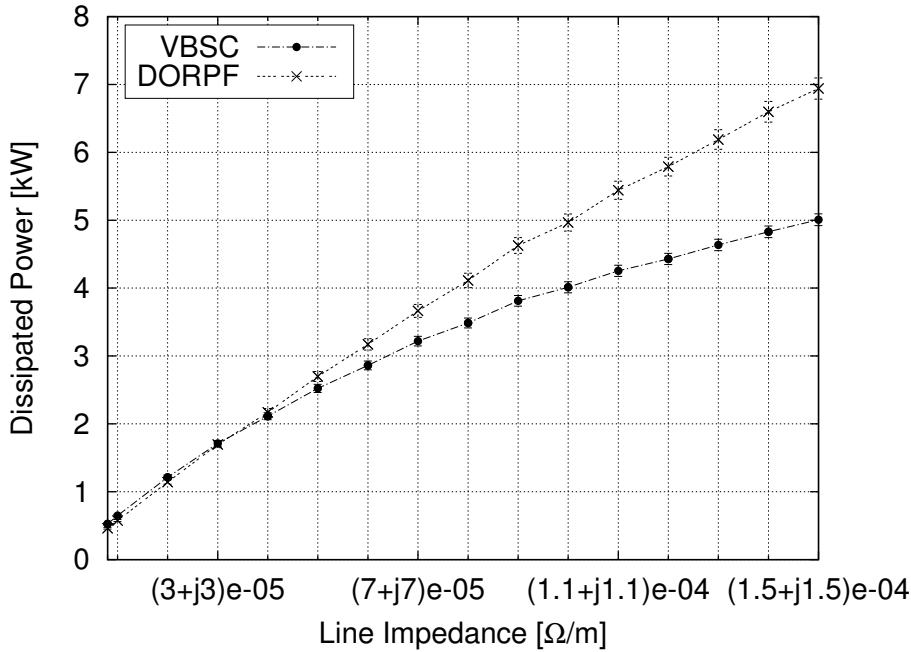


Figure 2.10. Average dissipated power vs specific line impedance for VBSC and DORPF. 15 nodes, 0.5 rewiring probability, 5 nodes are DGs. Reactive current injection.

techniques appear to be useful when the number of DGs is between 10% and 50% of the total number of nodes, regardless of the actual size of the grid. In this range, the distributed optimization techniques allow to save up to 15 kW with respect to ELC. When, instead, more than 50% of the nodes are DGs, the gain in terms of power loss with respect to the LC technique may not be worth the communication infrastructure needed by the distributed optimization techniques.

Fig. 2.13 shows the average PCC workload as a function of the percentage of broken links in the communication network. We note that when the percentage of broken links is in the range of 10%-50%, CBSC and VBSC significantly outperform the localized approach (ELC) which, as expected, is insensitive to link failures. However, when the percentage of broken links exceeds 50% of the total number of links, the gain with respect to ELC is modest and may not motivate a distributed approach. Thus, when link failures can be detected, a good option could be that of switching between distributed control (CBSC or VBSC) and ELC as a function of the percentage of broken links in the network.

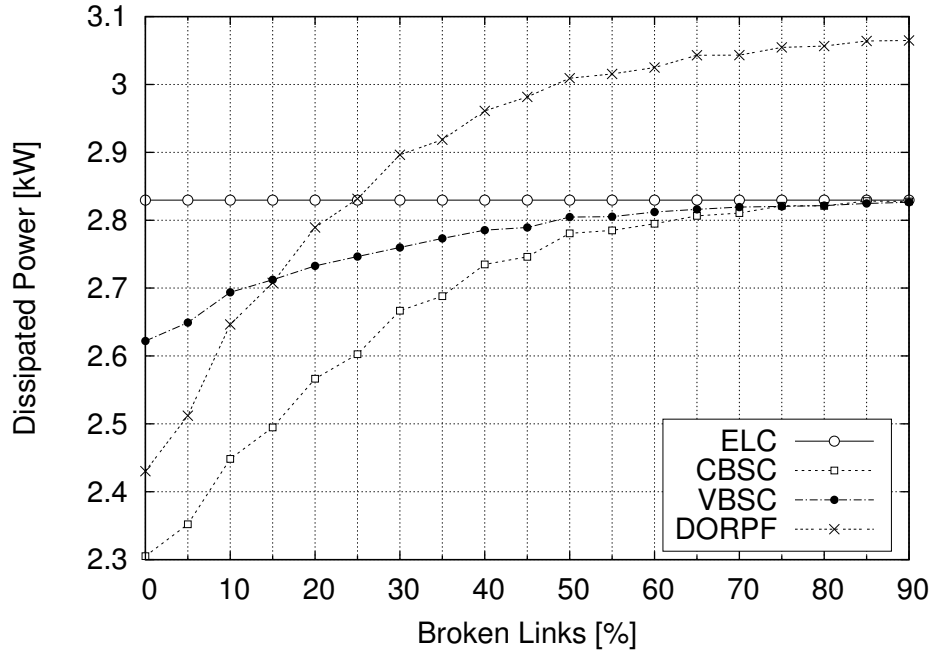


Figure 2.11. Average dissipated power vs the percentage of broken links for ELC, CBSC, VBSC and DORPF. 30 nodes, 9 nodes are DGs. Reactive current injection.

2.6.5 Impact of the EC Procedure

In Fig. 2.14 we show the average relative gain (expressed as a percentage), in terms of PCC workload reduction, obtained using CBSC together with EC as opposed to using CBSC in conjunction with the standard clustering technique of Fig. 2.12. In this plot we vary the percentage of DG nodes from 10% to 95%. Notably, when DGs are between 50% and 95% of the nodes, the gain ranges from 15% to 85%. However, in practice having more than 75% of the nodes that are DGs may be unlikely and, in addition, although the gain in this case is high in terms of percentage, the PCC workload reduction in terms of absolute value is rather small (see Fig. 2.12).

On the one hand, when DGs are between 40% and 75% of the nodes, the PCC workload reduction ranges between 3 and 8 kW. Note also that when the percentage of DGs is between 20% and 35%, standard clustering performs slightly better than EC. The highest gap in this case is obtained when 30% of the nodes are DGs, where standard clustering provides a 5% gain (i.e., about 3 kW) with respect to EC. This is due to the fact that when the percentage of DGs is small, the special clusters optimized by EC have bigger length on average with respect to the case where the percentage of DGs is higher (i.e., above 35%). Hence, a higher fraction

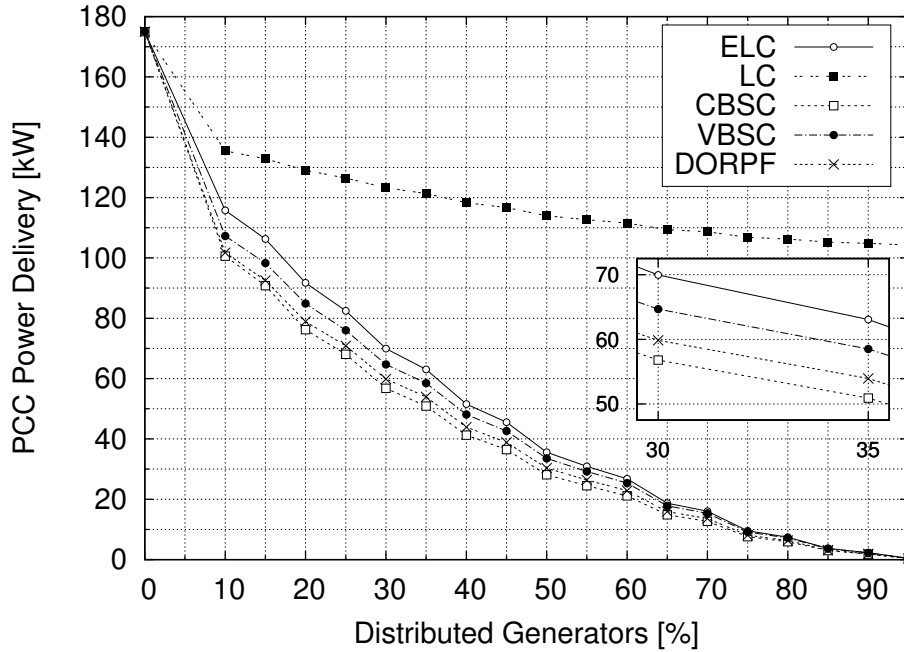


Figure 2.12. Average PCC workload vs the percentage of DGs over the total number of $N_{\text{tot}} = 30$ nodes for LC, ELC, CBSC, VBSC and DORPF. The number of DGs for each simulation run is obtained as $N = \lceil N_{\text{tot}}\xi \rceil$, where ξ is the percentage of DGs in the x-axis. Reactive current injection.

of the power fed by the DGs to the leaf nodes is wasted along the distribution lines. The PCC tries to compensate for the power dissipated on these branches injecting more reactive power and, in turn, the total power loss slightly grows.

2.6.6 Performance Assessment with Time Varying PV Generation and Power Demand

In this subsection, the performance of CBSC, VBSC and DOPRF is assessed when these operate in conjunction with time varying (and realistic) photovoltaic power generation and power demand, as described in Section 2.5. For the location we selected the city of Los Angeles (CA, US). All quantities in the simulations (energy generation, demand, control actions) evolve with a time granularity of 1 minute. With the described setup, the performance of CBSC, VBSC and DORPF in terms of PCC power delivery, dissipated power and reduction in power losses turned out to be very close. For this reason, the performance of these schemes is shown through a single line, referred to in the following plots as “Optimized”.

Figs. 2.15 and 2.16 show the power delivered by the PCC during a typical day of April

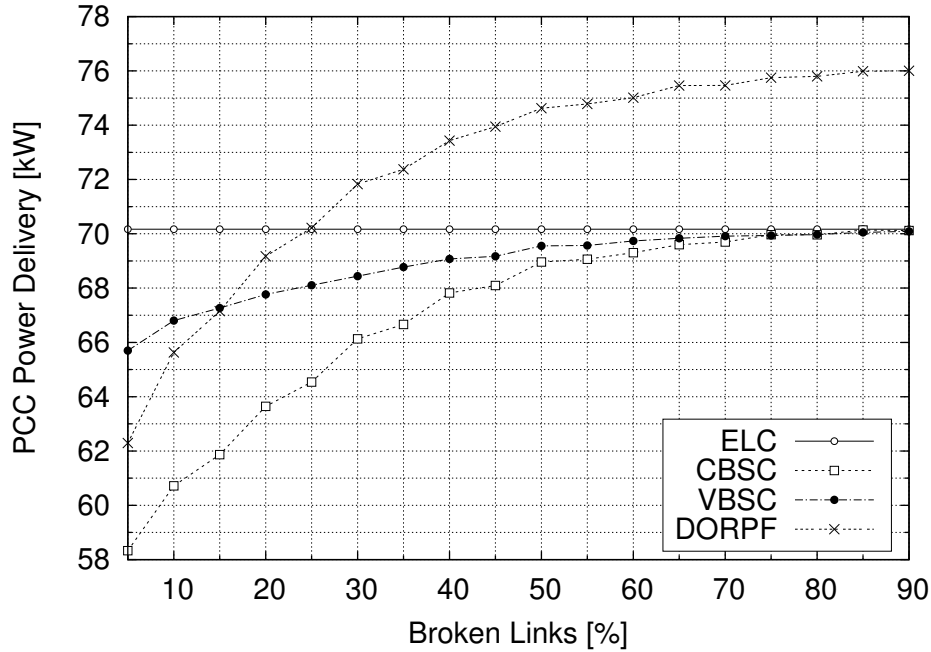


Figure 2.13. Average PCC workload vs the percentage of broken links for ELC, CBSC, VBSC and DORPF. 30 nodes, 9 nodes are DGs. Reactive current injection.

and December, respectively. The simulated traces start at 6 am and last for 24 hours. Each DG has a solar plant featuring a 28 Ah energy buffer (assumed full when simulations start) and a 4 kW-rated solar module, see Section 2.5.

Analyzing Fig. 2.15, it can be noticed that the optimized system provides improvements for roughly 20 hours, halving the PCC workload (“power demand” in the figure) in the best cases. Similar results are obtained when simulating a typical day of December, as shown in Fig. 2.16. However, in this case the period of time during which the optimized approach is effective shortens to about 14 hours. This result is expected and is due to the reduced light time experienced during the winter months in the northern hemisphere that, in turn, results in a diminished current inflow in the distributed energy buffers.

Fig. 2.17 shows the amount of power being dissipated along the distribution lines during a typical day of April. We observe that the power distribution losses are also halved by the optimization algorithms and that, during daytime, there are periods of time where the current generated by the PV plants exceeds that drained from the energy buffers. In these cases, the DGs effectively contribute to the grid’s electrical efficiency, while also being able to recharge their local batteries.

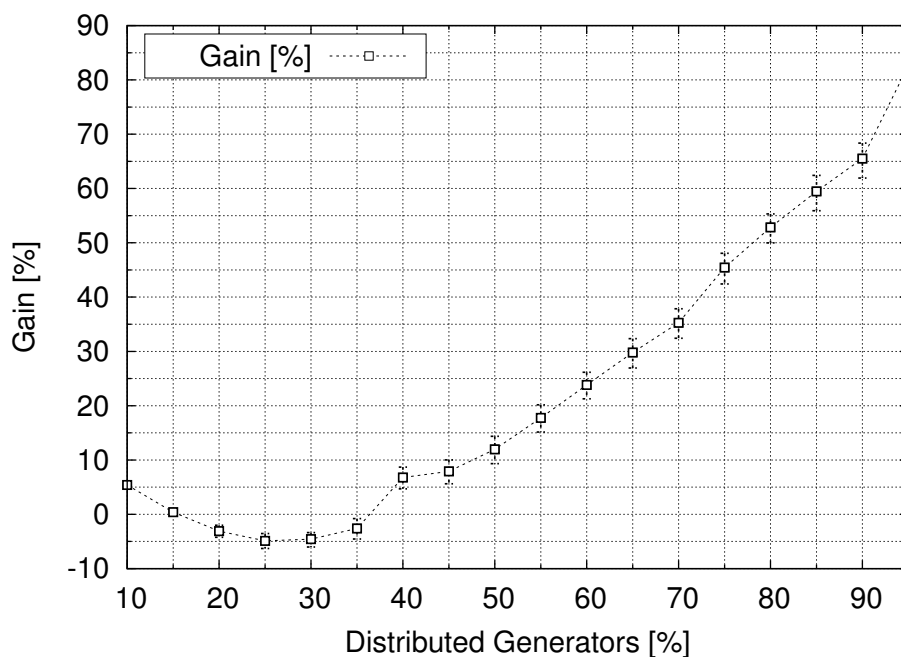


Figure 2.14. Average PCC power delivery gain obtained using EC vs the percentage of DGs. Reactive current injection.

Fig. 2.18 shows the average gain in terms of reduction of power losses, computed for a typical day of April. This gain increases linearly with the percentage of DGs in the grid. Also, even in the case where 100% of the nodes are DGs (not shown in the plot), the gain remains considerably smaller than 100%. In the considered scenario, this occurs as the distributed energy storage is not capable of sustaining the associated loads for a full day and this has to be compensated for through the injection of a certain amount of power by the PCC. Increasing the capacity of the local energy buffers would ameliorate this, but then the battery would be sizable and too expensive for its adoption by residential users.

We have also experimented with the network size by increasing it from 10 to 100 nodes. Our results reveal that the performance (normalized gain in terms of distribution losses and dissipated power) of the selected optimization techniques is invariant to the grid size and, in turn, the optimized approach can be effectively applied to a wide range of scenarios. These plots are not shown here due to space limitations.

Tab. 2.2 shows the average maximum gain G_m (reduction of distribution losses) and the number of hours in a day T_m during which the optimized solution provides a positive gain in terms of reduction of power losses, i.e., the DGs inject a non-zero energy flow. m indicates

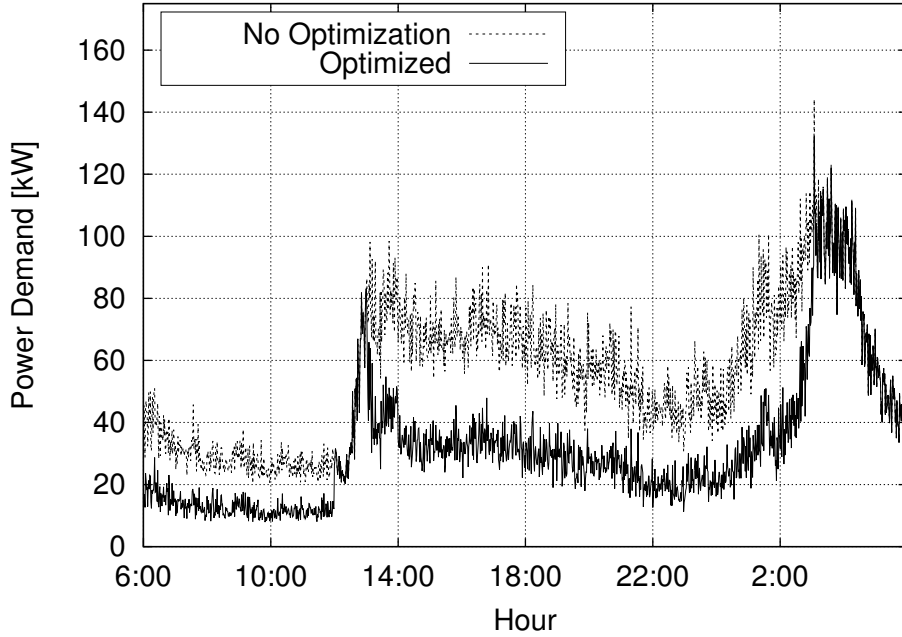


Figure 2.15. *PCC power delivery vs time of a typical day of April. 50% of nodes are DGs. Reactive current injection.*

the month, i.e., April or December. We observe that, while the maximum gain steadily increases when increasing the percentage of DGs, the increase in T_m becomes marginal as the DG percentage grows beyond 30%. In this case, due to the abundance of DGs sharing the control action, the percentage of energy that each of them is required to inject into the grid becomes a small fraction of that entering the node during the day. Thus, T_m is dominated by the energy inflow (meteorological conditions, size and type of harvester), by the end user's battery capacity and its power demand (which governs the amount of energy that is drained from the local battery for self-powering).

2.6.7 Lessons Learned

Our performance evaluation reveals the impact of communications on the selected optimization techniques over a large number of power grid topologies (generated so as to resemble actual power grids structures) and sheds some light on the effectiveness of the selected schemes. Specifically, when detailed information about the grid state can be retrieved, the CBSC algorithm gives the best results in terms of power loss minimization, reduction in the aggregate power demand, and resilience to communication link failures. When, instead, only

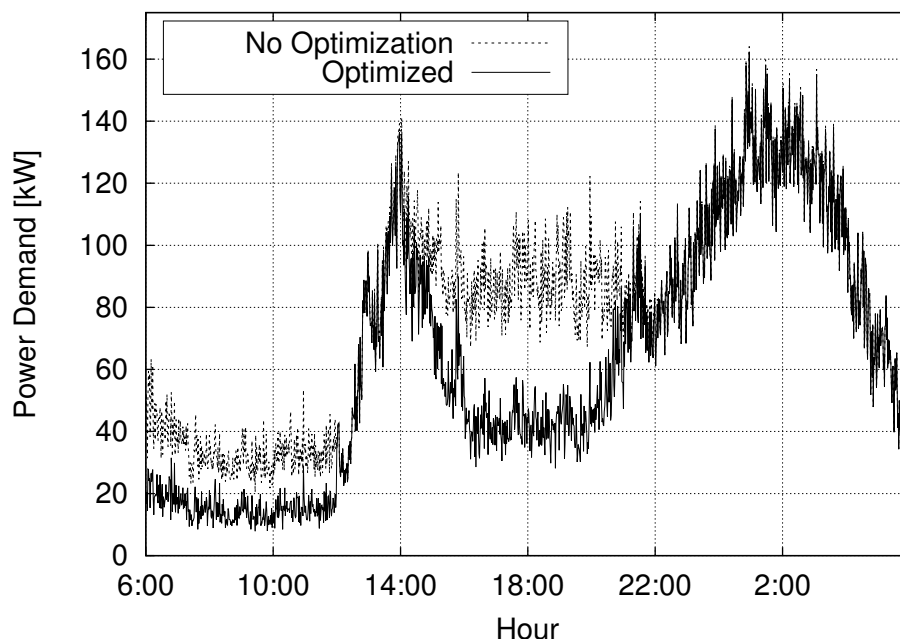


Figure 2.16. *PCC power delivery vs time of a typical day of December. 50% of nodes are DGs. Reactive current injection.*

partial information can be retrieved (i.e., when each DG can only collect information about its neighboring DGs) the optimization technique should be carefully selected. When the specific line impedance is small and link failures are rare events, the DORPF algorithm ensures the fastest convergence rate. On the other hand, when no exact information about the specific line impedance is available or link failures happen frequently, VBSC, despite exhibiting a slow convergence rate, is the most robust solution. CBSC, VBSC and DORPF exhibit a slightly oscillatory behavior with respect to the dissipated power when the percentage of DGs or the percentage of broken communication links varies. This is an intrinsic characteristic of the distributed optimization techniques and does not depend on the number of samples collected to obtain the presented numerical results.

Notably, the algorithms' performance, in terms of convergence time, resilience to link failures and specific line impedance, varies widely. However, configurations exist for which convergence is achieved within only ten communication steps and the aggregate power demand of the micro-grid can be roughly halved even when just 30% of the nodes have communication and control capabilities.

Finally, results in the presence of realistic power demand and distributed generation from

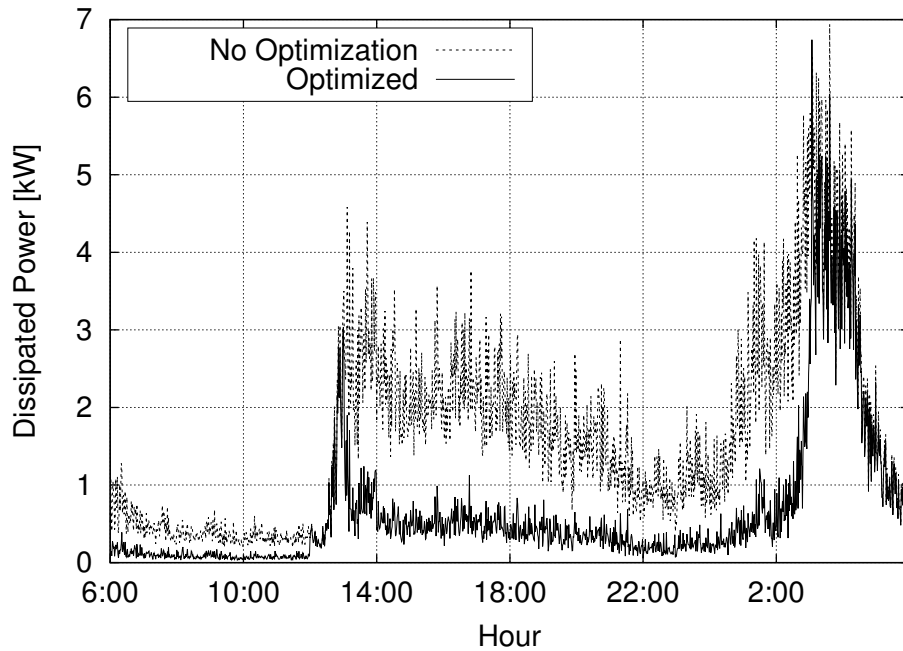


Figure 2.17. *Dissipated power vs time of a typical day of April. 50% of nodes are DGs. Reactive current injection.*

solar sources reveal that the optimized techniques can be quite beneficial for prolonged periods of time during typical days of April (considered here as the best case) and December (worst case). That is, distribution losses will be halved in the best cases and the same will occur for the power demand from the PCC. These results encourage further research, such as the adaptive temporal management of the energy reserve in the distributed buffers, to adapt the algorithms' behavior to the power demand profile or other quality of service criteria.

2.7 Conclusions

In this chapter, we have considered the design of a communication infrastructure to be exploited by power loss minimization schemes in micro-grids, which are assessed using a novel co-simulation methodology. Clustering and communication protocols have been designed to fit at best the considered technical scenario. Our co-simulation approach made it possible to obtain statistically relevant measures for the various optimization schemes, highlighting the respective strengths and weaknesses in the presence of realistic communication and electricity grid topologies, power demand and energy inflow from photovoltaic sources. We stress that

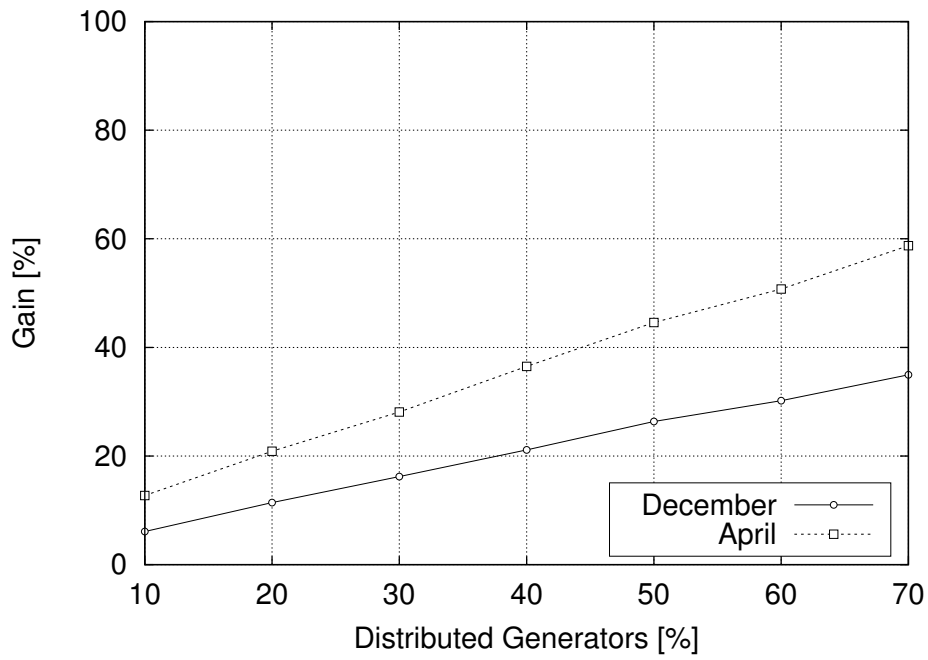


Figure 2.18. Average gain in power dissipation reduction vs percentage of DGs for a typical day of April. Reactive current injection.

the evaluation framework presented here can promptly be extended to future optimization techniques and different performance objectives.

Table 2.2. *Effectiveness of optimal algorithms vs percentage of DGs. Maximum gains in terms of reduction of power losses and number of hours in a day during which the optimal distributed power injection is effective.*

DGs %	G_{Dec} [%]	T_{Dec} [h]	G_{Apr} [%]	T_{Apr} [h]
10	25.5	14.15	24.8	19.7
20	41.3	14.97	40.5	20.08
30	57	15.13	56.5	20.2
40	68.6	15.2	68.3	20.21
50	77.5	15.2	77.2	20.26
60	84.8	15.23	84.6	20.33
70	90.3	15.33	90.1	20.36

3.1 Introduction

We consider electricity grids where distributed energy sources (DESs) from renewables (e.g., photovoltaic panels or wind-powered micro turbines) exist and may act as energy producers to provide ancillary services. In the considered scenario, an overlay communication infrastructure [23] is utilized to orchestrate the DESs in a distributed fashion with the objective of minimizing power losses. In this respect, various options are possible, going from the use of wireless cellular networks to the ad hoc deployment of optical fiber cables. However, a preferred option, that reduces deployment costs while guaranteeing complete control by the utility, is to exploit the power cables for communication, implying the adoption of powerline communication (PLC) technology [21]. Among the possible capabilities of a communication and control architecture for smart grids [11], in the present chapter we focus on the *minimization of power losses*.

We note that the current flowing in the electrical transmission cables yields a partial power dispersion (in the form of heat) that contributes to economical and environmental costs. By suitably setting the amount of active/reactive power injected by DESs these power losses can be reduced, whilst sustaining the connected local loads. This translates into a decreased power demand to the mains, which lessens the use of high voltage lines and the associated operational cost for the utility.

Early works on the reduction of power losses focused on centralized solutions [4,25], which are however hardly scalable as the grid size increases and new DESs are dynamically added. Moreover, they require a full knowledge of the grid, in terms of topology, load activity and

DES power availability, thus also inducing a significant communication overhead. Distributed solutions were investigated in, e.g., [5–7, 27]. While often being suboptimal, these are more flexible and have lighter requirements in terms of communication.

We observe that in the existing literature the communication infrastructure was often taken for granted and the communication patterns among nodes were not optimized. Most papers considered a sequential adjustment of the current injected from the smart nodes, i.e., at any given time, a single node updates the amount of current injected, while the remaining ones do not apply any change. This approach assures grid stability and induces a token-ring communication strategy where, at any given time, a single node has the token and implements the control action, requesting and sending data over the communication network. We stress that the order by which the token is passed among the nodes has not been considered in previous works, although this affects the convergence rate of the control algorithms as well as the power drained during the optimization process.

In this chapter, we aim at optimizing the token exchange procedure among smart nodes in order to either reduce the token path length or to maximize the convergence rate of selected optimization algorithms for power loss minimization. Specifically, we investigate the importance of the scheduling rule that is utilized for the token assignment, assessing the impact of optimal control sequences as well as that of an original and lightweight heuristic approach. Two relevant power loss minimization algorithms, namely, the current based surround control (CBSC) [6, 26], and the distributed optimal reactive power flow control (DORPF) [7, 28], which have been proven to significantly reduce power losses in smart micro grids are considered. The performance of these schemes is then tested over a large number of grids that are statistically generated according to established literature models [24].

The rest of the chapter is organized as follows. Section 3.2 presents the considered electrical grid model, and provides a short overview of the two selected control techniques. The optimization of the token assignment strategy is addressed in Section 3.3. Details on the grid generation methodology are provided in Section 3.4, which is then used in Section 3.5 to obtain numerical results in terms of total dissipated power. Our concluding remarks are given in Section 3.6.

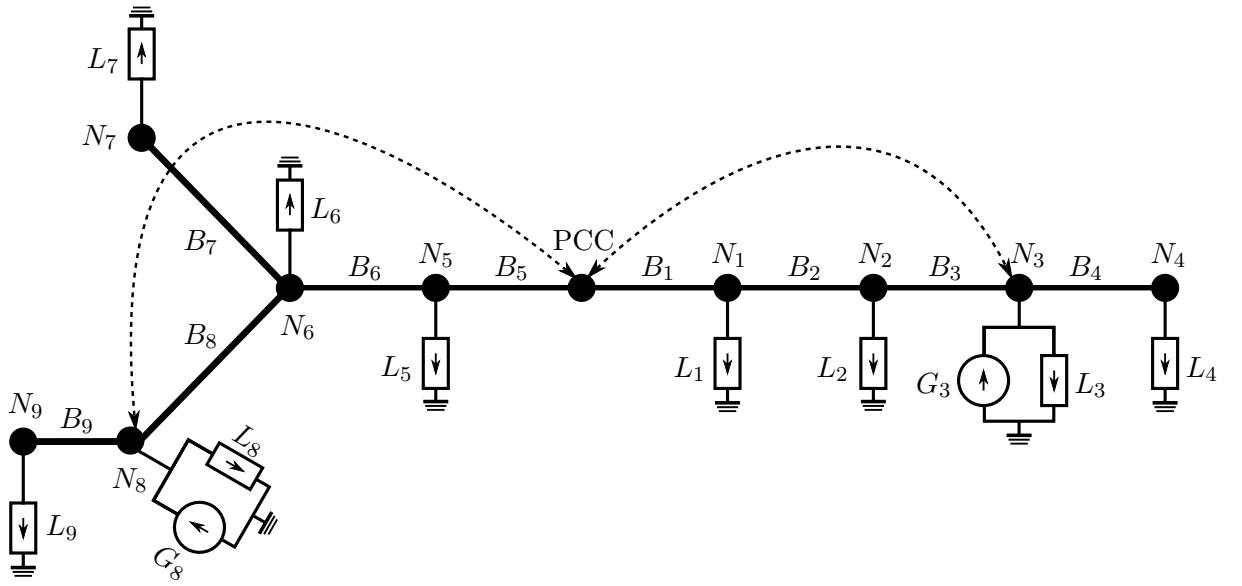


Figure 3.1. Power micro grid example. Think lines represent line impedances, whereas dashed lines represent logical communication links.

3.2 System Model

In this section, we specify the electrical and communication models for the micro grid. In addition, we briefly review the selected optimization techniques, highlighting their communication requirements.

3.2.1 Grid Model

We model the micro grid electrical topology as a directed tree. The root of the tree represents the point of common coupling (PCC), the other nodes represent loads, distributed energy sources (DESs) and connection points. Loads are represented either as constant resistive-inductive series impedances or as constant current sources. DESs are modeled as current sources, which may be connected in parallel to a load, which is referred to as the *associated* load (DESs are always assumed to feed their associated loads). Some of the nodes are equipped with smart meters and powerline communication (PLC) transceivers and, in turn, are able to take electrical measures and to communicate using the power lines. These nodes are referred to as *smart nodes* (SNs) and are identified by indices $1, \dots, N$ with N being the total number of SNs. SNs identifiers are assigned by the PCC and remain fixed during the optimization.

The communication capability of SNs induces a logical overlay communication network

built on top of the power grid physical topology. The communication network is exploited to exchange local electrical measurements to minimize the distribution power losses and the total power demand to the PCC.

Fig. 3.1 shows a micro grid example with added communication capabilities. The set of nodes and branches are respectively denoted by $\mathcal{N} = \{\text{PCC}, N_i : i = 1, \dots, 9\}$ and $\mathcal{B} = \{B_j : j = 1, \dots, 9\}$. Load L_i is connected to node N_i for $i = 1, \dots, 9$. DESs G_3 and G_8 are connected to nodes N_3 and N_8 and respectively feed the associated loads L_3 and L_8 . In Fig. Fig. 3.1 the SNs are the PCC, N_3 and N_8 .¹ The dashed lines connecting these SNs highlight the logical communication network structure, while communication data is exchanged over power cables thanks to PLC.

3.2.2 Distributed Optimization Algorithms

Local Control (LC) [5, 29] decreases the amount of power injected by the PCC by allowing DESs to directly feed their associated loads. This technique requires no communication among nodes and, in turn, the set of SNs is empty. The following distributed optimization algorithms apply this technique as the starting point for their distributed optimization.

Current Based Surround Control (CBSC) [6, 26] groups the nodes into *clusters*. Clusters are defined by checking, for any pair of DESs, whether their connecting path includes any other DES or the PCC. If this is not the case, a *cluster* is defined as the set containing the two DESs, the associated nodes, and all the nodes between them in the electrical network topology. For each cluster, the DES that is closest to the PCC is elected as the cluster head (CH). In the case where one of the two DESs in the cluster is the PCC, this is elected as the CH (i.e., we assume that the PCC has better communication and computational resources with respect to the other nodes). Clusters in Fig. 3.1 are $C_1 = \{\text{PCC}, N_1, N_2, N_3\}$ and $C_2 = \{\text{PCC}, N_5, N_6, N_8\}$. The DESs inject the current (complex or reactive depending on the optimization policy) that is required by the loads in the respective cluster. The current injected for optimization purposes is scaled by a real factor $0 \leq \alpha \leq 1$ such that, referring to I_C as the total current needed in the cluster, the currents injected by the two DESs in the cluster are αI_C and $(1 - \alpha)I_C$. The parameter α is determined for each cluster according to

¹Note that communication can only occur among smart nodes, as the remaining ones are not equipped with the required PLC communication capabilities.

the instantaneous power demand from the loads therein and branch impedances. Hence, this technique requires that every node is a SN.

Distributed Optimal Reactive Power Flow Control (DORPF) [7, 28] requires that DESs are grouped into possibly overlapping clusters and that, for each of them, one of the nodes becomes the cluster head (CH). Also, within each cluster, the gradient of the power distribution loss is estimated through local measurements. Relying on the estimated gradient, the CH computes the set of reactive powers that have to be injected by the two DESs in its own cluster (one being associated with the CH) in order to minimize the distribution power losses and spreads this information among its neighboring DESs. While different clustering procedures are possible, as stated in [7], the most effective clustering technique is the one proposed in [6] (see CBSC above). This technique requires that only the nodes that are connected to DESs are SNs, thus relaxing the requirements on the nodes in terms of communication and complexity. Due to this, the same clustering approach of CBSC is also considered for DORPF.

3.3 Token Ring Control

CBSC and DORPF require that groups of nodes iteratively take a control action (i.e., inject a certain amount of power in the grid) in order to reduce as much as possible the distribution power loss. The PCC is considered as a SN during the optimization process and its identifier is 0. The procedure of having at any given time a single SN allowed to modify the injected current, before letting the next SN to operate is similar to the *token* ring approach widely used in communication networks. For the sake of clarity, we recall that the access to the communication medium is arbitrated through a special packet called *token*. At any given step, one of the SNs owns the *token*, being in charge of implementing the control action and communicating with other SNs. All the other SNs are only allowed to answer explicit requests from the *token* owner, but are not allowed to contact it in the first place. For what has been said so far, the communication network can be considered collision free. Therefore, we will use here the related terminology, where however *token* ownership is associated to the current control, rather than to the possibility to transmit information. Indeed, when a node has the *token* it may communicate (in a two-way fashion) with other nodes in order to collect the information need for the control action. However, only SN with the *token* initiates the

communications, while other nodes are only allowed to answer its requests. When the current *token* owner releases the *token*, the next owner is chosen according to a specific policy. Note that choosing the next owner corresponds to establishing an *order* (also referred to as control scheduling) for the execution of the control actions. Two policies for the owner selection are now discussed. The first ordering strategy aims at maximizing the convergence rate of the optimization algorithms. The second ordering strategy is considered as a comparison reference and simply aims at minimizing the length of the *token* path in each *token* round, i.e., minimize the communication overhead needed to move the token.

Heuristic for Convergence Rate Maximization: improving the convergence rate of the considered optimization algorithms has two main benefits. First, the optimization becomes more responsive to changes in the power demand from the loads. Second, further power is saved during optimization. The convergence rate can be improved by suitably tuning the order in which nodes perform the control action, i.e., defining a new *token* owner selection rule. The optimal (in the sense of maximum convergence rate) selection rule requires that at least one SN has a full knowledge of the network state, but, in this case, a centralized optimization approach would be the best choice. For this reason a *heuristic* selection rule, that does not increase the amount of information that each SN has to collect for the optimization purpose, is proposed. This rule is based on the observation that updates in clusters with a higher power demand should have a larger impact on the total power loss.

In details, any two clusters are referred to as *adjacent* if at least one pair of nodes belonging to the two clusters is connected by a line with no nodes in between. Hence, if a node belonging to the two clusters exists, the two clusters are adjacent. At the beginning of the optimization process, the *token* owner is uniformly chosen at random among the SNs by the PCC. At each optimization step, the *token* owner collects information about the actual power demand of all the adjacent clusters. The *token* is then passed to the head of the cluster with the highest power demand. If more CHs are eligible, one of them is chosen uniformly at random.

Token Path Length Minimization: as a baseline strategy we consider that obtained by minimizing the length of the *token* path. To this end, suitable SNs identifiers and a next owner updating rule have to be defined. The identifiers have to be assigned starting from 1 and visiting the nodes with a depth first pre-ordered tree traversal. If the current *token* owner is the SN with identifier i , then the next owner identifier will be $j = (i + 1) \bmod N$.

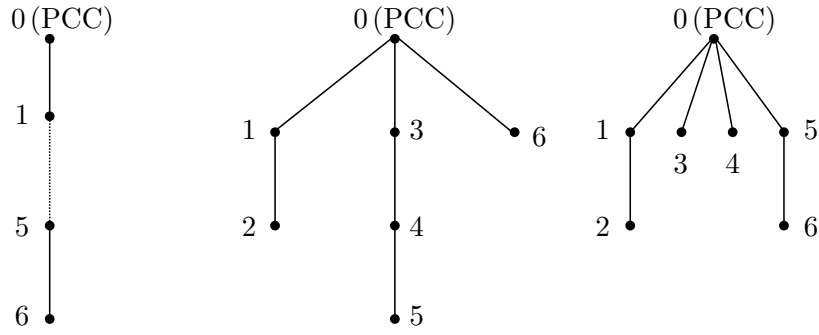


Figure 3.2. Random trees generated according to different rewiring probabilities p (from the left, $p = \{0, 0.5, 1\}$).

This procedure assures that the number of times the *token* has to jump between different subtrees is minimized, thus providing a more efficient communication solution, although in general suboptimal in terms of control algorithm convergence.

3.4 Electrical Grid Topology Generation

For a meaningful performance analysis, the selected optimization and scheduling algorithms are evaluated over a large number of power grid topologies. Toward this end, in this section a random power grid generation procedure, based on [8,24] and used in [25], is briefly reviewed. According to [8], many real world networks can be successfully represented as small-world graphs. These graphs are generated starting from a regular ring lattice with V vertices and degree k (which are user defined parameters). The generation process considers each edge of the graph and, according to a user defined *rewiring probability* probability p , one of the endpoints of the edge is changed. The *rewiring probability* is a tunable parameter determining the degree of randomness of the generated graph. A zero *rewiring probability* leads to a completely regular graph, while a unitary *rewiring probability* leads to a completely random graph. Most real world scenarios are neither suitable to a completely regular representation, nor to a completely random one, thus an intermediate probability is often best suited to represent real networks.

In [24], it is pointed out that the small-world graph generation procedure does not account for some peculiar characteristics of real world power grids. In particular, actual grid topologies exhibit a quite low average degree, which would lead to disconnected graphs. For this reason, in this chapter we adopt an ad hoc random graphs generation procedure based on small-world

graphs. Specifically, starting from a tree with V vertices, $V - 1$ branches, and exactly one leaf, each branch of the tree is iteratively rewired to a new endpoint according to the *rewiring probability* p . This process is carried out while ensuring that the graph remains connected and that no loops are generated. The procedure ends when all branches have been visited. The length property of each branch is then generated according to an exponential distribution. Also, an increasing p has two main effects on the generated graphs: the tree height is reduced and the maximum degree of the graph is increased. This implies that the PCC has a higher number of direct neighbor nodes as p increases.

Fig. 3.2 shows three examples of graphs generated using the described procedure. Note that with this technique the generated graphs are all trees, which is consistent with actual electrical network topologies. The leftmost graph of Fig. 3.2 has been generated using a *rewiring probability* $p = 0$, and hence it is the same tree as that from which the generation procedure starts (no rewiring is executed). The central graph and the rightmost one have been generated with *rewiring probabilities* of $p = 0.5$ and $p = 1$, respectively. We remark that increasing the rewiring probability has two main effects on the generated graphs: the tree height is reduced and the maximum degree of the graph is increased. This implies that the PCC has a higher number of direct neighbor nodes as p increases.

3.5 Numerical Results

In this section, the optimization algorithms of Section 3.2 are tested using the the two ordering (or *token* path selection) strategies of Section 3.3 over a large number of power grids, generated according to the procedure described in Section 3.4.

We considered networks with 15 and 50 nodes and two values of the rewiring probability: $p = 0.3$ and $p = 0.7$. Branch lengths are sampled (independently at random for each branch) from an exponential distribution with mean $\mu = 100\text{m}$. Power distribution cables are assumed to have constant section and, hence, constant impedance per meter. This impedance has been set to $(8 + j8)10^{-6}\Omega/\text{m}$. 30% of the nodes are connected to a DES. The nodes connected to DESs are chosen uniformly at random among the set of all nodes except the PCC. Each node (but the PCC) is connected to a load and loads are modeled as RL series impedances, whose values are chosen uniformly at random among the load types in Table 3.1. The PCC imposes a voltage reference of 230V and the grid frequency is 50Hz. The overlay communication network

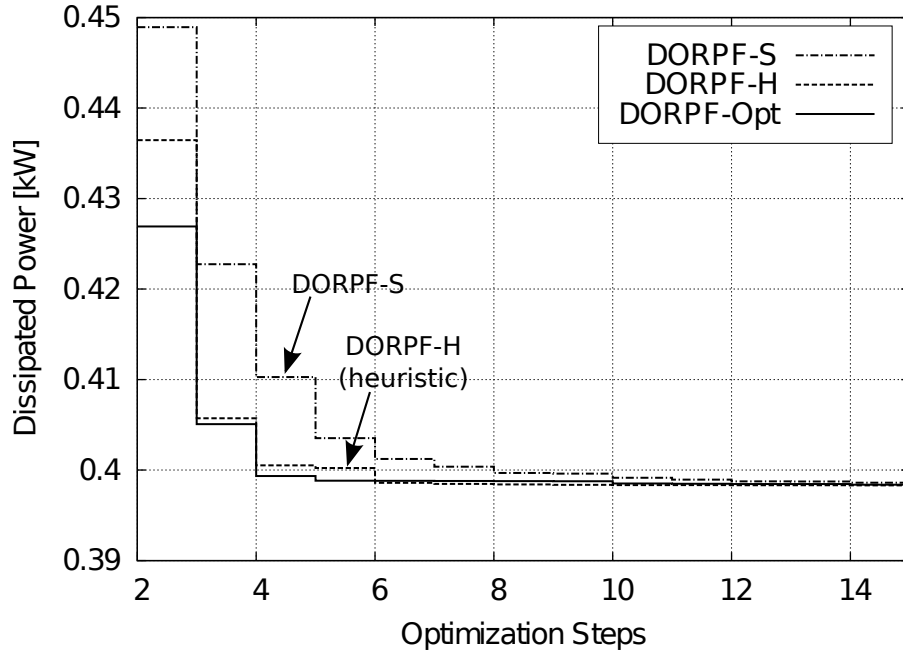


Figure 3.3. Dissipated power vs optimization steps for DORPF-S and DORPF-H and the power optimal strategy DORPF-Opt. 15 nodes, $p = 0.3$.

is assumed to be collision free. Moreover, it assumed that a routing protocol connecting each pair of SNs exists and that the communication links are error free.

Table 3.1. Resistance and inductance values of loads impedances.

Load type	R [Ω]	L [mH]
LT1	8.79	12.7
LT2	19.5	18.1
LT3	3.39	8.1

Next, we compare the two methods of Section 3.3 in terms of convergence rate and power expenditure during the optimization process. In the following, CBS and DORPF with the shortest token path policy will be denoted by CBSC-S and DORPF-S, respectively, while the same algorithms with the proposed heuristic for convergence rate maximization will be denoted by CBSC-H and DORPF-H, respectively.

Heuristic vs optimal scheduling: as a first set of results, in Fig. 3.3 we show the average power drained during the optimization process by DORPF-S, DORPF-H and an idealized version of DORPF, referred to here as “DORPF-Opt”, that has been obtained by adopting

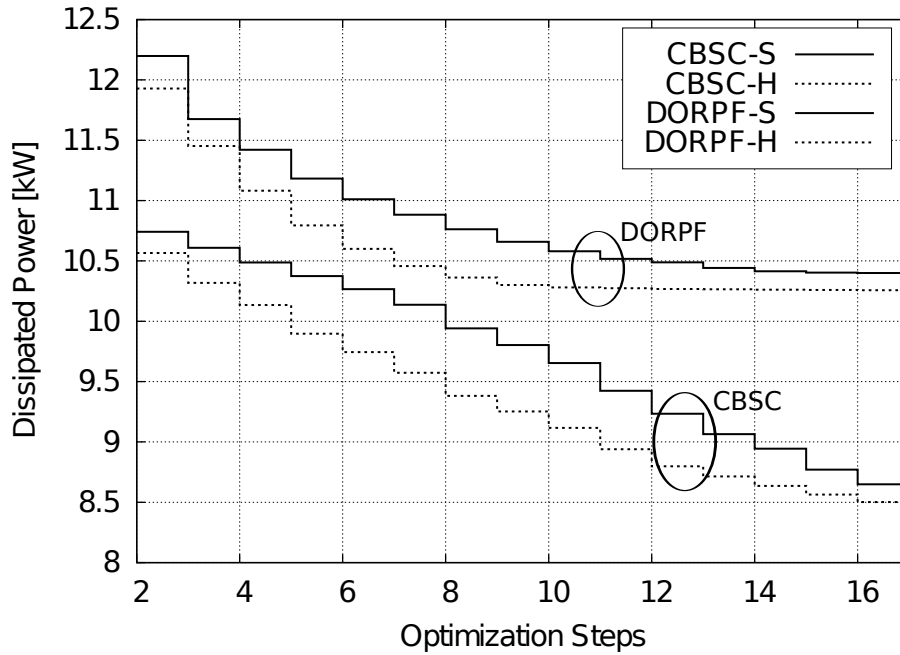


Figure 3.4. Dissipated power vs optimization steps for CBSC-S, CBSC-H, DORPF and DORPF-H. 50 nodes, $p = 0.3$.

the power optimal control sequence. The term *optimal* means that the sequence of nodes along the *token* path minimizes the energy drained during the execution of the algorithm. This optimal scheduling has been found through extensive search, an impractical approach whose complexity grows exponentially in the number of nodes and also requires full knowledge of electrical and communication topologies, DES and load (i.e., power demand) states. From Fig. 3.3, we see that our heuristic path selection (DORPF-H) performs very close to the power optimal scheme (DORPF-Opt), leading to gains in terms of convergence rate and energy expenditure.

Convergence rate: in Figs. 3.4 and 3.5 we compare DORPF against CBSC for $p \in \{0.3, 0.7\}$ and increasing the number of nodes to 50. A first noticeable result is that the *rewiring probability* p considerably affects the convergence rate of the considered optimization techniques. Specifically, from Fig. 3.4 we see that CBSC-S and DORPF-S converge within 17 optimization steps. For $p = 0.7$ (see Fig. 3.5) the convergence rate remains almost constant for DORPF-S, while for CBSC-S about 10 additional optimization steps are required.

These results demonstrate that the convergence rate of the selected algorithms is sensitive to the grid topology. In detail, when the grid topology exhibits a low degree of randomness

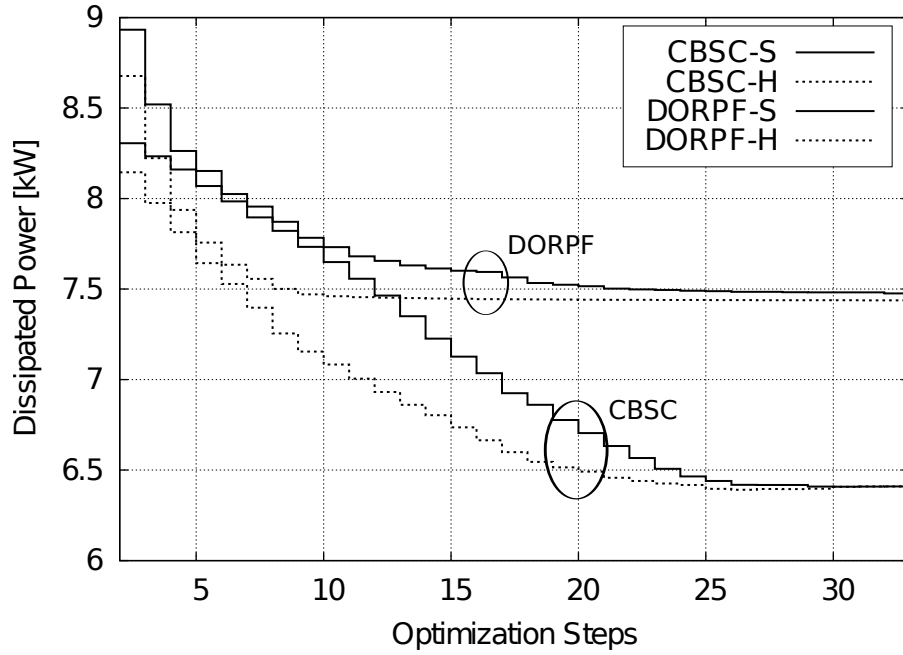


Figure 3.5. Dissipated power vs optimization steps for CBSC-S, CBSC-H, DORPF and DORPF-H. 50 nodes, $p = 0.7$.

(i.e., $p = 0.3$, Fig. 3.4), with the given setup, the maximum performance gap between CBSC-S and CBSC-H and between DORPF-S and DORPF-H is 0.5 kW and 0.4 kW, respectively. As the degree of randomness increases (i.e., $p = 0.7$, Fig. 3.5) the maximum gap between CBSC-S and CBSC-H rises to 0.7 kW, while the maximum gap between DORPF-S and DORPF-H remains almost constant. However, DORPF-H converges in only 11 optimization steps, while DORPF-S takes approximately 30 optimization steps to converge. We observe that a higher p , in terms of electrical topology, means that nodes have a higher number of direct neighbors. This implies a much richer setting for the optimization, as a higher number of choices in terms of neighbor selection is available at each optimization step. The better performance of CBSC demonstrates that this algorithm, in spite of its simplicity, has a more efficient search strategy in the solution space and this comes at the expense of its longer convergence time. Note also that there are two main benefits arising from the adoption of our heuristic approach. The first benefit is that the power grid becomes more responsive to power demand variations due to a faster optimization phase (shorter convergence time). The second benefit is that, a faster convergence makes it possible to save a certain amount of energy during the optimization, as we discuss in greater detail below.

Energy savings: in Fig. 3.6 we show the complementary cumulative distribution function (CCDF) describing the probability of saving an amount of energy greater than or equal to the value in the abscissa when using CBSC-H or DORPF-H. This graph has been obtained for grid topologies with 50 nodes and $p = 0.7$ by respectively integrating the power difference between CBSC-S and CBSC-H and between DORPF-S and DORPF-H for control steps of 1 minute each. For both CBSC and DORPF, the probability of saving energy during the optimization phase is greater than 90%. When using CBSC-H, savings can be as high as 2 MJ and this graph confirms the better optimization ability of this scheme. As an example, the probability of saving more than 0.5 MJ is 0.4 for CBSC, whereas it is 0.2 for DORPF. Also, it is worth noting that a small number of grid topologies exist for which CBSC-H and DORPF-H converge slower than CBSC-S and DORPF-S, respectively, although they converge to the same final point, which is algorithmic dependent but only weakly dependent on the selected *token* path. While these topologies do not affect the average performance (shown in Fig. 3.4), their impact can be observed in Fig. 3.6. In fact, there is a small but positive probability that the energy gain provided by our heuristic scheduling is negative. Similar results, not shown here due to space constraints, are obtained for $p = 0.3$.

To summarize, Fig. 3.6 shows that, for most of the grid topologies the heuristic approach proposed in this chapter provides considerable energy savings during each optimization phase. In addition, since the optimization is repeated whenever the electrical grid state changes (especially in terms of variation of power demands) the cumulative gain is much higher and proportional to the rate at which the optimization algorithms are executed. It is nevertheless worth noting that, since configurations exist for which the shortest *token* path procedure (DORPF-S and CBCS-S) guarantees faster convergence rates, the choice of the heuristic convergence rate enhancement procedure (DORPF-H and CBCS-H), despite its average behavior shown in Figs. 3.4 and 3.5, should be carefully evaluated before deployment.

3.6 Conclusions

In this chapter we have analyzed optimal and heuristic scheduling rules to arbitrate the current injection from distributed energy resources in electricity grids. To this aim, we have considered two recent optimization schemes for the reduction of power distribution losses, discussing their communication requirements and comparing their performance against that

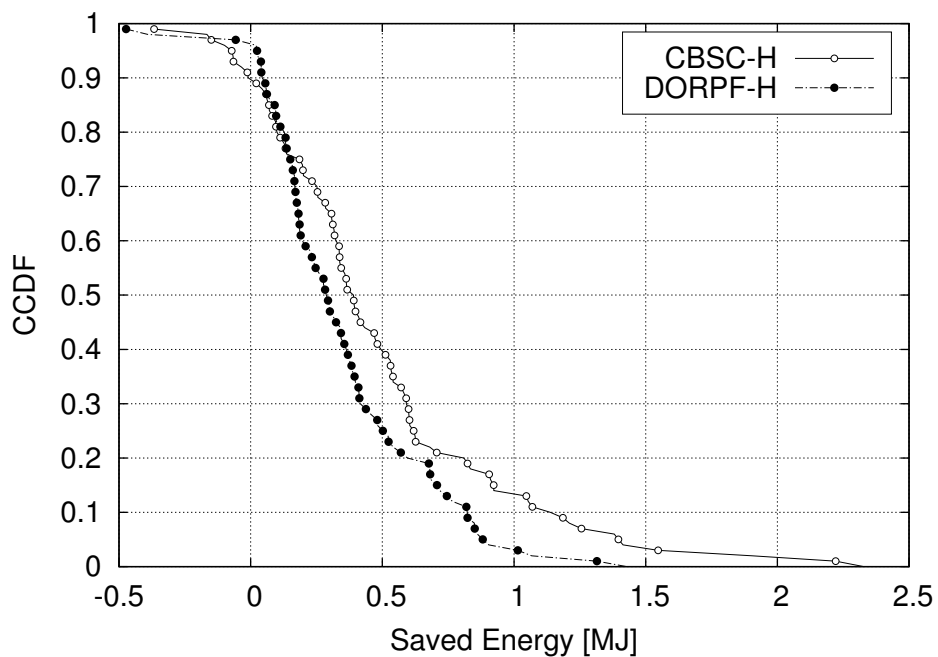


Figure 3.6. *CCDF of the energy saved by CBSC-H and DORPF-H with respect to CBSC-S and DORPF-S, respectively. 50 nodes, $p = 0.7$.*

of an idealized power optimal scheme. Our results reveal that the *execution order* (scheduling) for the distributed control actions matters and that substantial energy savings are possible through its careful design.

LOW-VOLTAGE MICROGRIDS will play a major role in future smart grids [32]. The presence of distributed micro-generation and energy storage owned by end users (referred to here as *prosumers*) results in a new paradigm for electrical grids and in a potentially new and vibrant market for technology manufacturers, service providers, energy traders, distributors, and regulatory boards. However, several challenges are still to be faced, in terms of technology, standards, rules, and economic models [33, 34]. According to this new paradigm, the distribution grid can be seen as a patchwork with the microgrids being its basic tiles and supporting the utility in terms of power quality, management of network dynamics, etc. Also, microgrids could be engineered so as to assure electrical continuity to the loads even in the case of grid failure. A major goal of microgrids is to integrate and effectively manage distributed energy resources (DERs), either as micro-generation (MG) or energy storage (ES). In fact, the increasing pervasiveness of renewable energy sources, mainly photovoltaic (PV), may lead to the misbehavior of the distribution grid due to over-production during daytime, while having a negative impact on the electrical market. Thus, the capability to control the energy in- and out-flow of microgrids, seen as an aggregate of entities (prosumer communities), plays a major role in ensuring stability, efficiency and cost-effectiveness of future smart grids. Toward this objective, each energy gateway (EG, i.e., the controller placed at the user's premises) must be properly driven, and the control architecture must be flexible and scalable, so as to accommodate any number of DERs and autonomously adapt to the power variations due to the loads and to the intermittent energy sources [35–41].

In this chapter, we propose a lightweight control approach to realize this vision, extending the work of [42] through a control architecture capable of guaranteeing the correct operation

of prosumer communities in an islanded operated scenario. In detail, the proposed control strategy adopts a master-slave approach, where the master role is played by the utility interface (UI), i.e., a three-phase inverter located at the point of common coupling (PCC) between the microgrid and the utility. The UI is equipped with energy storage (battery or super-cap) and, if necessary, with a backup generator (such as a micro-turbine, fuel cell, diesel gen-set, etc.), permanently performing as a voltage source. We assume that the microgrid operates in islanded mode, the UI acts as a grid-forming voltage source, as the mains, while the EGs act as current sources [42]. The purpose of the control strategy is to level peaks in the user demand, thus limiting the stage/production requirements to the UI. We achieve this goal by a semi-distributed approach, where the UI collects information on load and source activity and distributes a single control parameter that is then used locally to regulate the operation of ES and generators.

Note that an islanded operation mode entails an additional number of issues, including frequency and voltage control, which are not within the scope of this chapter. Here, we assume that some other control strategy takes care of these issues by operating at a suitably fast rate. Instead, our control operates at a slower rate (addressing slower variations of loads and sources) with the aim of ensuring the long-term sustainability of the microgrid.

A major advantage of our approach is the additional degree of freedom gained in the internal optimization of the microgrid, which is now seen by the utility as an *aggregate* user, with improved efficiency and control capabilities. Note that this might create new market opportunities and monetization strategies, since prosumer communities could upgrade their role and increase their contracting clout, by taking advantage of autonomous management. As a by-product, we are also able to control the microgrid when operating in a grid-connected mode, with the UI behaving as a grid-interactive UPS, and playing the role of the central controller for the microgrid.

To validate the proposed control strategy, a residential microgrid model, 100 kVA rated, is developed to simulate realistic power demand and energy generation processes. This model integrates real life data regarding power consumption (demand) and photovoltaic generation, featuring validated statistical models for both processes. Thanks to these tools, we evaluate the impact of the proposed control strategy (dealing with peak shaving at different time scales) on the performance of the microgrid and assess its peculiarities in terms of required energy

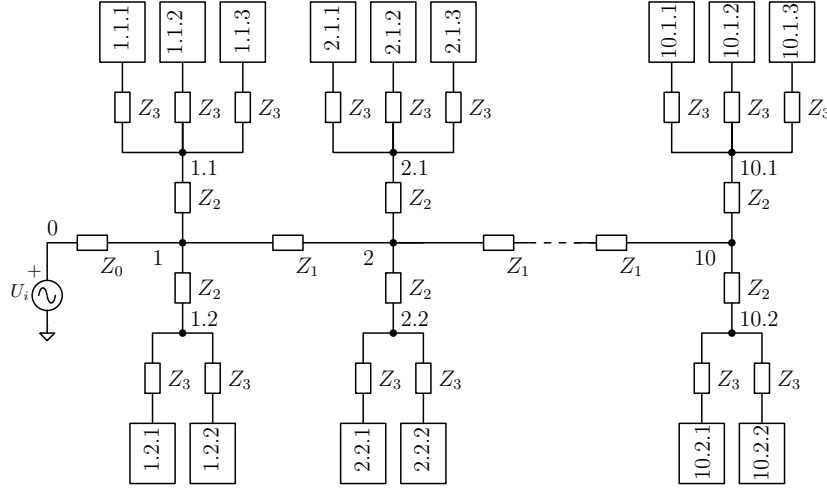


Figure 4.1. Schematic representation of the considered microgrid topology.

storage and load balancing capabilities. We note that the considered statistical approach for the energy sources and the loads leads to a more realistic system design methodology than considering, e.g., worst case scenarios.

The remainder of this chapter is structured as follows. In Section 4.1 we describe the system model, whereas our control algorithm is presented in Section 4.2. Simulation results are presented in Section 4.3 and our conclusions are drawn in Section 4.4.

4.1 System Model

We consider a low voltage, single phase residential microgrid, schematically represented in Fig. 4.1, with $K = 50$ end user nodes. At the PCC (node 0), the microgrid is equipped with a distinct unit, denoted three-phase utility interface (UI) with energy storage (UI-ES) capabilities and power capability of 100 kVA. Downstream from the PCC, the grid is composed of 10 topologically identical sections, each comprising 5 end users. The electrical network is represented by a tree with three levels of depth, with the end-users being its leaves (in Fig. 4.1, end-users are univocally identified by a triplet “i.j.k”). Each tree level is characterized by a characteristic interconnection impedance. As a result, besides the UI output impedance (Z_0), three additional interconnection impedances are considered, as reported in Tab. 4.1.

The UI is controlled as a voltage source and is capable of bidirectional communication (via power line or wireless) with any other node of the microgrid. $N = 15$ grid nodes, randomly distributed within the microgrid, are *active* nodes with micro-generation and energy storage

Table 4.1. *Microgrid interconnection impedances*

Tree level	Value	Unit
Zero level (PCC)	Z_0	$+j26 \text{ m}\Omega$
Level 1	Z_1	$173 + j44 \text{ m}\Omega$
Level 2	Z_2	$267 + j75 \text{ m}\Omega$
Level 3	Z_3	$705 + j157 \text{ m}\Omega$

capabilities. These nodes are interfaced to the grid through an energy gateway (EG), which operates as a current source and is capable of bidirectional communication with the UI. The remaining $M = K - N = 35$ nodes are passive nodes. Passive nodes, although possibly equipped with smart meters (SM), are not necessarily endowed with intelligent measurement or control devices. In grid-connected mode, the UI voltage reference is set by suitable active and reactive power control loops, while in islanded mode, the UI becomes the grid-forming voltage source for the entire microgrid. The EGs make their energy resources available, including their local energy storage. The active nodes perform as slaves and their EGs communicate with the UI, implementing distributed control actions. Although different power definitions can be used within the proposed approach, we consider conservative quantities for the active and reactive power, see [43]. Also, without loss of generality, we refer to single-phase variables, being aware that single-phase and three-phase loads may coexist in the same microgrid.

In grid-connected operation, the UI only supplies reactive power to perform ancillary functions, like power factor control at the PCC and load imbalance compensation. Moreover, the UI dispatches active and reactive power commands to the EGs. The EGs, in turn, make their residual power capability available to the UI, and possibly perform as active filters to mitigate current distortion. In grid-connected mode, any errors or delays in the power commands dispatched to EGs are non time-critical, since the power balance is ensured by the mains, at any time and in any condition. Instead, in islanded mode the UI becomes the voltage source for the entire microgrid, and makes use of its ES and/or backup unit to maintain the PCC voltage at the desired level. The power references dispatched to current-controlled EGs become then time-critical, since the power balance within the microgrid must

now be autonomously provided by the EGs and the UI. Therefore, suitably fast-rate control strategies must be deployed to ensure stability. Here we do not address this fast control. Rather, we focus on a longer-term control that avoids long lasting overconsumption. A degree of freedom is offered by load control, if any. In fact, if the power balance cannot be ensured by the available energy sources, the UI can ask the EGs to disconnect some low-priority loads to reduce the power demand.

4.2 Microgrid control strategy

Next, we describe how the microgrid can be controlled in grid-connected and islanded operation modes. At the beginning of every control period T_S (whose duration is a few line cycles) the UI, as the control master, polls all the nodes of the microgrid. The active nodes return the values of active and reactive power available for microgrid control. Note that the number of active and passive nodes can dynamically change, depending on how many end-users are actually connected to the microgrid. Moreover, active nodes perform as passive ones when their generated power is fully used to feed their local loads. Therefore, the control algorithm must be devised to allow dynamic adjustment of microgrid parameters. In detail, the data packet sent by the n -th EG (slave unit) to the UI (master controller) at the end of the ℓ -th control cycle includes:

- $P_{Gn}(\ell)$, $Q_{Gn}(\ell)$, the active and reactive power generated by the local power source during the ℓ -th cycle,
- $P_{Gn}^{\max}(\ell + 1)$ and $P_{Gn}^{\min}(\ell + 1)$, the estimate of the upper (max) and lower (min) limits of the active power from the local energy source in cycle $\ell + 1$, also taking into account the power that can be fed into (P_{Sn}^{in}) or drained from (P_{Sn}^{out}) the local ES. Since $P_{Sn}^{\text{out}} > 0$ and $P_{Sn}^{\text{in}} < 0$, it holds:

$$P_{Gn}^{\min}(\ell + 1) = P_{Gn}(\ell) - P_{Sn}^{\text{in}}(\ell + 1), \quad (4.1)$$

$$P_{Gn}^{\max}(\ell + 1) = P_{Gn}(\ell) + P_{Sn}^{\text{out}}(\ell + 1); \quad (4.2)$$

- $P_{Gn}(\ell + 1)$, the estimate of the active power that will be generated in the $\ell + 1$ -th cycle,
- $A_{Gn}(\ell + 1)$, the estimate of the nominal power flow capability of the EG, and

- $A_{Gn}^{\text{over}}(\ell + 1)$, the estimate of the overload power flow that can be temporarily sustained by the EG (e.g., for 10 – 100 grid cycles). The overload power rating is related to the instantaneous physical capability of the energy gateway. This parameter can vary in time, for example, as a consequence of thermal stresses.

Finally, the UI determines the active and reactive power, $P_{tot}^{PCC}(\ell)$ and $Q_{tot}^{PCC}(\ell)$, respectively, absorbed by the microgrid from the PCC and measured during the ℓ -th cycle.

To derive the subsequent control actions, the UI estimates the energy state of the microgrid by computing, on the basis of the collected data, the following quantities:

- the total power generated by the EGs in the ℓ -th cycle:

$$P_{Gtot}(\ell) = \sum_{n=1}^N P_{Gn}(\ell), \quad Q_{Gtot}(\ell) = \sum_{n=1}^N Q_{Gn}(\ell), \quad (4.3)$$

- the total power absorbed by the loads in the ℓ -th cycle:

$$P_{Ltot}(\ell) = P_{tot}^{PCC}(\ell) + P_{Gtot}(\ell), \quad (4.4)$$

$$Q_{Ltot}(\ell) = Q_{Ltot}^{PCC}(\ell) + Q_{Gtot}(\ell), \quad (4.5)$$

- the estimated power absorbed by the loads in the next cycle $\ell + 1$:

$$P_{Ltot}(\ell + 1) = P_{Ltot}(\ell) - P_{G0}(\ell + 1), \quad (4.6)$$

$$Q_{Ltot}(\ell + 1) = Q_{Ltot}(\ell) - Q_{G0}(\ell + 1), \quad (4.7)$$

where $P_{G0}(\ell + 1)$ and $Q_{G0}(\ell + 1)$ are the estimates of the active and reactive power that the UI expects to generate in the next control cycle $\ell + 1$.

- the expected available active and reactive power, in normal or overload conditions, from the distributed EGs in the next control cycle $\ell + 1$:

$$P_{Gtot}(\ell + 1) = \sum_{n=1}^N P_{Gn}(\ell), \quad (4.8)$$

$$P_{Gtot}^{\min}(\ell + 1) = \sum_{n=1}^N P_{Gn}^{\min}(\ell + 1), \quad (4.9)$$

$$P_{Gtot}^{\max}(\ell + 1) = \sum_{n=1}^N P_{Gn}^{\max}(\ell + 1), \quad (4.10)$$

$$Q_{Gn}^{\max}(\ell + 1) = \sqrt{A_{Gn}(\ell + 1)^2 - P_{Gn}(\ell + 1)^2}, \quad (4.11)$$

$$Q_{Gtot}^{\max}(\ell + 1) = \sum_{n=1}^N Q_{Gn}^{\max}(\ell + 1), \quad (4.12)$$

$$Q_{Gn}^{\text{over}}(\ell + 1) = \sqrt{A_{Gn}^{\text{over}}(\ell + 1)^2 - P_{Gn}(\ell + 1)^2}, \quad (4.13)$$

$$Q_{Gtot}^{\text{over}}(\ell + 1) = \sum_{n=1}^N Q_{Gn}^{\text{over}}(\ell + 1). \quad (4.14)$$

Then, the above estimates are used by the power-based control algorithm to determine the power contributions of the distributed generators.

The amount for power injected by the active nodes is finally obtained by means of two variables, α_P and α_Q , calculated by the UI and then broadcast to all EGs. In the following paragraphs, we describe how these coefficients are determined for the various operating modes.

4.2.1 Islanded Operation – Active Power

Next, we consider four cases, that are related to the amount of predicted power generation/consumption at the next cycle.

4.2.1.1 $P_{Ltot}(\ell + 1) < P_{Gtot}^{\min}(\ell + 1)$

in this case, the aggregated power demand ($P_{Ltot}(\ell + 1)$) is smaller than the minimum power that can be generated by the active nodes, although local accumulators are fully exploited. Thus $\alpha_P = 0$. Correspondingly, each active node generates a power reference:

$$P_{Gn}^*(\ell + 1) = P_{Gn}^{\min}(\ell + 1). \quad (4.15)$$

In case the total injected power exceeds the power demand, the surplus is stored in the UI accumulators, so as to assure the power balance of the microgrid.

4.2.1.2 $P_{Gtot}^{\min}(\ell + 1) \leq P_{Ltot}(\ell + 1) < P_{Gtot}(\ell + 1)$

here, the power absorbed by the loads can be directly provided by the active nodes. We set:

$$\alpha_P = \frac{P_{Ltot}(\ell + 1) - P_{Gtot}^{\min}(\ell + 1)}{P_{Gtot}(\ell + 1) - P_{Gtot}^{\min}(\ell + 1)}, \quad 0 \leq \alpha_P \leq 1. \quad (4.16)$$

Correspondingly, each active node generates an active power reference equal to:

$$P_{Gn}^*(\ell + 1) = P_{Gn}^{\min}(\ell + 1) + \alpha_P (P_{Gn}(\ell + 1) - P_{Gn}^{\min}(\ell + 1)). \quad (4.17)$$

4.2.1.3 $P_{Gtot}(\ell + 1) \leq P_{Ltot}(\ell + 1) \leq P_{Gtot}^{\max}(\ell + 1)$

the power absorbed by the loads can be delivered by the active nodes with the support of the distributed ES. Also in this case, the UI does not necessarily exchange active power with the grid, although it can restore the state of charge of its ES by summing the additional power to the load power. We set:

$$\alpha_P = 1 + \frac{P_{Ltot}(\ell + 1) - P_{Gtot}(\ell + 1)}{P_{Gtot}^{\max}(\ell + 1) - P_{Gtot}(\ell + 1)}, \quad 1 \leq \alpha_P \leq 2. \quad (4.18)$$

Correspondingly, each active node generates an active power reference equal to:

$$P_{Gtot}^*(\ell + 1) = P_{Gn}(\ell + 1) + (\alpha_P - 1) (P_{Gn}^{\max}(\ell + 1) - P_{Gn}(\ell + 1)). \quad (4.19)$$

4.2.1.4 $P_{Ltot}(\ell + 1) > P_{Gtot}^{\max}(\ell + 1)$

the power demand exceeds the maximum power that can be generated within the microgrid, even though distributed ES were fully exploited. In this case we set $\alpha_P = 2$. Correspondingly, each active node generates an active power reference equal to:

$$P_{Gn}^*(\ell + 1) = P_{Gn}^{\max}(\ell + 1). \quad (4.20)$$

In case the total power injected by the EGs is insufficient to satisfy the loads, the needed additional power is drained from the UI.

4.2.2 Islanded Operation – Reactive Power

4.2.2.1 $Q_{Ltot}(\ell + 1) \leq Q_{Gtot}^{\max}(\ell + 1)$

here, the reactive power can be delivered by the distributed EGs without overloading their power interfaces. In this case we set:

$$\alpha_Q = \frac{Q_{Ltot}(\ell + 1)}{Q_{Gtot}(\ell + 1)}, \quad 0 \leq \alpha_Q \leq 1. \quad (4.21)$$

Correspondingly, each active node generates a reactive power reference of:

$$Q_{Gn}^*(\ell + 1) = \alpha_Q \cdot Q_{Gn}^{\max}(\ell + 1). \quad (4.22)$$

4.2.2.2 $Q_{Ltot}(\ell + 1) > Q_{Gtot}^{\max}(\ell + 1)$

in this case, the desired reactive power can be generated through a controlled overload of the electronic power interfaces. In this case we set:

$$\alpha_Q = 1 + \frac{Q_{Ltot}(\ell + 1) - Q_{Gtot}^{\max}(\ell + 1)}{Q_{Gtot}^{\text{over}}(\ell + 1) - Q_{Gtot}^{\max}(\ell + 1)}, \quad 1 < \alpha_Q \leq 2. \quad (4.23)$$

Correspondingly, each active node generates a reactive power reference:

$$Q_{Gn}^*(\ell + 1) = Q_{Gn}^{\max}(\ell + 1) + (\alpha_Q - 1) (Q_{Gn}^{\text{over}}(\ell + 1) - Q_{Gn}^{\max}(\ell + 1)), \quad (4.24)$$

The α_P and α_Q coefficients allows the calculation of the power reference at the EGs. In compact form, for all the cases above it holds:

$$P_{Gn}^*(\ell + 1) = P_{Gn}^{\min} + (P_{Gn} - P_{Gn}^{\min}) \cdot \min(\alpha_P, 1) + (P_{Gn}^{\max} - P_{Gn}) \cdot \max(\alpha_P - 1, 0), \quad (4.25)$$

$$Q_{Gn}^*(\ell + 1) = Q_{Gn}^{\max} \cdot \min(\alpha_Q, 1) + (Q_{Gn}^{\text{over}} - Q_{Gn}^{\max}) \cdot \max(\alpha_Q - 1, 0), \quad (4.26)$$

4.2.3 Grid connected operation

In this case the UI is turned off, and the PCC delivers all the required power which is not provided by the local generators. In particular, as observed above, the control is non-critical since the mains ensure the power balance. The control master may ask the EGs to deliver any power level within their capacity (depending on the type of power source). For wind turbines or PV plants the best solution is to fully exploit their renewable energy, while for other types of sources (small hydro, fuel-cells, gas turbines) cost issues must be considered. In any event, the EGs can feed reactive power to demanding loads, thus reducing distribution losses, improving node voltage stability, and increasing the power factor at the PCC. Upon request from the UI, the EGs can also deliver or absorb more active power, at the expense of the energy reserve in their energy storage units. This can be done to meet internal needs such as node voltage stabilization, current limitation in the feeders or to respond to power demand from the utility.

The control strategy of Sections 4.2.1 and 4.2.2 can be directly adapted to the on-grid case. Indeed, setting $P_{Ltot}(\ell + 1) = P_{Gtot}(\ell + 1)$, we get $\alpha_P = 1$, forcing the distributed

sources to inject all the power they generate into the grid. Note that, we may overestimate the amount of generated power, $P_{Gtot}(\ell + 1)$, to accommodate several factors such as the amount of power needed to restore the state of charge of the local ESs. In any case, the UI provides the power required to maintain the balance between generated and absorbed powers. The UI may contribute to the reactive power compensation by computing Q_{G0} in (Eq. 4.7), and injecting the corresponding reactive power $Q_{Ltot}(\ell + 1)$ in the next cycle $\ell + 1$.

$$\begin{aligned} P_{Gn}^{\min} &= \text{sat}_{-A_n} (P_{Gn} + P_{Sn}^{\min}), \\ P_{Gn}^{\max} &= \text{sat}^{+A_n} (P_{Gn} + P_{Sn}^{\max}). \end{aligned} \quad (4.27)$$

In (Eq. 4.27) the saturation function $\text{sat}_L^U(\cdot)$ points out that the actual power than can be delivered is bounded by the power rating A_n of the EG inverter. Once these data have been collected from all grid nodes, the control master computes the total power consumed and generated within the microgrid as:

$$P_{Ltot} = \sum_K^{k=1} P_{Lk} = \sum_M^{m=1} P_{Lm} + \sum_N^{n=1} P_{Ln} \quad (4.28)$$

$$\begin{aligned} P_{Gtot} &= \sum_N^{n=1} P_{Gn}, \\ P_{Gtot}^{\min} &= \sum_N^{n=1} P_{Gn}^{\min}, \\ P_{Gtot}^{\max} &= \sum_N^{n=1} P_{Gn}^{\max}. \end{aligned} \quad (4.29)$$

Finally the control master executes a control algorithm that depends on the operating mode (grid-connected or islanded) and on the relative amount of generated and absorbed power. In the past, distance-based power sharing algorithms [44] have been explored. In this case, a simpler and almost equally effective algorithm can be used, that is now detailed.

Basically, EGs are driven by a couple of coefficients α_P and α_Q , referring respectively to the active and reactive power demand, which are computed by the UI and broadcasted to all EGs. Given α_P and α_Q , each EG controls the local power flow to the grid according to the

expressions:

$$P_{Gn}^*(l+1) = P_{Gn}^{\min} + (P_{Gn} - P_{Gn}^{\min}) \cdot \min(\alpha_P, 1) + (P_{Gn}^{\max} - P_{Gn}) \cdot \max(\alpha_P - 1, 0), \quad (4.30)$$

$$Q_{Gn}^*(l+1) = Q_{Gn}^{\max} \cdot \min(\alpha_Q, 1) + (Q_{Gn}^{\text{over}} - Q_{Gn}^{\max}) \cdot \max(\alpha_Q - 1, 0), \quad (4.31)$$

where, in (Eq. 4.30), the term $P_{Gn}^*(l+1)$ is the local active power reference for the next control cycle. Similarly, in (Eq. 4.31), $Q_{Gn}^*(l+1)$ represents the reactive power reference for the next control cycle and Q_{Gn}^{over} is the temporarily deliverable reactive power, exploiting the EGs overcurrent capability.

4.2.4 Islanded operation.

In this case the power balance must be ensured within the microgrid. We distinguish two situations:

4.2.4.1 Over-generation ($P_{Gtot} > P_{Ltot}$)

in this case, under steady-state conditions, the extra-power generated by renewable sources is stored in the distributed ES units depending on their state of charge, and the EGs are driven accordingly. The load transients are faced initially at the expense of the energy stored in UI-ES, and UI acts as a voltage source which automatically meets any dynamic power requests. Within few line cycles the EGs power commands are adapted to the new situation. The state of charge of UI-ES must be carefully controlled to ensure the capability to temporary store the excess of energy produced by the distributed generators or supply of the extra energy requested by the loads. If over-generation lasts too long, the power generated by renewable sources must be scaled down to meet the actual load power consumption. Also in this case the reactive power can be controlled by the EGs so as to meet local loads consumption and to stabilize node voltages. The coefficients α_P and α_Q for the $(l+1)$ control cycle are derived as a function of the generated and absorbed powers as follows:

$$\alpha_P = \frac{P_{Ltot}(l) - P_{Gtot}^{\min}(l)}{P_{Gtot}(l) - P_{Gtot}^{\min}(l)} \Rightarrow 0 \leq \alpha_P \leq 1 \quad (4.32)$$

$$\alpha_Q = \frac{Q_{Ltot}(l)}{Q_{Gtot}(l)} \Rightarrow 0 \leq \alpha_Q \leq 1 \quad (4.33)$$

4.2.4.2 Under-generation ($P_{Gtot} < P_{Ltot}$)

this is the most critical condition. Indeed, the power generated within the microgrid is not enough to fulfill loads demand, and the excess power must be provided by distributed ES units according to their state of charge. Obviously, this condition can be maintained for a limited time, during which the power balance must be ensured while preventing full discharge of UI-ES. There are two sub-cases to be considered.

- $P_{Ltot} \leq P_{Gtot}^{max}$: in this case, the extra power can be met by distributed ES units, without requiring the intervention of UI-ES. The control master shares the power and energy demand among the EGs according to a proper criterion. A good solution is to keep control over the state of charge of distributed ES (by active power control) while reducing the distribution loss within the microgrid (by reactive power control). This also limits the thermal stress in the feeders and helps stabilizing the voltage profiles.
- $P_{Ltot} > P_{Gtot}^{max}$: in this case, the control master temporarily asks distributed EGs to deliver maximum power P_{Gtot}^{max} , and takes the missing energy from UI-ES. Then, the backup generator is switched on, and its generated power is kept above load demand for some time, to restore the state of charge of ES devices. Reactive power contributions can be managed in the same way. Once the more stringent constraints on active power sharing among energy gateways are satisfied, the principle described above can be directly applied also for the reactive power. To this purpose, the reactive power available for distributed compensation can be computed on the basis of the data provided by microgrid nodes.

4.3 Results

In this section, we discuss the performance of the proposed control strategy considering the power microgrid of Section 4.1. The system, in terms of control, energy production and power demand, evolves in slotted time, where the slot duration is $T_S = 1$ minute. Before delving into the analysis of the results, in the following paragraphs, we briefly discuss the considered statistical models for the renewable energy sources and the end-user demand.

Also, we provide insights for a proper sizing of the UI when operated in islanded mode. To this end, we assume a UI with infinite generation and storage capabilities, and operate

the microgrid in islanded mode. By observing the requirements on the UI, we are then able to infer its sizing in a realistic deployment.

Renewable source model: energy traces for the photovoltaic sources have been obtained using the SolartStat tool [9]. In detail, energy generation statistics (cumulative distribution functions, cdf) have been generated for each month of the year and for each hour of the day for the city of Los Angeles. For the solar modules, we have considered the Panasonic N235B solar panel technology, accounting for a surface of about 10m^2 (delivering a nominal power of about 4kW). The solar modules have a tilt angle of 45° and an azimuthal displacement, with respect to the real South, of 30° . Hence, these cdfs have been utilized to generate the current harvested from each solar module with a time granularity of T_S .

Modeling power demand: an accurate statistical model has been derived from the household electric power consumption data set, available at [31]. This database contains fine-grained (one per minute) measurements of active and reactive power demand from residential structures, collected between December 2006 and November 2010. Following the approach of [9], we have obtained power demand cdfs for each month of the year, day of the week and hour of the day. A power demand process is then updated for each end-user every T_S seconds according to these statistics. Note that although the same cdf is considered for different end-users in the same time slot, their demands are independently drawn from this cdf.

Performance analysis: for comparison purposes, we introduce a simple algorithm, referred to as *Self Support*, where each EG makes local decisions without interacting with the UI. In detail, the highest priority of each EG corresponds to using the harvested energy to feed the local load. The excess energy, if any, is used to charge the local battery and the residual energy is injected into the grid.

Figs. 4.2 and 4.3 show the total power demand at the UI when the Self Support algorithm and the proposed control solution (referred to as Power Based) are used. In Fig. 4.4, we instead show the corresponding average state of charge of the local ESs. Moreover, we show the performance when no energy production / injection is accounted for (referred to in the plots as Power Demand). For these results, each active user has a battery with capacity of 28Ah operating at 240V. When the harvested energy is abundant (see Fig. 4.2), the proposed algorithm performs similarly to Self Support. As shown in Fig. 4.4, in April, Self Support and Power Based provide peak leveling while also charging the local batteries. From Fig. 4.3 we

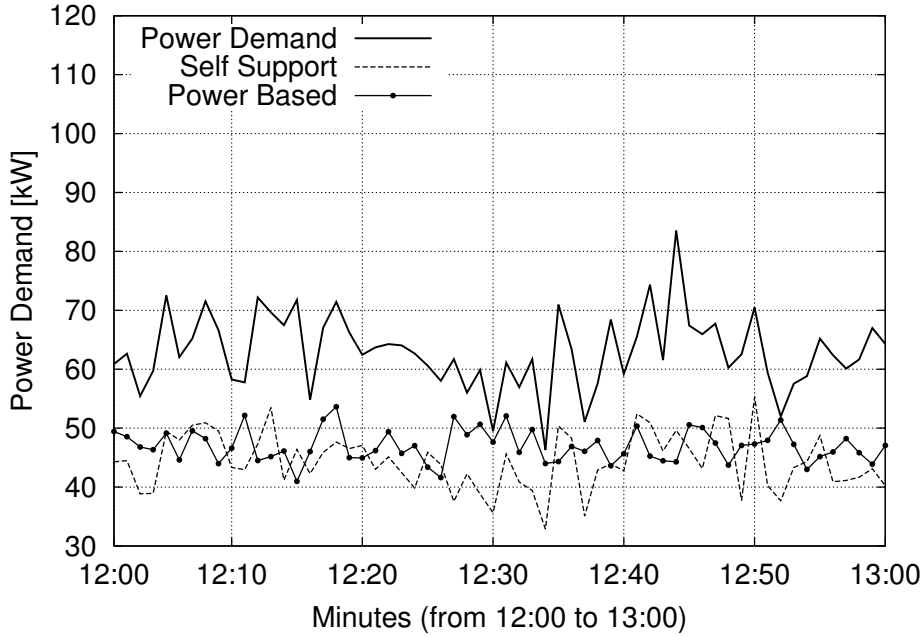


Figure 4.2. Total power demand at the UI for a typical day of April.

see that, as expected, the total demand is increased in December. In this case, the harvested energy is insufficient to fulfill the end-user demand and the distributed energy storage is utilized to support the loads and perform peak leveling. Power Demand accomplishes this task quite successfully, leveling the total demand at around $P_{G0}(\ell) = 40\text{kW}$ (that is an input parameter for the algorithm). The total power demand is thus more than halved at the expense (see Fig. 4.4) of a reduced energy reserve at the end-users. Note that our algorithm can effectively level the required power as long as there is some residual charge in the distributed batteries. In the considered example, the state of charge decreases of about 8Ah in an hour. This means that, considering an ideal behavior for the discharge process, the adopted storage units can guarantee a full support for about 3.5 hours in the considered setup (i.e., number of active users and reference value $P_{G0}(\ell)$).

The results of Figs. 4.5 and 4.6 are obtained as follows. We have considered a typical day of April and obtained the power demand and energy generation traces for all users (one sample per slot per trace). Thus, for each time slot, we have computed the difference between the total demand and the generated energy. The temporal average of this time series has been then used as the reference value $P_{G0}(\ell) \approx 15\text{kW}$ for the Power Based algorithm. Thus, we have run the Power Based algorithm for this same day, for these same traces and by

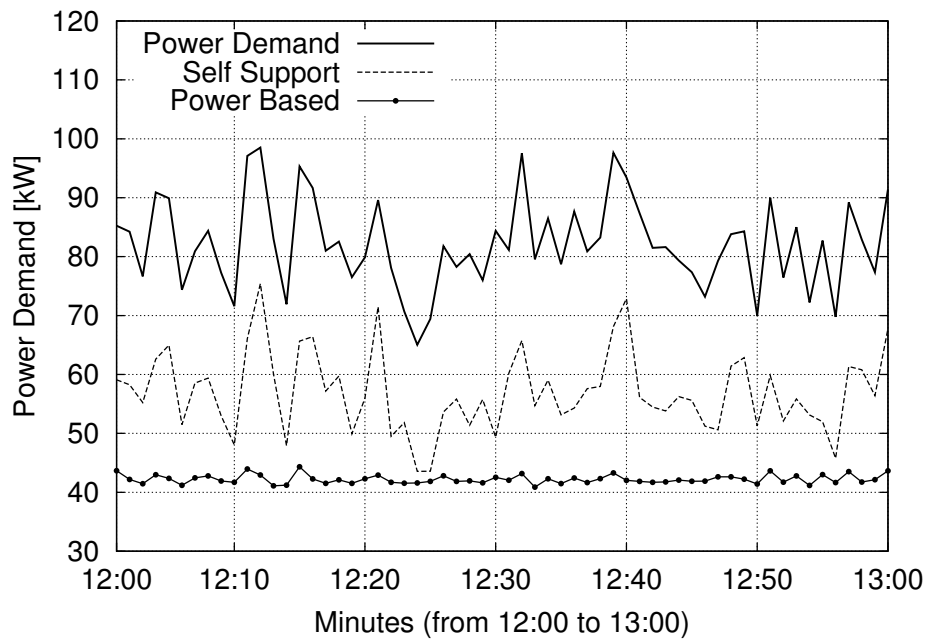


Figure 4.3. Total power demand at the UI for a typical day of December.

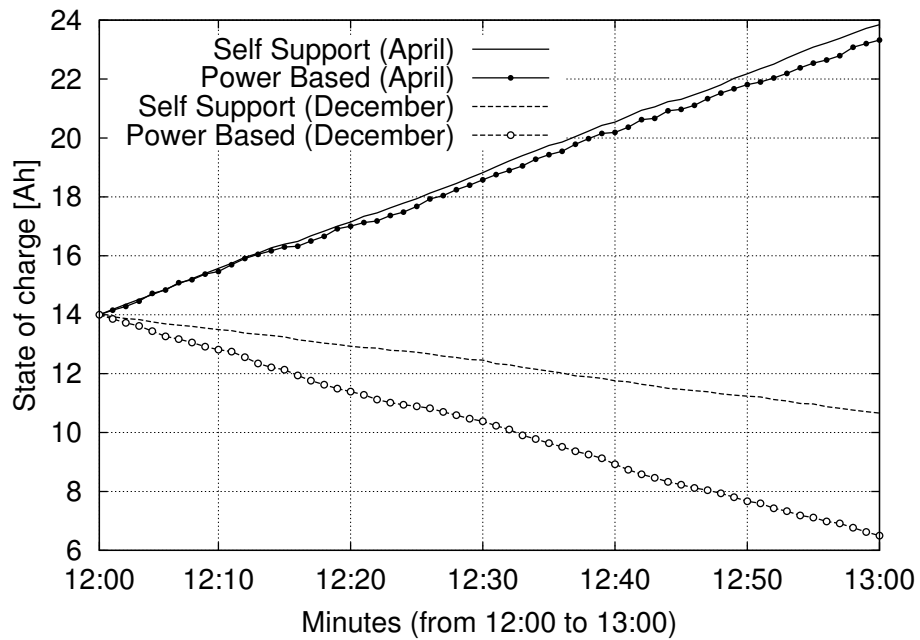


Figure 4.4. Average state of charge for an end-user storage unit (battery).

assuming a sufficiently large battery capacity (e.g., 200Ah at 240V) at each active user, so that the performance of the algorithm will not be affected by it. The rationale behind this is that we are trying to operate the network so that the minimum possible amount of power is required from the UI, by exploiting as much as possible the distributed energy generation capability of the active users. Fig. 4.5 shows the results of this experiment for a typical April's day and we see that Power Based effectively accomplishes the task of leveling the power demand around $P_{G0}(\ell) \approx 15\text{kW}$. We also observe that Power Based has a somewhat bimodal behavior: i) for a small energy (before 8 a.m. and after 3 p.m.) a more conservative behaviour is observed, slightly relaxing the total demand with respect to the target $P_{G0}(\ell)$; ii) when the energy income is abundant (between 8 a.m. and 3 p.m.) a better peak leveling is observed, taking advantage of (and lowering) the distributed energy reserve. Fig. 4.6 shows the state of charge of the battery of a typical end-user during the entire day. As seen from this plot, the required capacity is quite high and impractical due to economical and technological arguments. However, that capacity would assure the maximum exploitation of the energy production capabilities in the considered settings. As future avenues of research, note that increasing the number of active nodes would decrease the required capacity and we may also put a cap on it and check how that affects the performance as a function of the various system parameters.

4.4 Conclusions

In this chapter we have proposed a lightweight and effective algorithm for the energy management of prosumer communities. This algorithm provides satisfactory results, fulfilling its design objectives at the expense of a truly limited communication overhead (the transmission of a pair of reference values to each active user per time slot). We shed some light on battery sizing showing that, given a proper dimensioning of the storage capacity, self-sustainability is indeed possible and the proposed approach is able to reduce the total power required to the mains from a minimum of one half to a maximum of one sixth for the considered network setup. These figures, as well as the required storage capacity at the end-user side, highly depend on the number of users with energy harvesting and storage capabilities. A more detailed study of these tradeoffs is left as a future work.

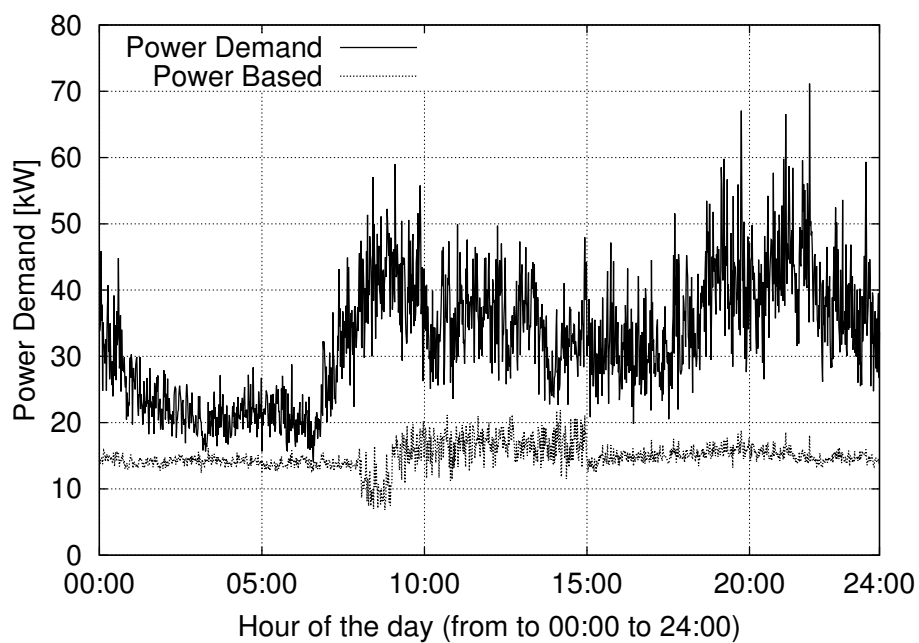


Figure 4.5. Total power demand at the UI for a typical day of April.

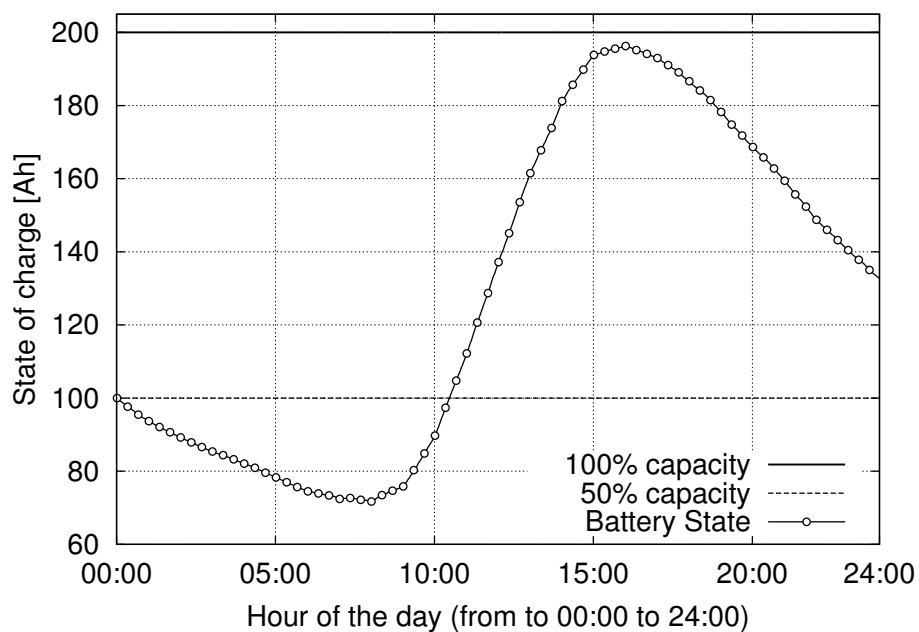


Figure 4.6. State of charge for a typical end-user in the month of April.

Optimized Energy Pricing for Smart Grid Efficiency Enforcement

5.1 Introduction

Two main phenomena are nowadays affecting traditional power distribution grids: on the one hand, the constantly increasing power demand calls for radical changes in the way the energy is generated and delivered to the final users, on the other hand, we are facing the worldwide diffusion of electrical power generation devices based on renewables [1, 10]. If injected into standard power lines without any coordination or control from grid operators, this ever increasing amount of renewable energy may destabilize current power grids, leading to instability problems, including power outages.

On this matter, recent work has shown how Distributed Energy Resources (DERs) can be used to boost the grid efficiency [11–14] in terms of power distribution losses minimization and reactive power compensation, frequency stability, peak shaving and to relieve electricity production plants from some of the power load [15]. In the last few years, several grid optimization techniques have been proposed [16–18], each exploiting some existing communication infrastructure and relying on online smart metering procedures [19]. This is to say that a coordinated and intelligent control of the distributed generation capabilities (from renewables) holds the potential on enhancing the electrical grid performance, controlling the aforementioned stability problems and, at the same time, increasing its hosting capacity.

In this chapter, we target residential micro grids where some of the end users behave as DERs, due to the exploitation of some form of renewable energy such as solar, wind, biomass, geothermal, etc. Each DER is equipped with an energy storage device (i.e., a battery) and

it is assumed to fulfill its own power needs. In addition, during each network cycle DERs can independently decide to either sell part of the stored energy to the main power supplier, which is addressed in this chapter as the Point of Common Coupling (PCC), or directly to some selected end users. In this chapter, end users buying energy are addressed as loads. Without any further regulation, DERs would sell their energy to the agents ensuring the highest revenues. This behavior could lead to non-efficient electrical conditions for the grid (i.e., high distribution power losses).

Previous work has shown how control techniques for DERs [4–7, 20] can significantly reduce distribution power losses while, at the same time, relieving the PCC from some of the power load. Instead of injecting all excess power into the grid, after local load satisfaction, the end users control their energy injection into the electricity grid in order to reduce the distribution power losses and the total power demand from the mains. It is worth noting, however, that *in real-world scenarios the power injection performed by the DERs is based on economical advantages*. Nowadays, each DER is willing to sell its surplus energy to the PCC in order to amortize the initial investment for the energy production plant (e.g., solar panels and energy storage) and its maintenance cost. For this reason, a new market model enforcing the DERs collaboration to the grid electrical efficiency is needed.

New market models for the smart grid have been studied so far in terms of demand response control and dynamic pricing strategies. Some work addressed the case where a single energy provider determines the best real time pricing policy, maximizing its own economical benefit [45, 46] or a specific quality of service function accounting for the main supplier revenue and the aggregated end users experience [47, 48]. Other research works exploit dynamic pricing policies in order to control the end users power demand, thus reducing the chance of events as, for example, power outages [49, 50]. None of these papers, however, accounts for actual grid electrical optimization techniques.

In this chapter we move a step forward, by *recognizing that real users will only change their behavior and positively contribute to the grid optimization if this will lead to economical benefits* (i.e., a monetary income). This entails the definition of new market models, whose aim is to incentivize the collaboration from the end-user possessing generation capabilities so that they will contribute to the energy efficiency of the power grid. Here, we devise an optimization framework accounting for, on the one hand, the end users economical benefit (i.e., lowering

the energy consumers expenses and guaranteeing higher profit to the DERs) and, on the other hand, for the proper execution of a selected electrical optimization technique (so as to increase the energy efficiency of the power grid and assure its stability). The proposed market model is formulated as a multi-objective optimization problem. Each grid user (i.e., loads, DERs and the PCC) is assumed to act as a *rational agent* and hence it is assumed to always try to maximize its own benefit. In the considered scenario, each DER maximizes its own profit, each load minimizes its own expense and the PCC aims at maximizing the grid electrical efficiency. Energy can be traded directly among end users (i.e., DERs and loads) or among end users and the PCC. Each DER proposes to the loads individual prices for the energy trading. The loads can then decide whether to buy energy from the DERs (according to the proposed prices) or from the PCC (according to a fixed common price). The PCC enforces the grid electrical efficiency by applying a discount policy to the prices the DERs propose to the loads. This policy drives the best trading strategy (in terms of economical benefit) for each end-user while also driving the system toward the best electrical condition (according to a selected grid optimization technique). It is worth noting that the proposed model is transparent to the chosen grid optimization technique, and hence its range of application does not reduce to a single scenario and it does not exclude future improvements in terms of electrical optimization. Moreover, our model allows the PCC (i.e., the electrical utility) to decide the importance that is given into the optimization to each performance objective, i.e., end-user revenue *vs* grid electrical efficiency. This is achieved by means of a maximum discount factor that limits the individual discount that can be applied in the energy trading between DERs and loads. Our optimization must be performed at every network cycle in order to obtain the greatest benefit from it, however, the PCC is also able to set its own prices for buying and selling energy, so that our model can account for dynamic pricing and other long-term demand-response optimization techniques.

The rest of this chapter is structured as follows. Section 5.2 introduces the considered scenario. There, we present the electrical details of the considered grid model. Moreover, the communication requirements and infrastructure needed to support the proposed model are defined. Finally, the proposed market model and the interactions among the system agents are discussed.

Section 5.3 introduces the mathematical notation that is used throughout the chapter for

the market model, the associated multi-objective optimization problem and its solution.

Section 5.4 presents the multi-objective optimization problem that needs to be solved to find the energy trading strategy that best fits all the involved agents. In this section, we show that the considered optimization problem is not convex. Nevertheless, a bijective transformation yielding a convex version of the original problem is found and the solution of the new convex problem is discussed.

In Section 5.5, the electrical grid topology and the parameters used to obtain the numerical results are discussed.

In Section 5.6, the numerical results obtained through the setup discussed in Section 5.5 are shown and discussed.

Finally, in Section 5.7, the conclusions that can be drawn from the obtained results, assessing the validity of the proposed model are discussed.

5.2 Scenario

In this section, the electrical, communication and market scenarios considered in this chapter are presented.

5.2.1 Electrical Scenario

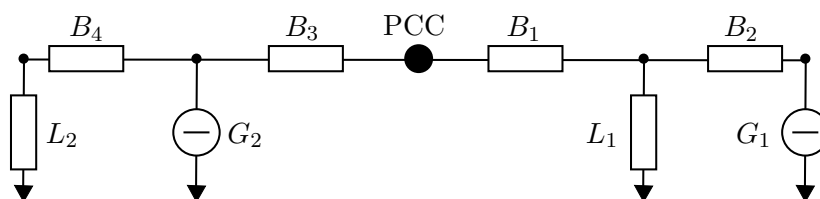


Figure 5.1. *Electrical network example.*

We consider a steady-state power micro grid. For computational ease, and without loss of generality, the considered grid is modeled as a directed tree. The root of the tree represents the Point of Common Coupling (PCC) and the other nodes represent loads and Distributed Energy Resources (DERs). Loads are either represented by constant complex impedances or by constant current sources, the PCC is modeled as a voltage generator setting the voltage reference for the entire grid, while DERs are modeled either as power or current generators.

This model has been widely considered in the literature, and in particular for power loss minimization algorithms [6, 7, 26–28].

In Fig. 5.1, an example of a power grid is shown. DER i and load j are denoted respectively by G_i and L_j . Distribution lines are assumed to have a constant section [6, 7], and hence each line has a constant impedance per unit length. The length of the z -th distribution line is denoted by B_z . Each DER is equipped with a finite-size energy storage device (e.g., rechargeable battery). The size of the energy storage devices determines the total amount of available power. Moreover, each DER is assumed to be feeding an associated load and to have the capability of injecting part of its energy surplus into the grid. The surplus power that DER G_i can inject in the grid is denoted by E_i . For the sake of terminology, the quantity E_i will be referred to as G_i 's surplus energy. In this chapter, it is assumed, without loss of generality, that $E_i > 0 \forall i$. Each load is assumed to have a non-zero power demand. The L_j 's power demand is denoted by D_j .

In the considered electrical scenario, a specific grid optimization technique is taken into account. It is worth noting that the proposed model is transparent with respect to the selected (electrical) grid optimization strategy as long as it deals with the selection of the amount of power that each DER must inject into the grid to boost its electrical efficiency.

5.2.2 Communication Scenario

Each node (i.e., loads, DERs and the PCC) in the grid is assumed to be equipped with a communication transceiver. The specific communication technology to be adopted depends on the requirements of the selected electrical optimization technique. These details are however neither considered here nor fundamental to the solution of presented optimization problem. In fact, our optimization framework is independent of the specific communication technology and infrastructure, as long as these allow the bi-directional communication between each pair of nodes.

5.2.3 Market Scenario

We propose a market scenario where each DER can either sell its surplus power to the PCC or directly to the loads. The monetary revenue that each DER obtains by selling (part of) its energy to the PCC is determined by a PCC-imposed unitary *buying price*. The monetary

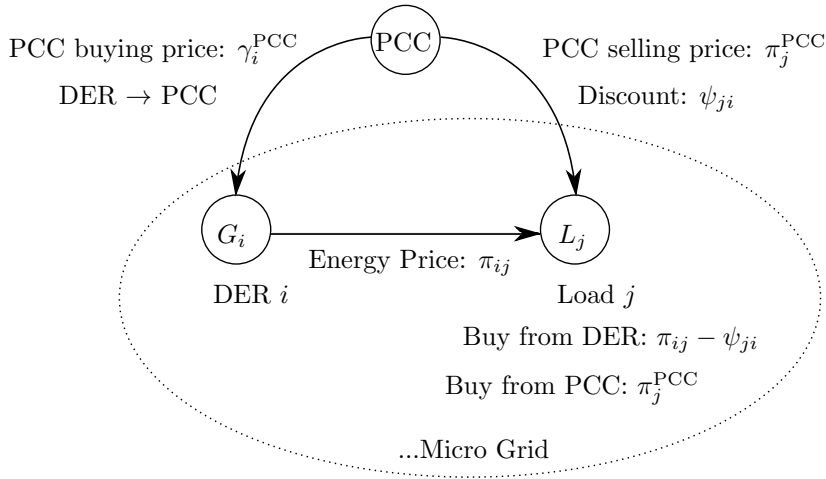


Figure 5.2. Market scenario example.

revenue that each DER obtains by selling its power directly to a specific load is determined by a DER-imposed unitary *selling price*. The latter price can differ from load to load, and is not controlled by the PCC. Also, each load can fulfill its power demand by buying the needed power from the PCC or directly from the DERs. DERs and loads are assumed to behave as *rational agents*. Thus, each DER will sell its power to the agents (PCC and loads) ensuring the highest revenue, while each load will buy the power it needs from the agents (PCC and DERs) ensuring the lowest expense.

Fig. 5.2 shows an example of the proposed market scenario. On the one hand, for each DER G_i , the PCC determines the unitary price γ_i^{PCC} . This is the unitary price that the PCC pays when buying power from DER G_i . On the other hand, for each load L_j the PCC determines the unitary price π_j^{PCC} . This is the unitary price that load L_j pays when buying power from the PCC. Moreover, each DER G_i proposes a unitary price π_{ij} to each load L_j . The unitary price π_{ij} determines the monetary revenue that G_i obtains when selling power to L_j . In order to move the grid electrical state toward the optimal solution (dictated by the selected electrical grid optimization technique), the PCC can apply a discount to the unitary prices proposed by the DERs to the loads. The discount proposed by the PCC to L_j when buying from G_i is denoted by ψ_{ji} , and the unitary price that L_j will pay to G_i will be $\pi_{ij} - \psi_{ji}$.

It is worth noting that, in the proposed model, the amount of power that G_i sells to the PCC is not injected into the grid. It is, instead, stored into G_i 's battery assuming that, at

any time, the PCC can claim its ownership and, in turn, force G_i to inject a fraction of that power into the grid. This assumption is needed so that the PCC can buy power from the DERs while, at the same time, enforcing the electrical grid's efficiency. In fact, in the DERs would inject into the grid the power they sell to the PCC, then all the available power would always be injected into the grid, making it impossible to minimize the distribution power losses.

5.3 Notation

In this section, the quantities involved in the optimization problem definition and solution and the corresponding notation are introduced.

Let \mathcal{G} be the set of active DERs in the grid, $|\mathcal{G}|=G$. Let \mathcal{L} be the set of active loads in the grid, $|\mathcal{L}|=L$.

5.3.1 Domains

Let:

$$\Pi = \{x \in \mathbb{R}_{++}^{G \times L} : x_{ij} \leq P_i, \forall i \in \mathcal{G}\} \quad (5.1)$$

be the set of matrices representing the unitary prices that the DERs can propose to the loads. The elements of Π will be denoted by Π_{ij} . The (ij) -th element of the matrix Π_{ij} is denoted by π_{ij} and represents the unitary price that G_i proposes to L_j , $\forall i \in \mathcal{G}, \forall j \in \mathcal{L}$. Let π_i and π_j denote the i -th row and the j -th column of Π_{ij} , respectively. Moreover, let $P_i, \forall i \in \mathcal{G}$ be the PCC imposed maximum unitary price that G_i can propose to the loads.

Let:

$$\mathbf{H} = \{x \in \mathbb{R}_+^{G \times (L+1)} : \sum_{j=0}^L x_{ij} = E_i, \forall i \in \mathcal{G}\} \quad (5.2)$$

be the set of matrices representing the amount of power that the DERs can sell to each buyer (the loads or the PCC). The elements of \mathbf{H} are denoted by \mathbf{H}_{ij} . The (ij) -th element of matrix \mathbf{H}_{ij} is denoted by η_{ij} and represents the amount of power that G_i sells to the j -th buyer (where $j = 0$ denotes the PCC and $j = 1, \dots, L$ denotes load L_j). Let η_i and η_j denote the i -th row and the j -th column of \mathbf{H}_{ij} , respectively.

Let:

$$\Delta = \{x \in \mathbb{R}_+^{L \times (G+1)} : \sum_{j=0}^G x_{ij} = D_i, \forall i \in \mathcal{L}\} \quad (5.3)$$

be the set of matrices representing the amount of power that the loads can buy from each seller (the DERs or the PCC). The elements of Δ are denoted by Δ_{ij} . The (ij) -th element of matrix Δ_{ij} is denoted by d_{ij} and represents the amount of power that load L_i buys from the j -th seller (where $j = 0$ denotes the PCC and $j = 1, \dots, G$ denotes G_j). Let d_i and d_j denote the i -th row and the j -th column of Δ_{ij} , respectively.

Let:

$$\Psi = \{x \in \mathbb{R}_+^{L \times G} : x_{ij} \leq \alpha \pi_{ji}, \forall i \in \mathcal{L}, \forall j \in \mathcal{G}\} \quad (5.4)$$

be the set of matrices representing the discounts that the PCC is willing to apply to the unitary prices that the DERs propose to the loads. We remark that *the discount policy is meant to drive the electrical grid state towards the optimal one, determined by the selected electrical optimization technique*. The elements of Ψ will be denoted by Ψ_{ij} . The (ij) -th element of the matrix Ψ_{ij} is denoted by ψ_{ij} and represents the discount that the PCC is willing to apply to the unitary price that G_j proposes to L_i . Moreover, let $0 \leq \alpha \leq 1$ be the PCC defined maximum discount factor (i.e., the PCC is willing to discount at most $(100\alpha)\%$ for each proposed unitary price).

Proposition 1. *The sets defined in Eqs. 5.1, 5.2, 5.3 and 5.4 are convex.*

Convexity of Π . Let $x_1, x_2 \in \Pi$ and $0 \leq \theta \leq 1$. Let $x_3 = \theta x_1 + (1 - \theta)x_2$, then:

$$\sum_{j=1}^L x_{3ij} = \theta \sum_{j=1}^L x_{1ij} + (1 - \theta) \sum_{j=1}^L x_{2ij}$$

Since $x_1, x_2 \in \Pi$, it holds true that: $\forall i \in \mathcal{G}, \sum_{j=1}^L x_{1ij} \leq P_i$ and $\forall i \in \mathcal{G}, \sum_{j=1}^L x_{2ij} \leq P_i$, hence:

$$\sum_{j=1}^L x_{3ij} \leq \theta P_i + (1 - \theta)P_i = P_i, \forall i \in \mathcal{G}$$

thus $x_3 \in \Pi$ □

Convexity of H . Let $x_1, x_2 \in H$ and $0 \leq \theta \leq 1$. Let $x_3 = \theta x_1 + (1 - \theta)x_2$, then:

$$\sum_{j=0}^L x_{3ij} = \theta \sum_{j=0}^L x_{1ij} + (1 - \theta) \sum_{j=0}^L x_{2ij}$$

Since $x_1, x_2 \in \mathbf{H}$, it holds true that: $\forall i \in \mathcal{G}, \sum_{j=0}^L x_{1ij} = E_i$ and $\forall i \in \mathcal{G}, \sum_{j=0}^L x_{2ij} = E_i$, hence:

$$\sum_{j=0}^L x_{3ij} = \theta E_i + (1 - \theta)E_i = E_i, \forall i \in \mathcal{G}$$

thus $x_3 \in \mathbf{H}$ □

Convexity of Δ . Let $x_1, x_2 \in \Delta$ and $0 \leq \theta \leq 1$. Let $x_3 = \theta x_1 + (1 - \theta)x_2$, then:

$$\sum_{j=0}^G x_{3ij} = \theta \sum_{j=0}^G x_{1ij} + (1 - \theta) \sum_{j=0}^G x_{2ij}$$

Since $x_1, x_2 \in \Delta$, it holds true that: $\forall i \in \mathcal{L}, \sum_{j=0}^G x_{1ij} = D_i$ and $\forall i \in \mathcal{L}, \sum_{j=0}^G x_{2ij} = D_i$, hence:

$$\sum_{j=0}^G x_{3ij} = \theta D_i + (1 - \theta)D_i = D_i, \forall i \in \mathcal{L}$$

thus $x_3 \in \Delta$ □

Convexity of Ψ . Let $x_1, x_2 \in \Psi$ and $0 \leq \theta \leq 1$. Let $x_3 = \theta x_1 + (1 - \theta)x_2$, then $x_{3ij} = \theta x_{1ij} + (1 - \theta)x_{2ij}, \forall i \in \mathcal{L}, \forall j \in \mathcal{G}$. Moreover $x_1 \in \Psi \implies x_{1ij} \leq \alpha \pi_{ji}, \forall i \in \mathcal{L}, \forall j \in \mathcal{G}$ and $x_2 \in \Psi \implies x_{2ij} \leq \alpha \pi_{ji}, \forall i \in \mathcal{L}, \forall j \in \mathcal{G}$, hence: $x_{3ij} \leq \alpha(\theta \pi_{ji} + (1 - \theta)\pi_{ji}) = \alpha \pi_{ji}, \forall i \in \mathcal{L}, \forall j \in \mathcal{G} \implies x_3 \in \Psi$ □

Let $H_{ij} \in \mathbf{H}$, then define: $\tilde{H}_{i.} = \{k \in \{1, \dots, L\}, k : \eta_{i,k} \neq 0\}$ and $\tilde{H}_{.j} = \{k \in \{1, \dots, G\}, k : \eta_{k,j} \neq 0\}$. These two sets determine the row and column indices, respectively, of the non zero elements of H_{ij} . Similarly, define:

$$\begin{aligned} \tilde{\Delta}_{i.} &= \{k \in \{0, \dots, G\} : d_{ik} \neq 0\} \\ \tilde{\Delta}_{.j} &= \{k \in \{1, \dots, L\} : d_{kj} \neq 0\} \end{aligned} \tag{5.5}$$

5.4 Multi-Objective Optimization Problem

The goal of this chapter is to propose an optimized market model aiming at increasing the DERs monetary revenue and reducing the loads expenses while enforcing the grid electrical efficiency. This goal is obtained by setting up and solving a multi-objective optimization problem. In this section, the multi-objective optimization problem will be defined and a convex formulation of this problem, allowing for standard interior-point solution methods, will be derived.

5.4.1 Objective Functions

Each DER will support the proposed market model only if it guarantees a higher monetary revenue with respect to the one that is nowadays implemented.

$$U_i^{\mathcal{G}}(\Pi_i, H_i) = \sum_{j=1}^L \pi_{ij} \eta_{ij} + (E_i - \sum_{j=1}^L \eta_{ij}) \gamma_i^{\text{PCC}} \quad (\forall i \in \mathcal{G}) \quad (5.6)$$

Let (Eq. 5.6) represent the monetary revenue of the i -th DER when selling the E_i amount of energy to the loads, as specified by the vector H_i . and using the unitary prices defined by Π_i .

In opposition to the DERs behavior, each load will endorse the proposed market model only if it guarantees lower expenses with respect to the current market model.

$$U_i^{\mathcal{L}}(\Pi_i, \Delta_i, \Psi_i) = \sum_{j=1}^G (\pi_{ji} - \psi_{ij}) d_{ij} + (D_i - \sum_{j=1}^G d_{ij}) \pi_i^{\text{PCC}} \quad (\forall i \in \mathcal{L}) \quad (5.7)$$

Let (Eq. 5.7) represent the expense incurred by L_i when buying D_i energy from the DERs, as specified by the vector Δ_i . and according to the discounted unitary prices $\Pi_i - \Psi_i$.

In order to drive the grid towards the optimal working condition from the electrical point of view, the power demand vectors Δ_i , $\forall i \in \mathcal{L}$ must be as close as possible to the optimal ones (i.e., Δ_i^\diamond , $\forall i \in \mathcal{L}$). The proposed market model gives the PCC the capability to enforce this condition by imposing a discount ψ_{ij} to each unitary price π_{ji} that G_j proposes to L_i .

$$U_i^{\text{PCC}}(\Delta_i) = \|\Delta_i - \Delta_i^\diamond\|_2^2 \quad (\forall i \in \mathcal{L}) \quad (5.8)$$

The effect of the imposed discounts is determined, for each load L_i , by computing the squared distance between the L_i chosen demand vector Δ_i . and the most electrically efficient one Δ_i^\diamond . Let (Eq. 5.8) represent this distance. The goal of the PCC is to determine the best discount matrix Ψ_{ij} allowing the individual minimization of the distance between the L_i chosen demand vector and the most electrically efficient one. Each individual discount ψ_{ij} is upper bounded by a common quantity $0 \leq \alpha \leq 1$ representing the maximum fraction of π_{ji} that the PCC is willing to discount (i.e., $\psi_{ij} \leq \alpha \pi_{ji}$).

5.4.2 Constraints

The electrical state of the system induces a set of constraints modeling the physical consistency of the grid. Moreover, the PCC's will to enforce the electrical efficiency of the grid

induces an additional set of constraints limiting the maximum prices that the DERs can propose to the loads and the maximum discounts that can be applied to the aforementioned prices. In this subsection, these constraints will be presented and discussed.

$$\sum_{j=1}^L \eta_{ij} \leq E_i \quad \forall i \in \mathcal{G} \quad (5.9)$$

(Eq. 5.9) imposes that each DER $G_i \in \mathcal{G}$ sells exactly the surplus energy E_i . The meaning of this constraint is twofold: on the one hand, it means that G_i can not sell more energy than the amount remaining after fulfilling its own needs; on the other hand, it models the fact that the PCC is always willing to buy any excessing energy that the DERs are selling (as it happens in nowadays distribution grids).

$$\sum_{j=1}^G d_{ij} \leq D_i \quad \forall i \in \mathcal{L} \quad (5.10)$$

(Eq. 5.10) models the fact that the loads are not equipped with energy storage devices, and hence each load must buy the exact amount of energy needed to fulfill the present power demand.

$$\eta_{ij} = d_{ji} \quad \forall i \in \mathcal{G}, \forall j \in \mathcal{L} \quad (5.11)$$

(Eq. 5.11) models the fact that the amount of energy that DER $G_i \in \mathcal{G}$ is selling to load $L_j \in \mathcal{L}$ must be equal to the amount of energy that L_j is buying from G_i . Imposing these constraints assures that no agent in the grid can act maliciously compromising the electrical state of the grid.

$$\pi_{ij} \leq P_i \quad \forall i \in \mathcal{G}, \forall j \in \mathcal{L} \quad (5.12)$$

(Eq. 5.12) models the limits that the PCC imposes to the prices that the DERs propose to the loads. The goal of these limits is twofold: on the one hand, they act as market regulators preventing the prices from growing without control; on the other hand, they determine the maximum unitary discount that the PCC is willing to apply.

$$\psi_{ij} \leq \alpha \pi_{ji} \quad \forall i \in \mathcal{L}, \forall j \in \mathcal{G} \quad (5.13)$$

(Eq. 5.13) determines the maximum fraction of the unitary prices proposed by the DERs that can be discounted by the PCC.

5.4.3 Optimization Problem

According to the objective functions defined in (Eq. 5.6), (Eq. 5.7) and (Eq. 5.8) and the constraints introduced in (Eq. 5.9), (Eq. 5.10), (Eq. 5.11), (Eq. 5.12) and (Eq. 5.13), the following minimization problem can be formulated.

$$\begin{aligned}
& \underset{\Pi_{ij}, H_{ij}, \Delta_{ij}, \Psi_{ij}}{\text{minimize}} \begin{cases} \frac{1}{U_i^{\mathcal{G}}(\Pi_{i.}, H_{i.})} & \forall i \in \mathcal{G} \\ U_i^{\mathcal{L}}(\Pi_{i.}, \Delta_{i.}, \Psi_{i.}) & \forall i \in \mathcal{L} \\ U_i^{\text{PCC}}(\Delta_{i.}) & \forall i \in \mathcal{L} \end{cases} \\
& \sum_{j=1}^L \eta_{ij} \leq E_i \quad \forall i \in \mathcal{G}, \forall j \in \mathcal{L} \\
& \text{s.t.} \quad \sum_{j=1}^G d_{ij} \leq D_i \quad \forall i \in \mathcal{L} \\
& \pi_{ij} \leq P_i \quad \forall i \in \mathcal{G}, \forall j \in \mathcal{L} \\
& \psi_{ji} \leq \alpha \pi_{ij} \quad \forall i \in \mathcal{G}, \forall j \in \mathcal{L} \\
& \eta_{ij} = d_{ji} \quad \forall i \in \mathcal{G}, \forall j \in \mathcal{L}
\end{aligned} \tag{5.14}$$

Considering (Eq. 5.14), a first characterization of the solution can be given.

Proposition 2. *Let $\pi_{ji}(1 - \alpha) > \pi_i^{\text{PCC}}$ for some $j \in \{1, \dots, G\}$ and let Δ_i^* be the i -th row of the optimal demand matrix $\Delta_{ij}^* \in \Delta$, then $d_{ij}^* = 0 \forall \psi_{ij} \in]0, \alpha \pi_{ji}]$ and hence the optimal discount value ψ_{ij}^* admits infinite solutions.*

Proof of proposition 2. Let $\pi_{ji}(1 - \alpha) > \pi_i^{\text{PCC}}$ and let Δ_i^* be the optimal demand vector for load i . If $d_{ij}^* \neq 0$, then a new vector $\bar{\Delta}_i$ such that $\bar{d}_{ij} = 0$ and $\bar{d}_{i0} = d_{i0}^* + d_{ij}^*$ can be defined. It is true, by construction, that $U_i^{\mathcal{L}}(\bar{d}_i) < U_i^{\mathcal{L}}(\Delta_i^*)$, but this is not possible because Δ_i^* is optimal and hence $d_{ij}^* = 0$. \square

According to Prop. (2), if applying the maximum discount factor α to the price that G_j proposes to L_i , this price is still higher than the PCC imposed price, then no feasible discount can make L_j buy power from G_i .

Proposition 3. *Let $\pi_{ij} < \gamma_i^{PCC}$ for some $j \in \{1, \dots, L\}$ and let H_i^* be the i -th row of the optimal allocation matrix $H_{ij}^* \in H$, then $\eta_{ij}^* = 0$ and hence the optimal discount value ψ_{ji}^* admits infinite solutions.*

Proof of proposition 3. Let $\pi_{ij} < \gamma_i^{PCC}$ and let H_i^* be the optimal allocation vector for DG i . If $\eta_{ij}^* \neq 0$, then a new allocation vector \bar{H}_i such that $\bar{\eta}_{ij} = 0$ and $\bar{\eta}_{i0} = \eta_{i0}^* + \eta_{ij}^*$ can be defined. It is true, by construction, that $U_i^G(\bar{H}_i) > U_i^G(H_i^*)$, but this is not possible because H_i^* is optimal and hence $\eta_{ij}^* = 0$. \square

Prop. (3) states that if the revenue that G_i obtains selling its power to the PCC is greater than the maximum revenue that can obtain by selling it to L_j , then again there is no way for the PCC to enforce the electrical grid efficiency.

Prop. (2) and Prop. (3) state that, in order for the PCC to be able to enforce the grid electrical efficiency by applying a discount policy, the following conditions must hold true $\forall i \in \mathcal{G}, j \in \mathcal{L}$:

$$\pi_{ij} \geq \gamma_i^{PCC} \text{ and } \pi_{ij}(1 - \alpha) \leq \pi_j^{PCC} \quad (5.15)$$

Proposition 4. *Let η_{ij}^* , d_{ji}^* be the optimal ij -th allocation and ji -th demand values (according to the respective indexing) for the optimization problem in (Eq. 5.14), then, according to propositions 2 and 3, either:*

1. $\eta_{ij}^* = d_{ji}^* = 0$ if $\pi_{ij}(1 - \alpha) > \pi_j^{PCC}$ or $\pi_{ij} < \gamma_i^{PCC}$
2. $\eta_{ij}^* = d_{ji}^* \neq 0$ otherwise.

Proof. Considering propositions 2 and 3, and recalling that both the DERs and the loads are rational agents, the only case in which it is economically convenient for G_i to sell power to L_j is when it can get a higher revenue than the one it would obtain selling the same amount of power to the PCC. \square

Prop. (4) follows from Prop. (2) and Prop. (3). It states that the PCC can enforce the grid efficiency only if the conditions of (Eq. 5.15) are met. Moreover, it states that if these conditions are met, the rational behavior for DERs and loads will be to adhere to the discount policy proposed by the PCC and trading energy with the agents guaranteeing bigger revenues and smaller expenses for the DERs and loads respectively.

Proposition 5. Let π_{ij}^* be the optimal ij -th price value for the optimization problem in (Eq. 5.14), and let $\eta_{ij}^* = d_{ji}^* \neq 0$. Then, according to propositions 2, 3 and 4, it must hold true that:

1. $\pi_j^{PCC} < \pi_{ij}^* - \psi_{ji}$ for at least one value of ψ_{ji}
2. $\pi_{ij}^* > \gamma_i^{PCC}$

Proof. Considering propositions 2, 3 and 4 and recalling that loads are rational agents, the only case in which L_j will buy power from G_i is when the discounted price proposed by G_i is lower than the price it would pay to the PCC. Moreover, recalling that DERs are also rational agents, the only case in which G_i will sell power to L_j is the one in which its revenue is higher than the one it can get from the PCC. \square

Prop. (5) descends from Prop. (4). It states that, in order for the DERs and loads to adhere to the proposed model, the proposed discounts (limited to a fraction α of the proposed prices) must meet the rational behavior of the trading agents.

Solving the multi-objective minimization problem proposed in (Eq. 5.14) does not lead to a unique solution. Since the goals of the objective functions defined in (Eq. 5.6), (Eq. 5.7) and (Eq. 5.8) are contrasting. Hence, simultaneously minimizing these objective functions leads to a set of solutions called **Pareto Frontier (PF)**.

Proposition 6. The problem in (Eq. 5.14) is not convex.

Proof of proposition 6. In order to prove the non convexity of (Eq. 5.14) it is sufficient to show that one of its objective functions is not convex. Considering $U_i^G(\Pi_i, H_i)$, since $U_i^G(\Pi_i, H_i)$ is twice differentiable in its domain the Hessian matrix $H_{U_i^G(\Pi_i, H_i)}$ can be computed:

$$H_{U_i^G(\Pi_i, H_i)} = \left[\begin{array}{c|c} A & B \\ \hline B & A \end{array} \right]$$

where $A \in \{0\}^{L \times L}$ and B is the $L \times L$ identity matrix. $H_{U_i^G(\Pi_i, H_i)}$ is a permutation matrix. Let $z \in \mathbb{R}^{2L}$ and let $z_1, z_2 \in \mathbb{R}^L : z^T = [z_1^T z_2^T]$, then:

$$z^T H_{U_i^G(\Pi_i, H_i)} z = [z_2^T z_1^T] z$$

and hence $H_{U_i^G(\Pi_i, H_i)}$ is not positive semidefinite nor it is negative semidefinite. \square

According to Prop. (6), solving the problem in (Eq. 5.14) with standard convex multi-objective solution methods could not lead to the actual PF. In the following subsection, a convex transformation of the proposed problem, allowing for standard solution methods, will be discussed.

5.4.4 Geometric Programming Formulation

Since the DERs' and loads' objective functions can be expressed in posynomial form, the non-convex multi-objective minimization problem presented in (Eq. 5.14) can be formulated in a geometric programming framework [51–53]. In this subsection, the steps leading to this transformation will be presented and discussed.

Considering (Eq. 5.6), it can be expressed in the form:

$$U_i^{\mathcal{G}}(\Pi_i, \mathbf{H}_i) = \sum_{j=1}^L \pi_{ij} \eta_{ij} + \eta_{i0} \gamma_i^{\text{PCC}} \quad \forall i \in \mathcal{G} \quad (5.16)$$

Defining:

$$\alpha_j^{\mathcal{G}} = \begin{cases} 0 & \text{if } j = 0 \\ 1 & \text{otherwise} \end{cases} \quad (5.17)$$

and

$$c_{ij}^{\mathcal{G}} = \begin{cases} \gamma_i^{\text{PCC}} & \text{if } j = 0 \\ 1 & \text{otherwise} \end{cases} \quad (5.18)$$

and letting $\pi_{i0} \in \mathbb{R} \forall i \in \mathcal{G}$, then (Eq. 5.16) can be formulated as a posynomial function:

$$U_i^{\mathcal{G}}(\Pi_i, \mathbf{H}_i) = \sum_{j=0}^L c_{ij}^{\mathcal{G}} \pi_{ij}^{\alpha_j^{\mathcal{G}}} \eta_{ij} \quad \forall i \in \mathcal{G} \quad (5.19)$$

Similarly, (Eq. 5.7) can be re-formulated as:

$$U_i^{\mathcal{L}}(\Pi_i, \Delta_i, \Psi_i) = \sum_{j=1}^G (\pi_{ji} - \psi_{ij}) d_{ij} + d_{i0} \pi_i^{\text{PCC}} \quad \forall i \in \mathcal{L} \quad (5.20)$$

Defining:

$$\alpha_j^{\mathcal{L}} = \begin{cases} 0 & \text{if } j = 0 \\ 1 & \text{otherwise} \end{cases} \quad (5.21)$$

and

$$c_{ij}^{\mathcal{L}} = \begin{cases} \pi_i^{\text{PCC}} & \text{if } j = 0 \\ 1 & \text{otherwise} \end{cases} \quad (5.22)$$

Then (Eq. 5.20) can also be formulated as a posynomial function:

$$U_i^{\mathcal{L}}(\Pi_i, \Delta_i, \Psi_i) = \sum_{j=0}^G c_{ij}^{\mathcal{L}} \pi'_{ji}{}^{\alpha_j^{\mathcal{L}}} d_{ij} \quad \forall i \in \mathcal{L} \quad (5.23)$$

Where $\pi'_{ji} = \pi_{ji} - \psi_{ij}$.

Applying the geometric programming transformation detailed in [52], (Eq. 5.19) and (Eq. 5.23) can be transformed in convex functions:

$$U_i^{\mathcal{G}}(\Pi_i, \mathbf{H}_i) = \sum_{j \in \tilde{\mathbf{H}}_i} e^{\alpha_j^{\mathcal{G}} \log \pi_{ij} + \log \eta_{ij} + \log c_{ij}^{\mathcal{G}}} \quad (5.24)$$

$$U_i^{\mathcal{L}}(\Pi_i, \Delta_i, \Psi_i) = \sum_{j \in \tilde{\Delta}_i} e^{\alpha_j^{\mathcal{L}} \log \pi'_{ji} + \log d_{ij} + \log c_{ij}^{\mathcal{L}}} \quad (5.25)$$

For what has been said so far, the non-convex multi-objective minimization problem defined in (Eq. 5.14) can be transformed in a convex multi-objective minimization problem:

$$\begin{aligned} \min_{(\pi)_{ij}, (\eta)_{ij}, (d)_{ij}, (\psi)_{ij}} & \left\{ \begin{array}{ll} \log \left(\frac{1}{U_i^{\mathcal{G}}(\Pi_i, \mathbf{H}_i)} \right) & \forall i \in \mathcal{G} \\ \log \left(U_i^{\mathcal{L}}(\Pi_i, \Delta_i, \Psi_i) \right) & \forall i \in \mathcal{L} \\ U_i^{\text{PCC}}(\Delta_i) & \forall i \in \mathcal{L} \end{array} \right\} \\ \sum_{j=1}^L \eta_{ij} \leq E_i & \quad \forall i \in \mathcal{G}, \forall j \in \mathcal{L} \\ \sum_{j=1}^G d_{ij} \leq D_i & \quad \forall i \in \mathcal{L} \\ \text{s.t.} \quad \pi_{ij} \leq P_i & \quad \forall i \in \mathcal{G}, \forall j \in \mathcal{L} \\ \psi_{ji} \leq \alpha \pi_{ij} & \quad \forall i \in \mathcal{G}, \forall j \in \mathcal{L} \\ \eta_{ij} = d_{ji} & \quad \forall i \in \mathcal{G}, \forall j \in \mathcal{L} \\ \pi'_{ji} = \pi_{ji} - \psi_{ij} & \quad \forall i \in \mathcal{L}, \forall j \in \mathcal{G} \end{aligned} \quad (5.26)$$

5.4.5 Solution

The problem defined in (Eq. 5.26) can be addressed by mean of standard convex solution methods. Since the problem in (Eq. 5.26) is convex, the duality gap is zero and the Karush-Kuhn-Tucker (KKT) optimality conditions can be applied.

In order to apply standard convex optimization methods, the problem in (Eq. 5.26) must be scalarized. Let $\bar{\lambda} \in [0, 1]^{G+2L} : \sum_{i=1}^{G+2L} \lambda_i = 1$, then the convex and scalarized objective

function will be:

$$\begin{aligned}
U(\Pi_{ij}, \mathbf{H}_{ij}, \Delta_{ij}, \Psi_{ij}) &= \sum_{i=1}^G \lambda_i \log\left(\frac{1}{U_i^{\mathcal{G}}(\Pi_i, \mathbf{H}_i)}\right) + \\
&+ \sum_{i=1}^L \lambda_{i+G} \log(U_i^{\mathcal{L}}(\Pi_i, \Delta_i, \Psi_i)) + \\
&+ \sum_{i=1}^L \lambda_{i+G+L} U_i^{\text{PCC}}(\Delta_i)
\end{aligned} \tag{5.27}$$

Then, the scalarized convex minimization problem can be defined:

$$\begin{aligned}
&\min_{\Pi_{ij}, \mathbf{H}_{ij}, \Delta_{ij}, \Psi_{ij}} U(\Pi_{ij}, \mathbf{H}_{ij}, \Delta_{ij}, \Psi_{ij}) \\
&\quad \sum_{j=1}^L \eta_{ij} \leq E_i \quad \forall i \in \mathcal{G}, \forall j \in \mathcal{L} \\
&\quad \sum_{j=1}^G d_{ij} \leq D_i \quad \forall i \in \mathcal{L} \\
\text{s.t.} \quad &\pi_{ij} \leq P_i \quad \forall i \in \mathcal{G}, \forall j \in \mathcal{L} \\
&\psi_{ji} \leq \alpha \pi_{ij} \quad \forall i \in \mathcal{G}, \forall j \in \mathcal{L} \\
&\eta_{ij} = d_{ji} \quad \forall i \in \mathcal{G}, \forall j \in \mathcal{L} \\
&\pi'_{ji} = \pi_{ji} - \psi_{ij} \quad \forall i \in \mathcal{L}, \forall j \in \mathcal{G}
\end{aligned} \tag{5.28}$$

The problem detailed in (Eq. 5.28) is a standard convex minimization problem, hence, if the problem is feasible, an optimal solution is guaranteed to exist $\forall \bar{\lambda} \in [0, 1]^{G+2L} : \sum_{i=1}^{G+2L} \bar{\lambda}_i = 1$. The **Pareto frontier** is the set of all the optimal solutions obtained for every possible weight vector $\bar{\lambda}$. It is worth noting that, since all the points in the Pareto frontier are equally optimal, it is up to the final user to determine the particular weight vector satisfying his own needs.

5.5 Simulation Setup

In this section, the electrical grid topology and the electrical scenarios (in terms of power demand at the loads and power availability at the DERs) that have been used in order to assess the performance of the proposed optimization process are discussed.

In order to assess the performance of the model proposed in Section 5.4, the electrical grid of Fig. 5.1 has been considered as a case study. To determine the optimal power demand matrix, the Current Based Surround Control algorithm (CBSC, [6]) has been selected as

the electrical grid efficiency control technique, although we recall that other optimization techniques could be used in combination with our optimization framework.

CBSC groups the nodes into *clusters*. Clusters are defined by checking, for any pair of DERs, whether their connecting path includes any other DER or the PCC. If this is not the case, a *cluster* is defined as the set containing the two DERs, the associated nodes, and all the nodes between them in the electrical network topology. For each cluster, the DER that is closest to the PCC is elected as the cluster head (CH). In the case where one of the two DERs in the cluster is the PCC, this is elected as the CH (i.e., we assume that the PCC has better communication and computational resources with respect to the other nodes). The current injected for optimization purposes is scaled by a real factor $0 \leq \xi \leq 1$ such that, referring to I_C as the total current needed in the cluster, the currents injected by the two DERs in the cluster are ξI_C and $(1 - \xi)I_C$. The parameter ξ is determined for each cluster according to the instantaneous power demand from the loads therein and branch impedances. Hence, this technique requires that every node is a smart node (i.e., equipped with metering, communication and control capabilities).

The reason why the CBSC algorithm has been chosen is twofold. On the one hand, it allows to drive the grid to the theoretical optimal electrical regime, and hence it allows the assessment of the optimization process ability to drive the power grid toward its maximum electrical efficiency. On the other hand, the communication infrastructure requirements needed to implement CBSC are the same needed to implement the proposed optimization strategy. Both techniques, indeed, require that each node is equipped with a smart metering device (in order to determine the exact power availability, power demand and line impedance) and a transceiver (in order for each node to communicate the measured data to the selected receiver).

According to CBSC, the optimal power allocation matrix, for the considered grid topology, is:

$$\Delta_{ij}^{\circ} = \begin{bmatrix} B_2 \frac{D_1}{B_1 + B_2} & 0 \\ 0 & D_2 \end{bmatrix} \quad (5.29)$$

The length of the distribution lines has been set according to table Tab. 5.1.

The power demand of the loads has been set to 100 kW for both L_1 and L_2 . Hence, according to (Eq. 5.29) and Tab. 5.1, the optimal power demand matrix is:

Table 5.1. *Distribution lines length in meters*

\mathbf{B}_1	\mathbf{B}_2	\mathbf{B}_3	\mathbf{B}_4
50 m	50 m	45 m	90 m

Table 5.2. *DERs Power Availability*

\mathbf{G}_1	50kW	60kW	100kW
\mathbf{G}_2	100kW	90kW	100kW

$$\Delta_{ij}^{\diamond} = \begin{bmatrix} 50\text{kW} & 0 \\ 0 & 100\text{kW} \end{bmatrix} \quad (5.30)$$

Given the optimal power demand matrix of (Eq. 5.29), three electrical scenarios have been considered. The first scenario will be referred to as *tight power offer* and it addresses the case where the individual available power for each DER equals the total power that it should inject according to CBSC.

The second scenario that has been considered is referred to as *unbalanced tight power offer* and it allows to study the case where the total available power equals that dictated by CBSC, but the individual power availability does not match the CBSC requirements. In this case, the optimal electrical grid conditions can not be reached.

The third scenario that has been taken into account is referred to as *loose power offer*. This scenario considers the case where the total power availability exceeds the total power demand.

The DERs power availability for each considered scenario is shown in Tab. 5.2.

5.6 Results

In this section, the experimental results obtained by applying the proposed optimization process to the case study described in Section 5.5 are shown.

For each scenario introduced in Section 5.5, the performance of the optimization process has been assessed in terms of:

- the DERs monetary gain with respect to the case where the surplus power is entirely sold to the PCC;

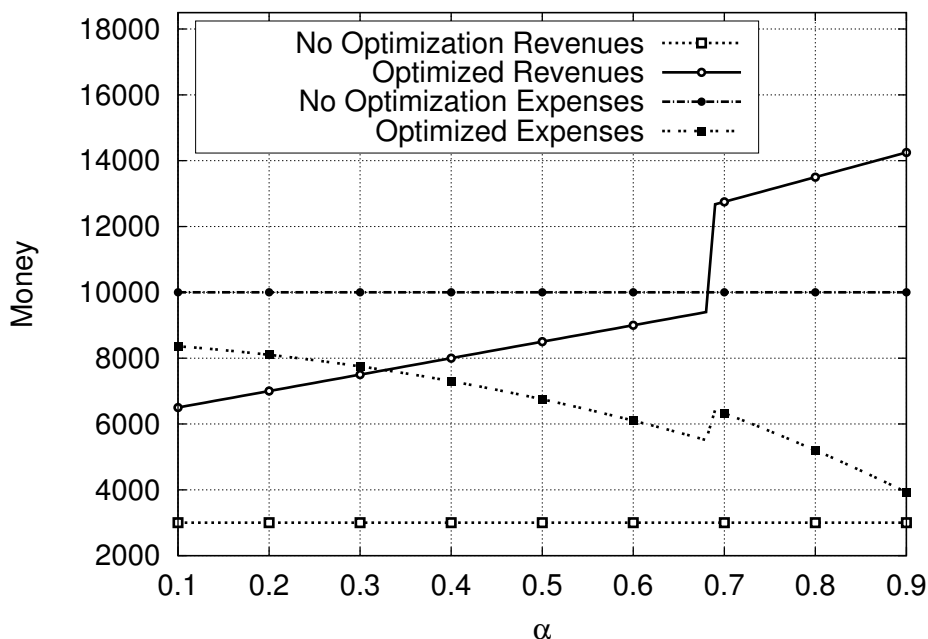


Figure 5.3. Aggregated revenue and aggregated expense. Tight money case.

- the loads expenses with respect to the case in which all the required power is bought from the PCC;
- the achieved electrical efficiency with respect to the theoretical optimal conditions achieved by CBSC.

5.6.1 Tight Power Offer

In this section, the tight power offer scenario is addressed. In this case, both G_1 and G_2 sell the exact amount of power dictated by the PCC. Fig. 5.3 shows the DERs aggregate revenue and the loads aggregate expense obtained through the proposed optimization when the maximum discount factor α varies from 10% to 90%. As a term of comparison, the aggregate revenue obtained by DERs and the aggregate expense incurred by the loads when no optimization is applied (i.e., the surplus power is sold in full to the PCC by the DERs and all the required power is bought from the PCC by the loads) have been plotted. A first noticeable result is that, for every value of α , the optimized aggregate revenue is always larger than that in the non-optimized scenario. Moreover, the aggregate expense is always smaller than the non-optimized one. This behavior is highly desirable, since it guarantees to all the

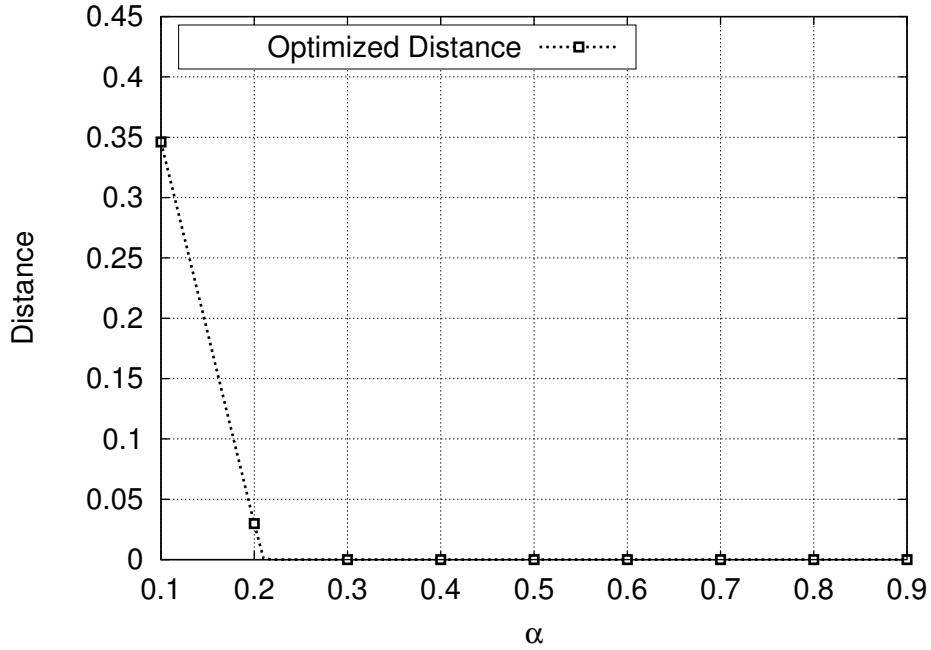


Figure 5.4. *Electrical efficiency in terms of distance from optimal electrical condition. Tight money case.*

agents involved in the energy trading process that endorsing the proposed optimization leads to a *substantial economical convenience*.

When computing the distance from the electrically efficient condition, the norm of the difference $\Delta_{i,\cdot} - \Delta_{i,\cdot}^\diamond$ is computed for each load $i \in \mathcal{L}$. The plotted distance is thus the sum of the L individual distances. Fig. 5.4 shows, for $\alpha = 10\%, \dots, 90\%$, the distance between the power demand matrix obtained through the proposed optimization and the optimal one obtained through CBSC. It can be noticed that when the maximum discount factor reaches 21%, the electrical efficiency obtained through the proposed optimization equals the theoretical optimal electrical efficiency obtained by CBSC.

Fig. 5.3 and Fig. 5.4 show that, for a maximum discount factor of 21% on the prices proposed by the DERs to the loads, a Pareto optimal solution that guarantees the maximum achievable electrical efficiency while allowing to double the aggregate revenue of DERs with respect to the non-optimized case. Moreover, by endorsing the proposed optimization scheme, the consumers will incur sensibly smaller expenses.

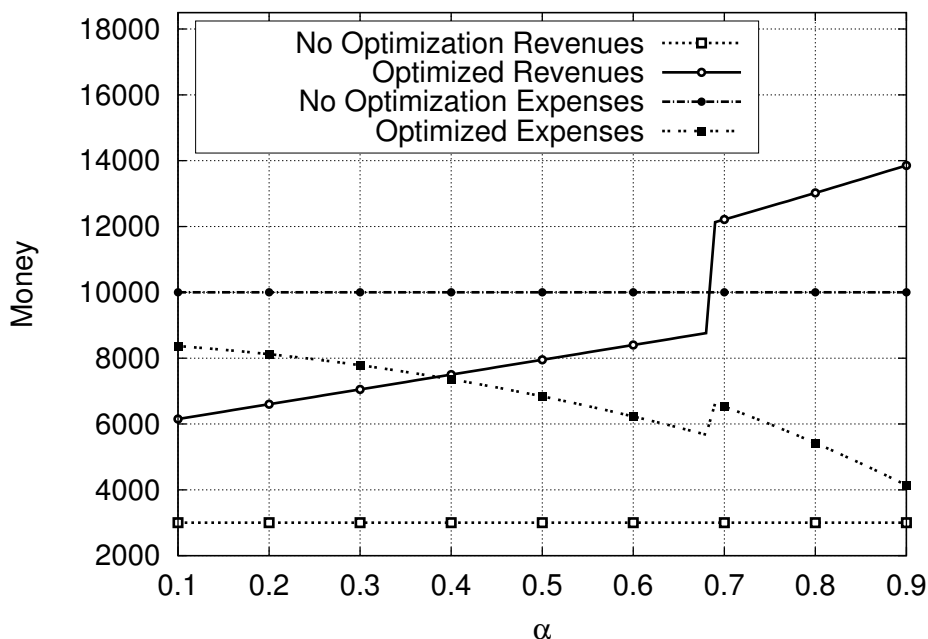


Figure 5.5. *Aggregated revenue and aggregated expense. Unbalanced tight money case.*

5.6.2 Unbalanced Tight Power Offer

In this section, the unbalanced tight power offer scenario is addressed. In this case, G_1 is willing to sell more power than the amount dictated by the CBSC algorithm, while G_2 , on the contrary, is selling less power than what dictated by CBSC. Fig. 5.5 shows the DERs aggregate revenue and the loads aggregate expense obtained through the proposed optimization when the maximum discount factor α varies from 10% to 90%. As a term of comparison, the aggregate revenue obtained DERs and the aggregate expense in which the loads incur when no optimization is applied to the system (i.e., all the surplus power is sold to the PCC by the DERs and all the needed power is bought from the PCC by the loads) have been plotted. As in the previous case, endorsing the proposed optimization will lead to economical benefits for both the DERs and the loads. Fig. 5.6 shows, as for the previous case, the distance between the power demand matrix obtained through the proposed optimization and the optimal one obtained through CBSC. The considered scenario does not allow to reach the theoretical optimal electrical efficiency. As a matter of fact, even though the total available power equals the one needed by CBSC, G_1 has more available power than what is needed, while G_2 has less available power than that required. Hence, no configuration exists for which the power allocation matrix obtained through the proposed optimization approach can match the

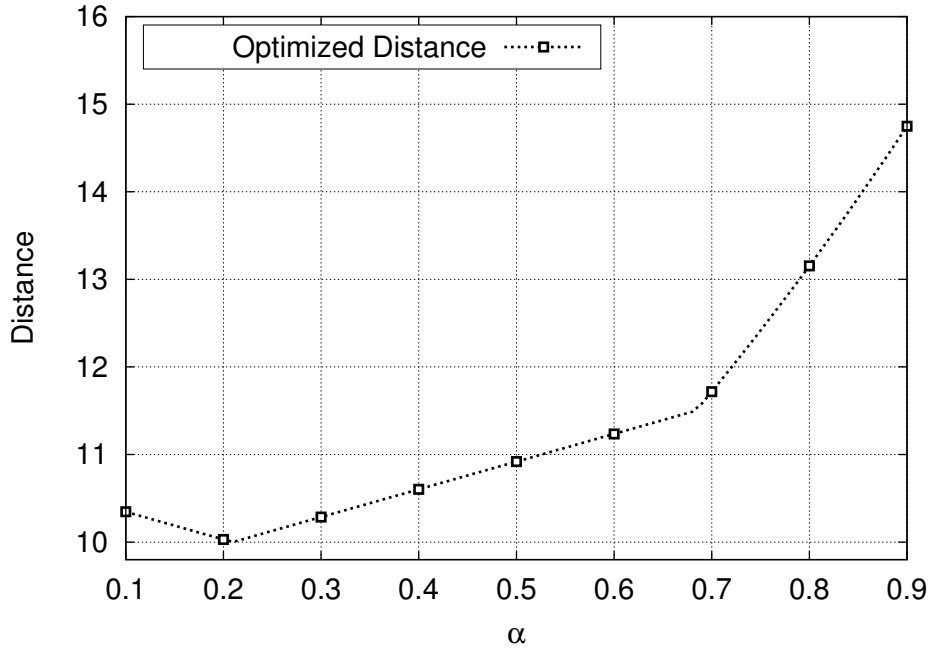


Figure 5.6. *Electrical efficiency in terms of distance from optimal electrical condition. Unbalanced tight money case.*

optimal power demand matrix. It can nevertheless be noted that, for a maximum discount factor of $\alpha = 20\%$, the optimization process reaches the minimum achievable distance from the theoretical optimal working condition. In contrast with the previous case, in this scenario there exists, for the selected weight vector λ , a single maximum discount factor that allows to maximize the electrical grid efficiency. This behavior is due to the fact that configurations exist for which DERs and loads individual interests drive the grid toward a non-optimal power allocation condition (i.e., G_1 , instead of selling 10 kW to the PCC, it starts trading with L_2 inducing a sub-optimal electrical efficiency).

As for the previous case, Fig. 5.5 and Fig. 5.6 show that the proposed optimization always ensures economical benefits for both DERs and loads while, at the same time, leading to an increased electrical grid efficiency.

5.6.3 Loose Power Offer

This section addresses the loose power offer scenario. In this case, G_1 sells more power than what dictated by CBSC, while G_2 sells the exact amount of power dictated by the CBSC algorithm.

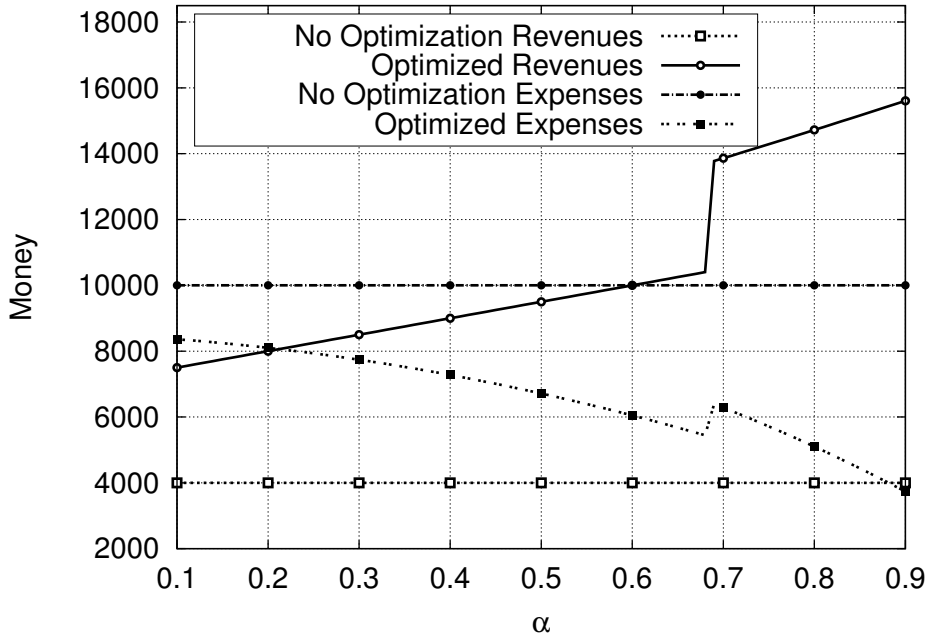


Figure 5.7. Aggregated revenue and aggregated expense. Loose money case.

Fig. 5.7 shows the performance of the proposed optimization in terms of economical benefits for the DERs and the loads. As for the previous cases, it can be noted that the proposed optimization always guarantees higher revenues and smaller expenses with respect to the case where the PCC is the only agent trading electrical power (i.e., all power has to be uniquely sold to or bought from the PCC).

Fig. 5.8 shows that for $\alpha = 20\%$ the optimal electrical configuration is reached. In this case, G_1 sells 50 kW to L_1 and the remaining available power is sold to the PCC. As α grows, G_1 starts selling more power to L_1 and hence the distance from the optimal electrical condition starts increasing. As for the previous case, for the selected weight vector λ , a single value of α exists for which the electrical efficiency is maximized (i.e., the distribution power losses are minimized).

The presented results show that, for every considered power configuration, the proposed optimization approach results in substantial economical benefits and is likely to drive the power grid toward its maximum electrical efficiency. It is worth noting that, in the considered examples, the discount factor that is required to reach the electrical grid efficiency is never higher than 21%. This is appealing as it shows that the maximum discount remains rather small, irrespective of the network configuration. This may be especially convenient for the

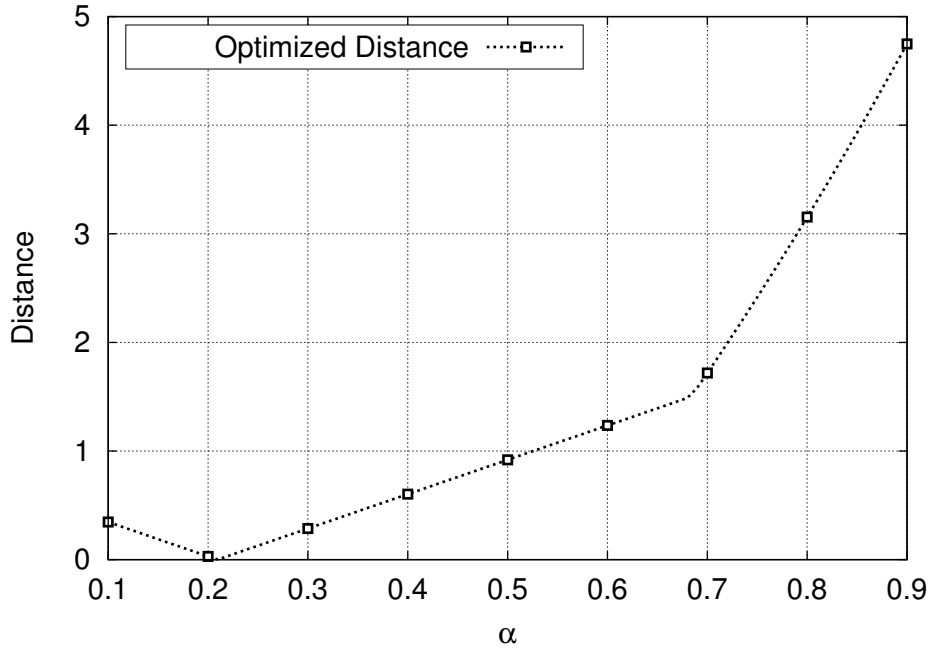


Figure 5.8. *Electrical efficiency in terms of distance from optimal electrical condition. Loose money case.*

grid operator in practical scenarios.

5.7 Conclusions

In this chapter, an original market model for smart grids has been presented. The proposed framework jointly accounts for end users economical benefits and electrical grid efficiency maximization. This model has been formally described in terms of a non convex multi-objective optimization problem. The non convex multi-objective problem has then been transformed into a convex one through a bijective transformation based on geometric programming. Optimal trading and discount policies have been devised through the solution of the convex version of the considered problem. The performance of the proposed market model has then been tested in terms of achievable economical benefit for the end users (i.e., the DERs aggregate profit and the loads aggregate expense). Three power configurations have been considered and the proposed optimization framework has been evaluated for each of them for an example network setup. The first configuration relates to the case where the power availability of DERs matches the optimal power allocation matrix dictated by

the CBSC algorithm. The second configuration relates to the case in which the total power availability from DERs exactly matches the total power demand from the loads, but the optimal configuration can not be reached as DERs are not able to individually inject the needed amount of power. The third configuration relates to the case where the power availability exceeds the total power demand. Numerical results show that for each of the three considered configurations, the proposed market model guarantees considerable economical benefits for both the DERs and the loads. Moreover, it is shown that the smart grid can be always driven to a solution where its electrical efficiency is optimal and this entails the use of discount factors smaller than 21%.

In this doctoral thesis, several aspects involving the emerging smart grid technology have been considered. The main considered aspects are the impact of communication impairments and of control action scheduling on the performance of distributed power loss minimization techniques, the design of a new peak shaving procedure and the definition of an original market model accounting for optimal pricing policies allowing for the enforcement of the grid electrical efficiency.

In the first chapter, a reference simulation framework for the performance assessment of distributed power loss minimization techniques has been designed. Using this framework, the performance of four selected state-of-the-art grid optimization techniques has been assessed in the presence of communication link failures and real-world photovoltaic power generation and power demand traces. Numerical results have shown that the performance of these techniques, in terms of power loss minimization, convergence time and PCC workload reduction vary greatly as the grid connectivity (in terms of percentage of working communication links) decreases. However, in most cases the correct configuration of the selected algorithms allows for a convergence time performance of a few line cycles, leading to substantial improvements in terms of power losses and corresponding amount of power drained from the mains.

In the second chapter, we assessed the impact that the control action scheduling has on the convergence rate of two state-of-the-art distributed power loss minimization techniques. The optimal scheduling that maximizes the convergence rate of the selected techniques has been devised and a heuristic and lightweight scheduling algorithm has been designed. Numerical results have shown that the proposed scheduling strategy allows to save up to 2 MJ during each network cycle.

In the third chapter, we designed a lightweight and distributed peak shaving algorithm. Numerical results based on real-world photovoltaic power generation and power demand traces show that the proposed strategy makes it possible to efficiently level out peaks in the aggregated grid power demand when even a small fraction of the end-users is equipped with photovoltaic panels and energy storage devices.

In the fifth chapter, we proposed a new energy market model accounting for distributed energy sources from renewables, and the trading of the locally generated energy with other users or with the grid operator. Smart metering devices and a suitable communication infrastructure are accounted for to drive the market optimization, while jointly looking at the electrical state of the power grid. Specifically, we have developed a multi-objective optimization problem whose solution yields the optimal energy pricing strategies, i.e., yielding the maximum economical benefits for the agents involved in the energy trading, while enforcing the grid electrical efficiency. Numerical results show that the proposed optimization greatly outperforms the non-optimized scenario both in terms of economical benefit and electrical efficiency.

List of Publications

The work presented in this thesis has appeared in the articles reported below.

Journal papers

- [J1] **Riccardo Bonetto**, Michele Rossi, Stefano Tomasin and Michele Zorzi, “Networking for Power Loss Minimization in Smart Micro Grids: Design Rules and Performance Assessment”, [arXiv:1311.6949]. Submitted to *IEEE Transactions on Industrial Informatics*.

Conference papers

- [C1] **Riccardo Bonetto**, Nicola Bui, Michele Rossi and Michele Zorzi, “McMAC: a power efficient, short preamble Multi-Channel Medium Access Control protocol for wireless sensor networks”, *Workshop on NS3 (WNS3) 2012*, Sirmione, Italy, 23 March 2012.
- [C2] **Riccardo Bonetto**, Nicola Bui, Vishwas Lakkundi, Alexis Olivereau, Alexandru Serbanati and Michele Rossi, “Secure Communication for Smart IoT Objects: Protocol Stacks, Use Cases and Practical Examples”, *IEEE IoT-SoS Workshop*, San Francisco, CA, US, 2012.
- [C3] **Riccardo Bonetto**, Stefano Tomasin and Michele Rossi, “When Order Matters: Communication Scheduling for Current Injection in Micro Grids”. Accepted for presentation at *IEEE International Conference on Industrial Technology 2015 (ICIT2015)*, Seville, ES, 17-19 March 2015.
- [C4] **Riccardo Bonetto**, Tommaso Caldognetto, Simone Buso, Michele Rossi, Stefano Tomasin and Paolo Tenti, “Lightweight Energy Management of Islanded Operated Mi-

crogrids for Prosumer Communities”. Accepted for presentation at *IEEE PES Conference on Innovative Smart Grid Technologies 2015 (ISGT2015)*, Washington, DC, U.S., 17-20 February 2015.

Bibliography

- [1] EIA, “Annual energy outlook 2013 with projections to 2040,” Office of Communications, EI-40 Forrestal Building, Independence Avenue, S.W. Washington, DC 20585, 2013.
- [2] F. Blaabjerg, R. Teodorescu, M. Liserre, and A. Timbus, “Overview of control and grid synchronization for distributed power generation systems,” *IEEE Trans. Industrial Electronics*, vol. 53, no. 5, pp. 1398–1409, Oct. 2006.
- [3] R. Majumder, “Reactive power compensation in single-phase operation of microgrid,” *IEEE Trans. Industrial Electronics*, vol. 60, no. 4, pp. 1403–1416, Apr. 2013.
- [4] A. Tsikalakis and N. Hatziargyriou, “Centralized control for optimizing microgrids operation,” *IEEE Trans. Energy Conversion*, vol. 23, no. 1, pp. 241–248, Mar. 2008.
- [5] K. Turitsyn, P. Sulc, S. Backhaus, and M. Chertkov, “Local control of reactive power by distributed photovoltaic generators,” in *Proc. First IEEE International Conference on Smart Grid Communications (SmartGridComm)*, Gaithersburg, MD, U.S., Oct. 2010.
- [6] A. Costabeber, P. Tenti, and P. Mattavelli, “Surround control of distributed energy resources in micro-grids,” in *Proc. IEEE International Conference on Sustainable Energy Technologies (ICSET)*, Kandy, Sri Lanka, Dec. 2010.
- [7] S. Bolognani and S. Zampieri, “Distributed control for optimal reactive power compensation in smart microgrids,” in *Proc. 50th IEEE Conference on Decision and Control and European Control Conference (CDC-ECC)*, Orlando, FL, U.S., Dec. 2011.

-
- [8] D. J. Watts and S. H. Strogatz, "Collective dynamics of 'Small-World' networks," *Nature* 393, pp. 440–442, Apr. 1998.
- [9] M. Miozzo, D. Zordan, P. Dini, and M. Rossi, "SolarStat: Modeling photovoltaic sources through stochastic markov processes," in *IEEE International Energy Conference and Exhibition (ENERGYCON)*, Dubrovnik, Croatia, May 2014.
- [10] IEA, "Key world energy statistics," 9 rue de la Fédération, 75739 Paris Cedex 15, France, 2013.
- [11] S. Goel, S. F. Bush, and D. Bakken, Eds., *IEEE Vision for Smart Grid Communications: 2030 and Beyond*. 3 Park Avenue New York, NY, USA: IEEE, 2013.
- [12] A. Yokoyama, H. Akagi, Y. Hayashi, K. Ogimoto, and H. Ishii, "A national project on optimal control and demonstration of the Japanese smart grid for massive integration of photovoltaic systems," in *Proc. 3rd IEEE PES International Conference and Exhibition on Innovative Smart Grid Technologies (ISGT Europe)*, Berlin, Germany, Oct. 2012.
- [13] A. A. Bayod-Rjula, "Future development of the electricity systems with distributed generation," *Elsevier Energy*, vol. 34, no. 3, pp. 377 – 383, Dec. 2009.
- [14] Y. Hayashi, "Trend and future view of voltage control for distribution systems with distributed generators," *IEEJ Trans. Power and Energy*, vol. 129, pp. 491–494, Feb. 2009.
- [15] J. Carrasco, L. Franquelo, J. Bialasiewicz, E. Galvan, R. Guisado, M. Prats, J. Leon, and N. Moreno-Alfonso, "Power-electronic systems for the grid integration of renewable energy sources: A survey," *IEEE Trans. Industrial Electronics*, vol. 53, no. 4, pp. 1002–1016, Aug. 2006.
- [16] F. Blaabjerg, Z. Chen, and S. Kjaer, "Power electronics as efficient interface in dispersed power generation systems," *IEEE Trans. Power Electronics*, vol. 19, no. 5, pp. 1184–1194, Sept. 2004.
- [17] P. Tenti, D. Trombetti, E. Tedeschi, and P. Mattavelli, "Compensation of load unbalance, reactive power and harmonic distortion by cooperative operation of distributed

- compensators,” in *Proc. 13th European Conference on Power Electronics and Applications (EPE)*, Barcelona, Spain, Sept. 2009.
- [18] P. Vytelingum, T. D. Voice, S. D. Ramchurn, A. Rogers, and N. R. Jennings, “Agent-based micro-storage management for the smart grid,” in *Proc. 9th International Conference on Autonomous Agents and Multiagent Systems (AAMAS)*, Toronto, Canada, Jul. 2010.
- [19] M. Ciobotaru, R. Teodorescu, P. Rodriguez, A. Timbus, and F. Blaabjerg, “Online grid impedance estimation for single-phase grid-connected systems using PQ variations,” in *Proc. IEEE Power Electronics Specialists Conference (PESC)*, Orlando, FL, U.S., Jun. 2007.
- [20] P. Vovos, A. Kiprakis, A. Wallace, and G. Harrison, “Centralized and distributed voltage control: Impact on distributed generation penetration,” *IEEE Trans. Power Systems*, vol. 22, no. 1, pp. 476–483, Feb. 2007.
- [21] S. Galli, A. Scaglione, and W. Zhifang, “For the grid and through the grid: The role of power line communications in the smart grid,” *Proceedings of the IEEE*, vol. 99, no. 6, pp. 998–1027, Mar. 2011.
- [22] “IEEE approved draft standard for low frequency (less than 500 khz) narrow band power line communications for smart grid applications,” *IEEE Std. 1901.2-2013*, 2013.
- [23] N. Bui, M. Rossi, and M. Zorzi, *IEEE Vision for Smart Grid Communications: 2030 and Beyond*. 3 Park Avenue New York, NY, USA: IEEE, 2013, ch. Networking Technologies for Smart Grid.
- [24] G. A. Pagani and M. Aiello, “Power grid network evolutions for local energy trading,” *arXiv:1201.0962 [physics.soc-ph]*, Feb. 2012.
- [25] T. Erseghe and S. Tomasin, “Power flow optimization for smart microgrids by SDP relaxation on linear networks,” *IEEE Trans. Smart Grid*, vol. 4, no. 2, pp. 751–762, Jun. 2013.

- [26] P. Tenti, A. Costabeber, P. Mattavelli, and D. Trombetti, "Distribution loss minimization by token ring control of power electronic interfaces in residential microgrids," *IEEE Trans. Industrial Electronics*, vol. 59, no. 10, pp. 3817–3826, Oct. 2012.
- [27] A. Costabeber, T. Erseghe, P. Tenti, S. Tomasin, and P. Mattavelli, "Optimization of micro-grid operation by dynamic grid mapping and token ring control," in *Power Electronics and Applications (EPE 2011)*, Birmingham, United Kingdom, Aug. 2011, pp. 1–10.
- [28] S. Bolognani and S. Zampieri, "Convergence analysis of a distributed voltage support strategy for optimal reactive power compensation," in *Proc. 3rd IFAC Workshop on Distributed Estimation and Control in Networked Systems*, Santa Barbara, CA, U.S., Sept 2012.
- [29] K. Turitsyn, P. Sulc, S. Backhaus, and M. Chertkov, "Options for control of reactive power by distributed photovoltaic generators," *Proceedings of the IEEE*, vol. 99, no. 6, pp. 1063–1073, Jun. 2011.
- [30] W. H. Kersting, "Radial distribution test feeders," in *Proc. IEEE Power Engineering Society Winter Meeting*, Columbus, OH, U.S., Jan. 2001.
- [31] K. Bache and M. Lichman, "UCI Machine Learning Repository," 2013. [Online]. Available: <http://archive.ics.uci.edu/ml>
- [32] L. Tao, C. Schwaegerl, P. Mancarella, G. Strbac, N. Hatziargyriou, and B. Buchholz, "European Roadmap for Microgrids," in *Proc. CIGRE*, Paris, France, Aug. 2010.
- [33] R. Ipakchi and F. Albuyeh, "Grid of the future," *IEEE Power and Energy Magazine*, vol. 7, no. 2, pp. 55–62, Feb. 2009.
- [34] H. Farhangi, "The path of the smart grid," *IEEE Power and Energy Magazine*, vol. 8, no. 1, pp. 18–28, Jan.-Feb. 2010.
- [35] J. Rocabert, G. Azevedo, A. Luna, J. Guerrero, J. Candela, and P. Rodriguez, "Intelligent connection agent for three-phase grid-connected microgrids," *IEEE Trans. Power Electronics*, vol. 26, no. 10, pp. 2993–3005, Oct. 2011.

- [36] R. Anderson, A. Boulanger, W. Powell, and W. Scott, "Adaptive stochastic control for the smart grid," *IEEE Proceedings*, vol. 99, no. 6, pp. 1098–1115, May 2011.
- [37] A. Dimeas and N. Hatziargyriou, "Operation of a multiagent system for microgrid control," *IEEE Trans. Power Systems*, vol. 20, no. 3, pp. 1447–1455, Aug. 2005.
- [38] J.-Y. Kim, J.-H. Jeon, S.-K. Kim, C. Cho, J. H. Park, H.-M. Kim, and K.-Y. Nam, "Cooperative control strategy of energy storage system and microsources for stabilizing the microgrid during islanded operation," *IEEE Trans. Power Electronics*, vol. 25, no. 12, pp. 3037–3048, Dec. 2010.
- [39] A. Mohsenian-Rad, V. Wong, J. Jatskevich, R. Schober, and A. Leon-Garcia, "Autonomous demand-side management based on game-theoretic energy consumption scheduling for the future smart grid," *IEEE Trans. Smart Grids*, vol. 1, no. 3, pp. 320–331, Nov. 2010.
- [40] D. Forner, T. Erseghe, S. Tomasin, and P. Tenti, "On efficient use of local sources in smart grids with power quality constraints," in *Proc. First IEEE Int. Conf. on Smart Grid Commun. (SmartGridComm)*, 2010, pp. 555–560.
- [41] T. Erseghe and S. Tomasin, "Power flow optimization for smart microgrids by sdp relaxation on linear networks," *IEEE Trans. Smart Grid*, vol. 4, no. 2, pp. 751–762, 2013.
- [42] E. Serban and H. Serban, "A control strategy for a distributed power generation microgrid application with voltage- and current-controlled source converter," *IEEE Trans. Power Electronics*, vol. 25, no. 12, pp. 2981–2992, Dec. 2010.
- [43] P. Tenti, H. K. Morales, and P. Mattavelli, "Conservative Power Theory, a Framework to Approach Control and Accountability Issues in Smart Microgrids," *IEEE Trans. Power Electronics*, vol. 26, no. 3, pp. 664–673, May 2011.
- [44] P. Tenti, A. Costabeber, T. Caldognetto, and P. Mattavelli, "Improving microgrid performance by cooperative control of distributed energy sources," in *Proc. IEEE Energy Conversion Congress and Exposition (ECCE)*, Denver, CO, US, Sep. 2013.

- [45] Q. L. Ping, Y. Zhang, H. Jianwei, and W. Yuan, "Demand response management via real-time electricity price control in smart grids," *IEEE Journal on Selected Areas in Communications*, vol. 31, no. 7, pp. 1268–1280, July 2013.
- [46] P. Samadi, A.-H. Mohsenian-Rad, R. Schober, V. Wong, and J. Jatskevich, "Optimal real-time pricing algorithm based on utility maximization for smart grid," in *IEEE International Conference on Smart Grid Communications (SmartGridComm)*, Gaithersburg, MD, U.S., Oct 2010.
- [47] C. Joe-Wong, S. Sen, H. Sangtae, and C. Mung, "Optimized day-ahead pricing for smart grids with device-specific scheduling flexibility," *IEEE Journal on Selected Areas in Communications*, vol. 30, no. 6, pp. 1075–1085, July 2012.
- [48] S. Ali, R. Ahmad, and K. K. Hyeun, "A study of pricing policy for demand response of home appliances in smart grid based on m2m," in *IEEE International Conference on Frontiers of Information Technology (FIT)*, Islamabad, PK, Dec 2012.
- [49] P. Samadi, A. Mohsenian-Rad, R. Schober, V. Wong, and J. Jatskevich, "Optimal real-time pricing algorithm based on utility maximization for smart grid," in *IEEE International Conference on Smart Grid Communications (SmartGridComm)*, Gaithersburg, MD, U.S., Oct 2010.
- [50] H. Chong and S. Sarker, "Dynamic pricing for distributed generation in smart grid," in *IEEE Green Technologies Conference*, Denver, CO, U.S., April 2013.
- [51] S. Boyd and L. Vandenberghe, *Convex Optimization*. New York, NY, U.S.: Cambridge University Press, 2004.
- [52] S. Boyd, S. Kim, L. Vandenberghe, and A. Hassibi, "A tutorial on geometric programming," *Optimization and Engineering*, vol. 8, no. 1, pp. 67–127, 2007. [Online]. Available: <http://dx.doi.org/10.1007/s11081-007-9001-7>
- [53] M. Kaisa, *Nonlinear Multiobjective Optimization*. Springer Science and Business Media U.S., 1998.